

CONTINUING EVOLUTION OF DIAMIDO-SUPPORTED MOLYBDENUM IMIDO
ORGANOMETALLIC CHEMISTRY

By

THOMAS M. CAMERON

A DISSERTATION PRESENTED TO THE GRADUATE SCHOOL
OF THE UNIVERSITY OF FLORIDA IN PARTIAL FULFILLMENT
OF THE REQUIREMENTS FOR THE DEGREE OF
DOCTOR OF PHILOSOPHY

UNIVERSITY OF FLORIDA

2002

TO LUCILE, MELISSA, AND GERRY

ACKNOWLEDGMENTS

My undergraduate and Los Alamos experiences, shaped by Professor S. A. Westcott and Dr. R. Tom Baker, respectively, were certainly memorable and will never be forgotten. The skills I learned while working with Westcott and Baker have served me throughout graduate school. The time and effort they put forth guiding and helping me is evident in the work outlined in this dissertation, and were it not for these two individuals, I would never have continued my education in chemistry on the graduate level.

Los Alamos is where I first met Professor James M. Boncella, who was visiting on sabbatical at the time. Based on our interaction, I decided to work for him as a graduate student and followed him back to UF. It was an excellent decision. Professor Boncella, with his never-ending knowledge of organometallic chemistry, has been responsible for my growth as a chemist over the last five years. Together we have made some interesting chemical discoveries and have published these results in leading journals in our field. I have enjoyed the time spent with him. Perhaps our paths will cross again in the future.

Dr. Khalil Abboud has made great contributions to this dissertation. He has solved all of the structures reported herein, and it was always a pleasure to work with him. Without his hard work there would be, without a doubt, fewer structural studies in this report.

Our work would not have been complete without the excellent support of Dr. Ion Ghiviriga. Over the past years Ion has taught me a great deal about 2-D NMR and has

contributed to our work by characterizing several organometallic species. I will never forget the seven-course dinners at Ion's place, his generosity, and his hospitality. I just wish there were time to learn more from him. I thank Professor Michael Scott for all of his help over the years and for access to his automatic coffee machine. I will always remember the time spent with Tim Foley. He is a remarkable individual and things will not be the same without him. Thanks also go to Jeff for happy drinking days and Bob Shelton for setting up all of the DFT calculations mentioned in this work.

I could not have accomplished any of this work without my loving parents, Lucile and Gerry. They have supported me unwaveringly for the last 27 years, never asking for anything in return. Had it not been for their encouragement, I could never have lasted. I do not know what I would have done without them. I love them both with all of my heart.

Had I not made this journey to and through graduate school, I would never have met Melissa. She alone has made this experience worthwhile and has given my life a new meaning. Her strength, love, and support have helped me through difficult times. It has often seemed like the world was trying to keep us apart, but I believe that destiny brought us together, and together we will remain. I have missed her dearly since her graduation, and it is as if a part of me left with her. But we will soon be together again.

TABLE OF CONTENTS

	<u>page</u>
ACKNOWLEDGMENTS	iii
LIST OF TABLES	ix
LIST OF FIGURES	x
ABSTRACT.....	xiv
CHAPTER	
1 METAL IMIDES AND AMIDES	1
Nitrogen Donor-Based Ligands in Early Metal Chemistry	1
Imido Ligands	2
Amido Ligands.....	6
Reactive Imido-Diamido Complexes.....	7
Group 4 imido-diamido complexes	9
Group 6 imido-diamido complexes	10
Scope of the Dissertation	14
2 SYNTHESIS OF LEWIS BASE-STABILIZED MOLYBDENUM COMPLEXES: SOURCES OF REACTIVE MOLYBDENUM(IV).....	16
Generation of Imido-Diamido Pyridine Complexes	16
Synthesis and Characterization of [Mo(NPh)(Py) ₂ (<i>o</i> -(Me ₃ SiN) ₂ C ₆ H ₄)] (47).....	16
Metal <i>d²</i> vs. <i>d⁰</i> Electronic Configuration and Diamido Ligand Folding	20
Synthesis and Characterization of [Mo(NPh) <i>trans</i> (Py) ₂ (CO)(<i>o</i> -(Me ₃ SiN) ₂ C ₆ H ₄)] (48).....	24
C-N Activation of an Amido Ligand: Synthesis of Imido-Bridged 49 from 47	30
Generation of Imido-Diamido P(OMe) ₃ Adducts.....	31
Synthesis and Characterization of [Mo(NPh)(P(OMe) ₃) ₃ (<i>o</i> -(Me ₃ SiN) ₂ C ₆ H ₄)] (50).....	31
Synthesis and Characterization of [Mo(NPh)(P(OMe) ₃) ₂ CO(<i>o</i> -(Me ₃ SiN) ₂ C ₆ H ₄)] (51).....	33
Generation of Imido-Diamido PMe ₃ Adducts	35
Synthesis and Characterization of [Mo(NPh)(PMe ₃) ₃ (<i>o</i> -(Me ₃ SiN) ₂ C ₆ H ₄)] (52) ...	35
Synthesis and Characterization of [Mo(NPh)(PMe ₃) ₂ CO(<i>o</i> -(Me ₃ SiN) ₂ C ₆ H ₄)] (54).....	36
Generation of Imido-Diamido PMe ₂ Ph Adducts	41

Synthesis and Characterization of $[\text{Mo}(\text{NPh})(\text{PMe}_2\text{Ph})_2(o\text{-(Me}_3\text{SiN)}_2\text{C}_6\text{H}_4)]$ (55).....	41
Synthesis and Characterization of $[\text{Mo}(\text{NPh})(\text{PMe}_2\text{Ph})_2\text{CO}(o\text{-(Me}_3\text{SiN)}_2\text{C}_6\text{H}_4)]$ (56).....	43
Synthesis and Characterization of $[\text{Mo}(\text{NPh})(\text{DMPE})(o\text{-(Me}_3\text{SiN)}_2\text{C}_6\text{H}_4)\text{-}\mu\text{-}$ $(\text{DMPE})\text{Mo}(\text{NPh})(\text{DMPE})(o\text{-(Me}_3\text{SiN)}_2\text{C}_6\text{H}_4)]$ (57).....	44
Generation of an Imido-Diamido Arduengo Carbene (Imidazol-2-Ylidene) Adduct ..	46
Summary	51
3 SYNTHESIS AND REACTIVITY OF A MOLYBDENUM IMIDO-DIAMIDO STRETCHED DIHYDROGEN COMPLEX	53
Characterization of Dihydrogen Complexes.....	54
Solution NMR Spectroscopy: d_{HH} and $^1J_{\text{H-D}}$	55
Solution NMR Spectroscopy: d_{HH} and NMR Relaxation Time (T_1).....	55
Molybdenum Imido-Diamido Stretched Dihydrogen Complexes.....	56
Characterization of $[\text{Mo}(\text{NPh})(\text{PMe}_3)_2(\text{H}_2)(o\text{-(Me}_3\text{SiN)}_2\text{C}_6\text{H}_4)]$ (60)	57
Characterization of $[\text{Mo}(\text{NPh})(\text{PMe}_2\text{Ph})_2(\text{H}_2)(o\text{-(Me}_3\text{SiN)}_2\text{C}_6\text{H}_4)]$ (66)	63
Bonding in Molybdenum Imido-Diamido Stretched Dihydrogen Complexes	65
Reaction of 50 and 57 with Dihydrogen Gas	66
Reaction of 52 with Phenylsilane and Diphenylsilane.....	68
Summary	68
4 SYNTHESIS, CHARACTERIZATION, AND REACTIVITY OF A MOLYBDENUM (IV), η^4-BUTADIENE COMPLEX AND η^2-ALKYNE COMPLEXES	71
Early Transition Metal Butadiene Complexes.....	71
Molybdenum Imido-Diamido Butadiene Complexes.....	73
Synthesis and Characterization of η^4 -Butadiene Complex $[(\text{Mo}(\text{NPh})\text{-}\eta^4\text{-(H}_2\text{C=CHCH=CH}_2)(o\text{-(Me}_3\text{SiN)}_2\text{C}_6\text{H}_4)]$ (73)	74
Reactivity of $[(\text{Mo}(\text{NPh})\text{-}\eta^4\text{-(H}_2\text{C=CHCH=CH}_2)(o\text{-(Me}_3\text{SiN)}_2\text{C}_6\text{H}_4)]$ (73) with 2-Butyne.....	78
Reactivity of $[(\text{Mo}(\text{NPh})\text{-}\eta^4\text{-(H}_2\text{C=CHCH=CH}_2)(o\text{-(Me}_3\text{SiN)}_2\text{C}_6\text{H}_4)]$ (73) with Acetone: Formation of $[(\text{Mo}(\text{NPh})(\text{CH}_2\text{CH=CHCH}_2\text{C}(\text{Me})_2\text{O})$ $(o\text{-(Me}_3\text{SiN)}_2\text{C}_6\text{H}_4)]$ (77)	84
Synthesis and Characterization of η^4 -MVK Complex $[(\text{Mo}(\text{NPh})\text{-}\eta^4\text{-}$ $(\text{O=C}(\text{Me})\text{CH=CH}_2)(o\text{-(Me}_3\text{SiN)}_2\text{C}_6\text{H}_4)]$ (78)	85
Summary	88
Early Transition Metal Alkyne Complexes.....	88
Synthesis and Characterization of Molybdenum Imido-Diamido Alkyne Complexes $[(\text{Mo}(\text{NPh})\text{-}\eta^2\text{-(RCCR)}(o\text{-(Me}_3\text{SiN)}_2\text{C}_6\text{H}_4)]$ (R = Me (75), Ph (79), SiMe ₃ (80)).....	89
Reaction of $[(\text{Mo}(\text{NPh})\text{-}\eta^2\text{-(PhCCPh)}(o\text{-(Me}_3\text{SiN)}_2\text{C}_6\text{H}_4)]$ (79) with tert-Butyl Isocyanide	91
Summary	96

5 REACTIVITY OF MOLYBDENUM OLEFIN AND ARENE COMPLEXES WITH UNSATURATED SUBSTRATES	98
Reaction of Molybdenum Olefin Complexes with Imines: The Synthesis of Molybdenum Imido-Diamido η^2 -Imine Complexes.....	98
Reaction of Molybdenum Olefin Complexes with Acetone and Aldehydes: The Synthesis of Oxametallacyclopentanes.....	105
Reactivity of Arene Complexes with Acetone.....	109
6 EXPERIMENTAL DATA	112
General Methods.....	112
Synthesis and Characterization.....	113
[Mo(NPh)(Py) ₂ (<i>o</i> -(Me ₃ SiN) ₂ C ₆ H ₄)] (47)	113
[Mo(NPh) <i>trans</i> (Py) ₂ (CO)(<i>o</i> -(Me ₃ SiN) ₂ C ₆ H ₄)] (48)	114
Imido-Bridged, Bimetallic 49	114
[Mo(NPh)(P(OMe) ₃) ₃ (<i>o</i> -(Me ₃ SiN) ₂ C ₆ H ₄)] (50).....	115
[Mo(NPh)(P(OMe) ₃) ₂ CO(<i>o</i> -(Me ₃ SiN) ₂ C ₆ H ₄)] (51).....	115
[Mo(NPh)(PMe ₃) ₃ (<i>o</i> -(Me ₃ SiN) ₂ C ₆ H ₄)] (52)	115
[Mo(NPh)(PMe ₃) ₃ (<i>o</i> -(Me ₃ SiN)(NH)C ₆ H ₄)] (53)	116
[Mo(NPh)(PMe ₃) ₂ CO(<i>o</i> -(Me ₃ SiN) ₂ C ₆ H ₄)] (54).....	116
[Mo(NPh)(PMe ₂ Ph) ₂ (<i>o</i> -(Me ₃ SiN) ₂ C ₆ H ₄)] (55)	116
[Mo(NPh)(PMe ₂ Ph) ₂ CO(<i>o</i> -(Me ₃ SiN) ₂ C ₆ H ₄)] (56)	117
[Mo(NPh)(DMPE)(<i>o</i> -(Me ₃ SiN) ₂ C ₆ H ₄)- μ -(DMPE)Mo(NPh)(DMPE) (<i>o</i> -(Me ₃ SiN) ₂ C ₆ H ₄)] (57)	117
[Mo(NPh)IMes(<i>o</i> -(Me ₃ SiN) ₂ C ₆ H ₄)] (59).....	118
[Mo(NPh)(PMe ₃) ₂ (H ₂)(<i>o</i> -(Me ₃ SiN) ₂ C ₆ H ₄)] (60)	118
[Mo(NPh)(PMe ₂ Ph) ₂ (H ₂)(<i>o</i> -(Me ₃ SiN) ₂ C ₆ H ₄)] (66)	119
[Mo(NPh)(PMe ₂ Ph) ₂ (<i>o</i> -(Me ₃ SiN)(NH)C ₆ H ₄)] (67)	119
[Mo(NPh)(P(OMe) ₃) ₃ (<i>o</i> -(Me ₃ SiN)(NH)C ₆ H ₄)] (68)	119
Synthesis and Characterization of 71	119
[(Mo(NPh)- η^4 -(H ₂ C=CHCH=CH ₂)(<i>o</i> -(Me ₃ SiN) ₂ C ₆ H ₄)] (73)	120
[(Mo(NPh)- η^4 -(2,3-dimethyl-1,3-cyclohexadiene)(<i>o</i> -(Me ₃ SiN) ₂ C ₆ H ₄)] (74)	121
[(Mo(NPh)- η^4 -(2,3-dimethyl-1,3-cyclohexadiene)(<i>o</i> -(Me ₃ SiN) ₂ C ₆ H ₄)] (<i>in situ</i>) (74).....	121
Intermediates [<i>syn</i> -(Mo(NPh)(C(Me)=C(Me)CH ₂ CHCH ₂ CH ₂) (<i>o</i> -(Me ₃ SiN) ₂ C ₆ H ₄)] (76a) and [<i>anti</i> -(Mo(NPh)(C(Me)=C(Me) CH ₂ CHCH ₂ CH ₂ (<i>o</i> -(Me ₃ SiN) ₂ C ₆ H ₄)] (76b).....	121
[(Mo(NPh)(CH ₂ CH=CHCH ₂ C(Me) ₂ O)(<i>o</i> -(Me ₃ SiN) ₂ C ₆ H ₄)] (77)	122
[(Mo(NPh)- η^4 -(O=C(Me)CH=CH ₂)(<i>o</i> -(Me ₃ SiN) ₂ C ₆ H ₄)] (78)	122
[(Mo(NPh)- η^2 -(MeCCMe)(<i>o</i> -(Me ₃ SiN) ₂ C ₆ H ₄)] (75).....	122
[(Mo(NPh)- η^2 -(PhCCPh)(<i>o</i> -(Me ₃ SiN) ₂ C ₆ H ₄)] (79)	123
[(Mo(NPh)- η^2 -(Me ₃ SiCCSiMe ₃)(<i>o</i> -(Me ₃ SiN) ₂ C ₆ H ₄)] (80)	123
Reaction of [(Mo(NPh)- η^2 -(PhCCPh)(<i>o</i> -(Me ₃ SiN) ₂ C ₆ H ₄)] (79) with <i>tert</i> -Butyl Isocyanide: Synthesis and Characterization of 82	123

[Mo(NPh)- η^2 -PhN=C(H)Ar(<i>o</i> -(Me ₃ SiN) ₂ C ₆ H ₄)] (Ar = C ₆ H ₄ - <i>p</i> -OMe) (83)	124
[Mo(NPh)- η^2 -PhN=C(Me)Ph(<i>o</i> -(Me ₃ SiN) ₂ C ₆ H ₄)] (84)	124
[Mo(NPh)EtNC(H)ArC(H)ArNEt(<i>o</i> -(Me ₃ SiN) ₂ C ₆ H ₄)] (Ar = C ₆ H ₄ - <i>p</i> -OMe) (85)	125
[Mo(NPh)BzNC(H)ArC(H)ArNBz(<i>o</i> -(Me ₃ SiN) ₂ C ₆ H ₄)] (Ar = C ₆ H ₄ - <i>p</i> -OMe) (86)	125
[(Mo(NPh)(C(Me) ₂ CH ₂ C(Me) ₂ O)(<i>o</i> -(Me ₃ SiN) ₂ C ₆ H ₄)] (88)	126
[(Mo(NPh)(C(H)PhCH ₂ C(Me) ₂ O)(<i>o</i> -(Me ₃ SiN) ₂ C ₆ H ₄)] (89)	126
[(Mo(NPh)(C(H)PhCH ₂ C(Et) ₂ O)(<i>o</i> -(Me ₃ SiN) ₂ C ₆ H ₄)] (90)	127
[(Mo(NPh)(C(H)PhCH ₂ C(CH ₂) ₅ O)(<i>o</i> -(Me ₃ SiN) ₂ C ₆ H ₄)] (91)	127
[(Mo(NPh)(C(Me) ₂ CH ₂ C(H)(C ₆ H ₄ - <i>p</i> -OMe)O)(<i>o</i> -(Me ₃ SiN) ₂ C ₆ H ₄)] (92)	128
Reactivity of Arene Complexes with Acetone	128
LIST OF REFERENCES	129
BIOGRAPHICAL SKETCH	139

LIST OF TABLES

<u>Table</u>	<u>page</u>
2-1 X-ray data for crystal structures 19 , 47 , and 48	19
2-2 X-ray data for crystal structures 49 , 50 , and 51	38
2-3 X-ray data for crystal structures 55 , 57 , and 59	50
4-1 X-ray data for crystal structures 73 , 74 , and 78	77
4-2 X-ray data for crystal structures 75 and 80	94
5-1 X-ray data for crystal structures 84 , 85 , and 88	100

LIST OF FIGURES

<u>Figure</u>	<u>page</u>
1-1 Metal-imido multiple-bond interactions	2
1-2 General valence bond description of possible metal-imido interactions	3
1-3 Representation of a generic metal ($d\pi$)-imido ($p\pi$) multiple-bonding interaction...	4
1-4 $\text{Mo}(\text{NPh})_2(\text{S}_2\text{CNEt}_2)_2$ (1)	4
1-5 $\text{Cp}^*_2\text{Ta}(\text{NPh})\text{H}$ (2)	5
1-6 Current multidentate amido ligands in organometallic chemistry	9
1-7 Synthesis of Group 4 imido-diamido complexes	10
1-8 Reactivity of Group 4 imido-diamido complexes	11
1-9 Molybdenum (17) and tungsten (18) imido-diamido dichlorides	11
1-10 Synthesis of molybdenum and tungsten dialkyl complexes	12
1-11 Reactivity of tungsten dialkyls with Bu^tNC	12
1-12 Formation of molybdenum and tungsten alkylidene adducts	13
1-13 Formation and reactivity of metallacycle 36	13
1-14 Molybdenum olefin complexes and the synthesis of arene complexes	14
2-1 Synthesis of $[\text{Mo}(\text{NPh})(\text{Py})_2(o-(\text{Me}_3\text{SiN})_2\text{C}_6\text{H}_4)]$ (47)	17
2-2 Enlarged region of the ^1H NMR spectrum of 47 at -20°C	17
2-3 Thermal ellipsoid plot of 47 (50% probability thermal ellipsoids)	18
2-4 Space-filling model of 47 . Steric crowding hinders pyridine ligand rotation	20
2-5 Thermal ellipsoid plot of 19 (50% probability thermal ellipsoids)	21
2-6 Diamido ligand folding in molybdenum imido-diamido complexes	23

2-7	Ligand-folding and a general 3 orbital $4e^-$ interaction.....	23
2-8	Model systems for DFT studies on 19 and 47	24
2-9	Optimized geometries for 19a , 19b , and 19c , emphasizing ligand folding.....	25
2-10	Important MO interactions for 19c	26
2-11	Important MO interaction for 47c	27
2-12	Synthesis of [(Mo(NPh) <i>trans</i> (Py) ₂ (CO)(<i>o</i> -(Me ₃ SiN) ₂ C ₆ H ₄)] (48), Py = pyridine.....	28
2-13	Thermal ellipsoid plot of 48 (50% probability thermal ellipsoids).....	29
2-14	C-N activation of the <i>o</i> -(Me ₃ SiN) ₂ C ₆ H ₄ ligand in 47	31
2-15	Thermal ellipsoid plot of 49 (50% probability thermal ellipsoids).....	32
2-16	Synthesis of [Mo(NPh)(P(OMe) ₃) ₃ (<i>o</i> -(Me ₃ SiN) ₂ C ₆ H ₄)] (50).....	32
2-17	Thermal ellipsoid plot of 50 (50% probability thermal ellipsoids).....	34
2-18	Thermal ellipsoid plot of 51 (50% probability thermal ellipsoids).....	37
2-19	Thermal ellipsoid plot of 52 (50% probability thermal ellipsoids).....	39
2-20	Thermal ellipsoid plot of 53 (50% probability thermal ellipsoids).....	40
2-21	Synthesis of [(Mo(NPh)(PMe ₃) ₂ (CO)(<i>o</i> -(Me ₃ SiN) ₂ C ₆ H ₄)] (54).....	41
2-22	Synthesis of [Mo(NPh)(PMe ₂ Ph) ₂ (<i>o</i> -(Me ₃ SiN) ₂ C ₆ H ₄)] (55).....	42
2-23	Thermal ellipsoid plot of 55 (50% probability thermal ellipsoids).....	43
2-24	Synthesis of [Mo(NPh)(PMe ₂ Ph) ₂ CO(<i>o</i> -(Me ₃ SiN) ₂ C ₆ H ₄)] (56)	44
2-25	Synthesis of [Mo(NPh)(DMPE)(<i>o</i> -(Me ₃ SiN) ₂ C ₆ H ₄)-μ-(DMPE) Mo(NPh)(DMPE)(<i>o</i> -(Me ₃ SiN) ₂ C ₆ H ₄)] (57)	45
2-26	Thermal ellipsoid plot of 57 (50% probability thermal ellipsoids).....	46
2-27	Synthesis of [Mo(NPh)IMes(<i>o</i> -(Me ₃ SiN) ₂ C ₆ H ₄)] (59).....	48
2-28	Thermal ellipsoid plot of 59 (50% probability thermal ellipsoids).....	49
2-29	Carbon monoxide complexes and νCO (cm ⁻¹)	52
3-1	General bonding in H ₂ complexes	54

3-2	Generation and reactivity of H ₂ complex 60	57
3-3	No H/D exchange between N-D and Si-H sites at 20°C	58
3-4	Spectra (¹ H NMR) of the H ₂ and H-D ligands of 60 and 60D (-20°C).....	59
3-5	Relaxation time vs. temperature plot for 60 , ln <i>T</i> ₁ vs. K ⁻¹	60
3-6	Potential mechanism for the formation of 53	61
3-7	Potential mechanism for the formation of 53	62
3-8	H and D do not partition equally between N and Si sites	62
3-9	Generation and reactivity of H ₂ complex 66	64
3-10	Spectra (¹ H NMR) of the H ₂ and H-D ligands of 66 and 66D (-20°C).....	64
3-11	Relaxation time vs. temperature plot for 66 , ln <i>T</i> ₁ vs. K ⁻¹	65
3-12	Bonding scenario for H ₂ complexes 60 and 66	66
3-13	Reaction of 50 and 57 with Dihydrogen Gas.....	67
3-14	Possible H ₂ complex in the DMPE system	67
3-15	Generation of cyclic 71 and 72	69
4-1	Synthesis of zirconocene butadiene complexes.....	72
4-2	Possible π^2 and σ^2 , π structures for <i>cis</i> -butadiene complexes	72
4-3	Reactivity of Cp ₂ Zr(butadiene) with a representative unsaturated substrate	73
4-4	Synthesis of [(Mo(NPh)- η^4 -(H ₂ C=CHCH=CH ₂)(<i>o</i> -(Me ₃ SiN) ₂ C ₆ H ₄)] (73)	74
4-5	Thermal ellipsoid plot of 73 (50% probability thermal ellipsoids).....	76
4-6	Reactivity of [(Mo(NPh)- η^4 -(H ₂ C=CHCH=CH ₂)(<i>o</i> -(Me ₃ SiN) ₂ C ₆ H ₄)] (73) with 2-butyne	79
4-7	Thermal ellipsoid plot of 74 (50% probability thermal ellipsoids).....	80
4-8	Structure of intermediate (76a), showing selected carbon (underlined) and proton chemical shifts, assigned by NMR spectroscopy	82
4-9	Structure of intermediate (76b), showing selected proton chemical shifts, assigned by NMR spectroscopy	82

4-10	Proposed mechanism for reaction of 73 with 2-butyne	83
4-11	Formation of $[(\text{Mo}(\text{NPh})(\text{CH}_2\text{CH}=\text{CHCH}_2\text{C}(\text{Me})_2\text{O})(o\text{-(Me}_3\text{SiN)}_2\text{C}_6\text{H}_4)]$ (77)...84	84
4-12	Proposed structure for 77 showing selected carbon (underlined) and proton chemical shifts, assigned by NMR spectroscopy.....	84
4-13	Possible methyl group exchange pathway	86
4-14	Thermal ellipsoid plot of 78 (50% probability thermal ellipsoids).....	87
4-15	Bonding in transition metal alkyne complexes.....	89
4-16	Synthesis of $[(\text{Mo}(\text{NPh})-\eta^2\text{-(RCCR)})(o\text{-(Me}_3\text{SiN)}_2\text{C}_6\text{H}_4)]$ (R = Me (75), Ph (79), SiMe ₃ (80)).....	90
4-17	Thermal ellipsoid plot of 75 (50% probability thermal ellipsoids).....	92
4-18	Thermal ellipsoid plot of 80 (50% probability thermal ellipsoids).....	93
4-19	Reaction of $[(\text{Mo}(\text{NPh})-\eta^2\text{-(PhCCPh)})(o\text{-(Me}_3\text{SiN)}_2\text{C}_6\text{H}_4)]$ (79) with Bu ^t NC: formation of 82	95
4-20	Proposed structure of 82 showing selected carbon (underlined) and proton chemical shifts, assigned by NMR spectroscopy.....	95
4-21	Proposed mechanism for the formation of 82	97
5-1	Synthesis of η^2 -imine complexes 83 and 84	99
5-2	Thermal ellipsoid plot of 84 (40% probability thermal ellipsoids).....	101
5-3	Reductive coupling of imines	103
5-4	Thermal ellipsoid plot of 85 (50% probability thermal ellipsoids).....	104
5-5	General scheme for the reductive coupling of organic molecules.....	106
5-6	Synthesis of oxametallacyclopentanes.....	106
5-7	Thermal ellipsoid plot of 88 (30% probability thermal ellipsoids).....	108
5-8	Structural assignment of 89 including assigned proton chemical shifts	109
5-9	Reaction of arene complexes with acetone	111
5-10	Possible equilibrium between an arene complex and a metallated species	111

Abstract of Dissertation Presented to the Graduate School
of the University of Florida in Partial Fulfillment of the
Requirements for the Degree of Doctor of Philosophy

CONTINUING EVOLUTION OF DIAMIDO-SUPPORTED MOLYBDENUM IMIDO
ORGANOMETALLIC CHEMISTRY

By

Thomas M. Cameron

December 2002

Chair: James M. Boncella

Department: Chemistry

We explore the synthesis and reactivity of diamido-supported molybdenum imido complexes based on the parent complex $[\text{Mo}(\text{NPh})\text{Cl}_2(o\text{-(Me}_3\text{SiN)}_2\text{C}_6\text{H}_4)]$. Reaction of olefin complexes $[\text{Mo}(\text{NPh})(\text{propene})(o\text{-(Me}_3\text{SiN)}_2\text{C}_6\text{H}_4)]$ (**37**) or $[\text{Mo}(\text{NPh})(\text{isobutylene})(o\text{-(Me}_3\text{SiN)}_2\text{C}_6\text{H}_4)]$ (**38**) with Lewis bases Py (pyridine), $\text{P}(\text{OMe})_3$, PMe_2Ph , DMPE, and IMes (1,3-Bis(2,4,6-trimethylphenyl)imidazol-2-ylidene) gives the corresponding adducts $[\text{Mo}(\text{NPh})(\text{Py})_2(o\text{-(Me}_3\text{SiN)}_2\text{C}_6\text{H}_4)]$ (**47**), $[\text{Mo}(\text{NPh})(\text{P}(\text{OMe})_3)_3(o\text{-(Me}_3\text{SiN)}_2\text{C}_6\text{H}_4)]$ (**50**), $[\text{Mo}(\text{NPh})(\text{PMe}_2\text{Ph})_2(o\text{-(Me}_3\text{SiN)}_2\text{C}_6\text{H}_4)]$ (**55**), $[\text{Mo}(\text{NPh})(\text{DMPE})(o\text{-(Me}_3\text{SiN)}_2\text{C}_6\text{H}_4)\text{-}\mu\text{-(DMPE)Mo}(\text{NPh})(\text{DMPE})(o\text{-(Me}_3\text{SiN)}_2\text{C}_6\text{H}_4)]$ (**57**), and $[\text{Mo}(\text{NPh})\text{IMes}(o\text{-(Me}_3\text{SiN)}_2\text{C}_6\text{H}_4)]$ (**59**), respectively. In this study, we report the X-ray structures of **47**, **50**, **55**, **57**, and **59**. We also discuss the reactivity of these complexes, as well as the PMe_3 adduct $[\text{Mo}(\text{NPh})(\text{PMe}_3)_3(o\text{-(Me}_3\text{SiN)}_2\text{C}_6\text{H}_4)]$ (**52**), with CO gas, generating $[\text{Mo}(\text{NPh})\text{-trans-(Py)}_2(\text{CO})(o\text{-(Me}_3\text{SiN)}_2\text{C}_6\text{H}_4)]$ (**48**), $[\text{Mo}(\text{NPh})(\text{P}(\text{OMe})_3)_2\text{CO}(o\text{-(Me}_3\text{SiN)}_2\text{C}_6\text{H}_4)]$ (**51**), $[\text{Mo}(\text{NPh})(\text{PMe}_3)_2(\text{CO})(o\text{-(Me}_3\text{SiN)}_2\text{C}_6\text{H}_4)]$ (**54**), and

[Mo(NPh)(PMe₂Ph)₂CO(*o*-(Me₃SiN)₂C₆H₄)] (**56**). We report the X-ray structures of **48** and **51**. We also present a DFT study comparing the bonding in complexes **47** and dialkyl complex [Mo(NPh)(Me)₂(*o*-(Me₃SiN)₂C₆H₄)] (**19**). These results indicate that the degree of ligand folding in complexes related to **19** may be influenced by steric factors. We report the X-ray structure of **19**. The unusual C-N activation reactivity of **47** is also discussed.

Dihydrogen complexes [Mo(NPh)(PMe₃)₂(H₂)(*o*-(Me₃SiN)₂C₆H₄)] (**60**) and [Mo(NPh)(PMe₂Ph)₂(H₂)(*o*-(Me₃SiN)₂C₆H₄)] (**66**) are formed by treatment of **52** and **55** with H₂ gas, respectively. The *d*_{H-H} of compounds **60** and **66**, as determined by *T*_{1(min)} and ¹*J*_{H-D}, are in good agreement and indicate that the H₂ ligand is slowly rotating. The reactions of **50** and **57** with H₂ gas are also presented.

Complexes **37** and **38** react with butadiene gas, generating [(Mo(NPh)η⁴-(H₂C=CHCH=CH₂)(*o*-(Me₃SiN)₂C₆H₄)] (**73**). We report the solid-state structure of **73**, showing that **73** is best described as a π²-butadiene complex, and we discuss the reactivity of **73** with 1.0 and 2.0 equiv of 2-butyne. Reaction of **73** with one equivalent of 2-butyne gives a molybdenum 2,3-dimethyl-1,3-cyclohexadiene complex (**74**). The X-ray structure of **74** is reported. Treatment of **73** with 2.0 equiv of 2-butyne gives [Mo(NPh)-η²-(MeCCMe)(*o*-(Me₃SiN)₂C₆H₄)] (**75**) and 1,2-dimethyl-1,4-cyclohexadiene as products. Complex **75** as well as [Mo(NPh)η²-(PhCCPh)(*o*-(Me₃SiN)₂C₆H₄)] (**79**) and [(Mo(NPh)-η²-(Me₃SiCCSiMe₃)(*o*-(Me₃SiN)₂C₆H₄)] (**80**) are synthesized independently and X-ray structures of **75** and **80** are presented. The allyl metallacycles [*syn*-(Mo(NPh)(C(Me)=C(Me)CH₂CHCHCH₂)(*o*-(Me₃SiN)₂C₆H₄)] (**76a**)

and [*anti*-(Mo(NPh)(C(Me)=C(Me)CH₂CHCHCH₂)(*o*-(Me₃SiN)₂C₆H₄))] (**76b**) are identified as intermediates in the reaction of **73** with 2-butyne by NMR spectroscopy.

Reaction of **38** with aldimines and ketimines gives η^2 -imine complexes [Mo(NPh)- η^2 -PhN=C(H)Ar(*o*-(Me₃SiN)₂C₆H₄)] (Ar = C₆H₄-*p*-OMe) (**83**) and [Mo(NPh)- η^2 -PhN=C(Me)Ph(*o*-(Me₃SiN)₂C₆H₄)] (**84**). The X-ray structure of **84** is reported. For less sterically demanding aldimines, the reductive coupling products [Mo(NPh)EtNC(H)ArC(H)ArNEt(*o*-(Me₃SiN)₂C₆H₄)] (Ar = C₆H₄-*p*-OMe) (**85**) and [Mo(NPh)BzNC(H)ArC(H)ArNBz(*o*-(Me₃SiN)₂C₆H₄)] (Ar = C₆H₄-*p*-OMe) (**86**) are isolated, and the X-ray structure of **85** is reported. Olefin complexes react with ketones and aldehydes, giving compounds [(Mo(NPh)(C(Me)₂CH₂C(Me)₂O)(*o*-(Me₃SiN)₂C₆H₄))] (**88**) and [(Mo(NPh)(C(H)PhCH₂C(Me)₂O)(*o*-(Me₃SiN)₂C₆H₄))] (**89**). The X-ray structure of **88** is reported.

CHAPTER 1 METAL IMIDES AND AMIDES

Organometallic chemistry is ultimately concerned with bonding interactions between transition metals and organic fragments through σ and/or π -bonds.¹ Transition metal fragments often stabilize reactive organic molecules and participate in catalytic carbon-carbon, carbon-nitrogen, carbon-hydrogen, and various other bond-forming and bond-breaking reactions. As such, modern organometallic chemistry has become an area rich in diverse chemical structure as well as a versatile tool for the synthetic chemist in the 21st century.

The reactivity observed at a metal center is highly dependent on the ancillary ligands that support that particular metal species. Electronic effects, such as π -loading (more ligand π -donor orbitals than metal π -acceptor orbitals), as well as the steric requirement of an ancillary ligand set dictate reactivity at the metal-center. Thus, efforts toward the derivitization of existing ancillary ligands and the discovery of new ligands with the goal of “tuning” reactivity at a metal-center are a major part of organometallic chemistry. Recent developments using this theme involve applications of imido and diamido ligands in organometallic synthesis.

Nitrogen Donor-Based Ligands in Early Metal Chemistry

Nitrogen donor-based ligands are common to the coordination sphere of early metals in organometallic chemistry and are prevalent in the literature. Ligands representative of this class include amines,¹ η^1 or η^2 nitriles,^{2,3} η^2 -imino-acyl ligands,^{4,5} terminal or bridging nitrosyls,⁶ terminal or bridging dinitrogen,⁷ nitrides,⁸ and

poly(pyrazolyl)borates.⁹ It is beyond the scope of this introduction to review each of these ligand types individually, and the reader is referred to the leading literature.

Organometallic complexes of η^2 -imine ligands are also known and are discussed in Chapter 5.

Imido Ligands

The area of transition-metal imido chemistry has experienced rapid and sustained growth over the last 20 years, and several excellent review articles have been written on the subject. The first major review to treat the topic was put forth by Nugent and Haymore.¹⁰ Wigley recently published an in-depth review,¹¹ while *Metal-Ligand Multiple Bonds* by Nugent and Mayer provides an excellent overview of imido complexes.¹² An extensive review of this work is not possible here. The subsequent discussion is limited to structural and bonding considerations in imido complexes.

The imido ligand is usually referred to as a closed-shell dianion, implying that the p orbitals of the ligand are filled. From a general standpoint, the imido or NR^{2-} ligand can coordinate to a metal center through a metal-nitrogen multiple bond involving one σ and either one or two additional π -interactions. In this way, it is possible to have a metal-nitrogen double-bond (**A**; one σ and one π -interaction) or triple-bond (**B**; one σ and two π -interactions) interaction (Figure 1-1).



Figure 1-1. Metal-imido multiple-bond interactions. **A**) A metal-nitrogen double-bond interaction; **B**) A metal-nitrogen triple-bond interaction. R = an organic functionality such as alkyl or aryl.

These bonding interactions can be described by a simple localized valence bond approach. In this treatment the hybridization at the imido nitrogen atom partially dictates the structural parameters of the imido ligand (Figure 1-2). In **C** the nitrogen atom is sp^2 hybridized implying, from a first approximation, a considerably bent R-N-M linkage (125° to 140°) with the lone pair occupying an $N(sp^2)$ hybrid orbital.¹⁰⁻¹² In such a situation, the imido ligand is formally considered a $2e^-$ donor for electron-counting purposes (the neutral method of e^- counting is used throughout this manuscript) and a formal metal-nitrogen double bond exists. Type **D** represents a linear structure that can arise when molecular orbital (MO) interactions do not allow for adoption of structure type **C**. The linear imide, represented by **E**, can come about when two π -interactions are present, forming a metal-nitrogen triple bond. Imides of type **E** contribute $4e^-$ to the electron count of a metal. For **E** the π -interactions are best described, in MO terms, as overlap between filled, imido, nitrogen-based p_x and p_y atomic orbitals and empty metal d_{xz} and d_{yz} atomic orbitals, respectively, as shown for a general case in Figure 1-3.

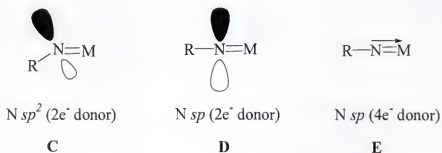


Figure 1-2. General valence bond description of possible metal-imido interactions

Few complexes of type **C** contain strongly bent-imido ligands. Of these compounds, the best known example is the molybdenum complex $\text{Mo}(\text{NPh})_2(\text{S}_2\text{CNEt}_2)_2$ (**1**) (Figure 1-4), a compound with one bent (type **C**; C-N-Mo = $139.4(4)^\circ$; N-Mo = $1.789(4)\text{ \AA}$) and one linear (type **E**; C-N-Mo = $169.4(4)^\circ$; N-Mo = $1.754(4)\text{ \AA}$) imido

ligand (the $169.4(4)^\circ$ angle is not linear, however, and as discussed below, type **E** imido linkages can have angles between 150° and 180°).¹³ With a bent-imido structure, **1** is formally considered an 18 e^- complex with the bent imido contributing 2 e^- and the linear imido contributing 4 e^- to the electron count. It has been proposed that the lone-pair electron localization in **C** can be attributed to a pair of electrons residing in a nitrogen-based MO on the bent-imido nitrogen, which is nonbonding with respect to the Mo-N interaction in **1**.

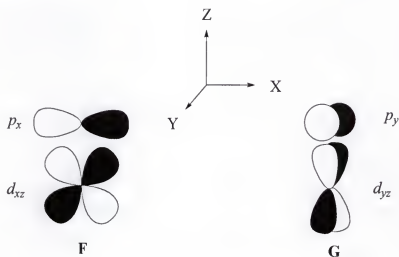


Figure 1-3. Representation of a generic metal ($d\pi$)-imido ($p\pi$) multiple-bonding interaction. **F**) interaction of an imido-based p_x with a metal-based d_{xz} orbital; **G**) interaction of an imido-based p_y with a metal-based d_{yz} orbital.

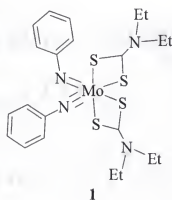


Figure 1-4. $\text{Mo}(\text{NPh})_2(\text{S}_2\text{CNEt}_2)_2$ (**1**)

Few examples of imido complexes conform to the limiting structure **D** in the literature. The $\text{Cp}^*_2\text{Ta}(\text{NPh})\text{H}$ complex (**2**) reported by Bercaw¹⁴ may be the closest related compound having a very long (1.831(10) Å) Ta-N bond and a linear Ta-N-C angle of 177.8(9)° (Figure 1-5). With a $2e^-$ donor imido ligand, **2** is an $18e^-$ complex, and the remaining imido electrons are not needed for bonding at the metal. The long Ta-N bond length, coupled with sp hybridization at the imido nitrogen (implied by the linearity of the imide), led most to conclude that the structure of **2** was best, although questionably defined in valence bond terms, as occupying a position halfway between **D** and **E**. Jørgensen¹⁵ put forth an accurate and elegant explanation of this bonding situation using extended Hückel calculations to clear the matter up. Increasing the imido angle causes an increase in the antibonding nitrogen-carbon (imido nitrogen-ipso carbon) overlap population in the HOMO (highest occupied molecular orbital), which destabilizes the bent-imido molecule (see Jørgensen¹⁵ for the full MO analysis). This example shows that this valence bond description can often be improved upon, in some cases by a substantial margin.

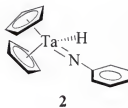


Figure 1-5. $\text{Cp}^*_2\text{Ta}(\text{NPh})\text{H}$ (**2**)

Most imido ligands encountered in organometallic and inorganic chemistry are those described by the limiting structure **E**, and most examples in this dissertation fall into this category. It is important to note that although **E** implies a linear R-N-M unit, in practice this angle can vary from approximately 150° to 180°. Experimental and

theoretical studies of complexes with metal-nitrogen triple-bond interactions have shown a very soft bending potential associated with this angle.¹⁶ It is therefore difficult to correlate the overall bond order to an R-N-M bond angle, and although such general approaches should be avoided, they still appear in the most current and respectable journals.¹⁷

In summary, while the valence bond treatment put forth is useful in gaining a basic understanding of metal-imido bonding, it is very limited. It seems that the best way to determine the true character of an imido complex is through a combination of reactivity, structural, and modern computational studies.

Amido Ligands

The widespread interest in amido ligands formulated as NH_2^- , NHR^- , or NR_2^- stems from their presence in a diverse array of compounds from the biologically significant, such as chlorophyll, to the area of inorganic chemistry, with the synthesis of amide-stabilized lanthanide metal centers. Putting aside the bioinorganic chemist's interest in the biologically significant amido-based ligands, initial exploration of metal-amides focused on structure and bonding as it compared to metal-carbon bonds of the time. This initial foray into metal-amido chemistry took place in the 1960s and early 1970s, and excellent reviews on the subject have been written.^{18,19} Researchers realized that the metal-amido bond in early metal complexes was rather inert in comparison to the metal-carbon bond; and they lost interest in the topic to pursue more interesting and lucrative chemistry, such as the developing field of early metal, metallocene-mediated polymerization.²⁰ Research in the field slowed until the inertness of the amido ligand was used to stabilize reactive early metal centers. Ironically, one such discovery involved the application of chelating *ansa*-monocyclopentadienyl-amido ligands to early

metal-olefin polymerization.²¹ The ability of a chelating amide to stabilize an early metal center, coupled with the synthetic ease and diversity of ligand design, led to a resurrection of metal-multidentate amido chemistry in the 1990s that has continued into this century.

Recent developments involving multidentate amido ligands have been reviewed.^{20,22} A list of precursors to some of the most important multidentate amido ligands in organometallic chemistry today is shown in Figure 1-6. These examples may be used to point out properties that make multidentate amides so useful. The availability of two substituent positions on an amide allow for the incorporation of this functionality into podand (**3**)^{23,24}-and macrocycle (**4**)²⁵-like systems. They allow the chemist to exert steric and electronic control during ligand design (**5**,²² **6**,²⁶ **7**²⁷) and allow the amide to be easily appended to other donor functionalities to better suit a metal center (**8**).²⁸ Furthermore, several synthetic strategies can be used to introduce amides to the coordination sphere of a metal.

These ligands are extremely useful in metal chemistry. For example, uranium species of trianionic **3** form dinitrogen complexes under appropriate conditions,²⁹ and Group 4 complexes of **5** and **6** are practical precursors to cationic olefin polymerization catalysts.^{22,26} Metal complexes of **7**, **8**, and related ligands are discussed in the next section, which is devoted to imido-diamido chemistry.

Reactive Imido-Diamido Complexes

The metal-imido multiple bonds impart unique properties to the imide and metal fragment, creating extremely reactive or stable molecules depending on the identity of the metal, the oxidation state, the imido substituent, and other ancillary ligands.³⁰ Multidentate amido ligands, when used as these ancillary ligands, should be key in tuning

reactivity at the metal center. It is thus reasonable to assume that one can create desired reactivity at an early metal center through judicious choice of both the imido and multidentate amido ligand. Some considerations must be taken into account here. For the purposes of this discussion, we will consider only diamido and imido ligands. An imide and a diamide contribute a total of +4 to the formal oxidation state of a metal complex. Most imido complexes are of d^0 , d^1 , and d^2 metal centers, and the metal-imido multiple bonding requires that the d orbitals involved in bonding be empty. Furthermore, the desired reactivity of the new compound must be considered; should the imide be reactive or should both the imide and multidentate amide behave as ancillary ligands? If Group 4 species are targeted, the metal in the resulting metal-imide-diamide, of the type $M(NR)_2(NR_2)_2$, will be in a formal +4 oxidation state. Useful functionalization will not be possible unless achieved through reactivity of the imido functionality. Synthesis of similar Group 5 complexes will suffer from the same disadvantages. Using a Group 6 metal in an analogous fashion could yield complexes of the type $M(NR)_2(NR_2)_2X_2$, allowing the metal to be functionalized at X. While high oxidation states and imido complexes are known for Groups 7 and 8, amides of these metals are rare. Applying the same idea to Group 9 or 10 metals will be difficult, for amides are not extremely good late-metal ligands, and most imido complexes must be of high-oxidation-state metal centers that are usually not available this late in the transition metal series. Based on this reasoning, efforts directed toward the synthesis of Group 6 imido-diamido complexes seem the most plausible. We have taken the above-mentioned approach for Group 6 metals; others have explored the possibilities from Groups 4 through 6. The important results are presented here.

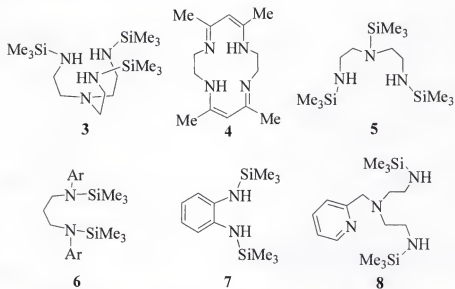


Figure 1-6. Current multidentate amido ligands in organometallic chemistry

Group 4 imido-diamido complexes

In general, the chemistry of Group 4 imido complexes is driven by reactive imido functionalities. Recently Mountford and coworkers³⁰ have made great strides in nonmacrocyclic-related developments in this area by focusing on the diamido ligands **5**, **8**, and **9** (Figures 1-6 and 1-7). The synthesis of relevant Group 4 metal complexes is shown in Figure 1-7. The reactivity of complex **13** with unsaturated organic compounds has been extensively studied and usually involves coupling reactions between the metal-imide and reactant. For example, **13** ($M = \text{Ti}$, $R = \text{butyl}^1$) reacted with 1-phenylpropyne at 80°C to give **15** and with 2,6-diisopropylphenyl isocyanate to afford **16** (Figure 1-8).³¹

Similar chemistry has also been reported for titanium aryl or alkyl imido complexes and tetraaza macrocyclic diamido ligands similar to **4** (Figure 1-6).^{25,32,33,34} Reactivity of this nature at the imido functionality is indeed important and has most recently been implicated in the metathesis of imines³⁵ and the hydroamination of unsaturated organic substrates.^{36,37,38} Perhaps the most remarkable imido reactivity has been observed by

Wolczanski and coworkers,³⁹ who reported C-H activation of saturated and unsaturated hydrocarbons by imido titanium species.

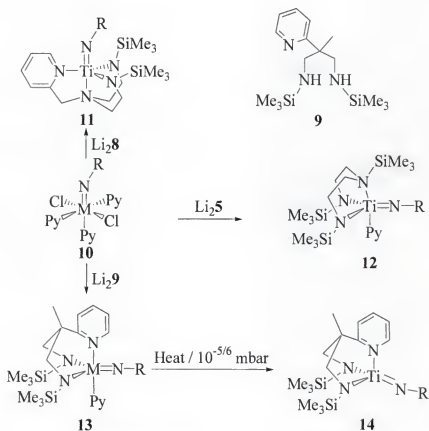


Figure 1-7. Synthesis of Group 4 imido-diamido complexes. For **10**: when M = Ti, R = butyl¹ or 2,6-C₆H₃Pr₂²; when M = Zr, R = 2,6-C₆H₃Pr₂.

Group 6 imido-diamido complexes

The imido-diamido complexes of the Group 6 metals do not generally have reactive imido functionalites. The imido and diamido ligands act as ancillary ligands and stabilize unusual complexes for these high-oxidation-state species. Mountford³⁰ has reported a few complexes of Group 6 imide-diamides with the ligand precursor **9**. In contrast, Boncella^{27,40} has developed extensive chemistry in this area starting from the two metal dichloride species shown in Figure 1-9.

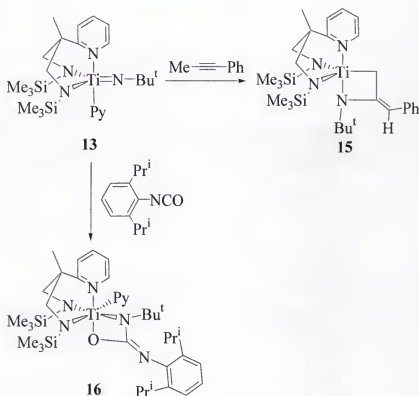


Figure 1-8. Reactivity of Group 4 imido-diamido complexes. Reactivity of 13 with 1-phenylpropyne and 2,6-diisopropylphenyl isocyanate.

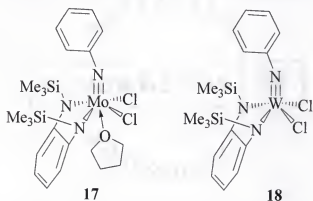


Figure 1-9. Molybdenum (17) and tungsten (18) imido-diamido dichlorides

Molybdenum and tungsten alkyl and alkylidene complexes. The dichlorides 17 and 18 were easily converted to alkyl complexes upon treatment with non- β -hydrogen-containing alkyl magnesium reagents (Figure 1-10).^{27,40} The reactivity of tungsten alkyls 24 and 26 has been explored with *tert*-butyl isocyanide (Bu^tNC)

(Figure 1-11).⁴¹ Complexes **24** and **26** inserted Bu^tNC into each metal alkyl bond, affording the η^2 -imino-acyl complexes **30** and **31**. When heated, **30** underwent a carbon-carbon coupling reaction giving **32**. This insertion and coupling chemistry has been well-documented for early metals with CO or isocyanides.^{4,5,41} Similar chemistry has not been seriously explored with the molybdenum alkyls **19-23**.

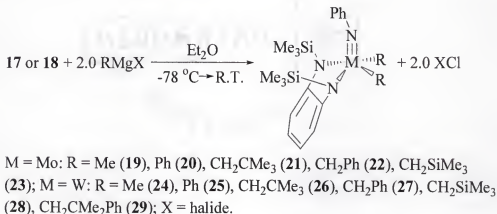


Figure 1-10. Synthesis of molybdenum and tungsten dialkyl complexes

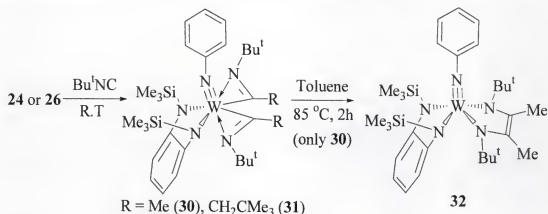


Figure 1-11. Reactivity of tungsten dialkyls with Bu^tNC

Treating complexes **21** and **26** with excess PMe₃ resulted in the formation of PMe₃ alkylidene adducts **33** and **34** through an α -abstraction process (Figure 1-12). Attempts to generate the base-free tungsten analogue of **34** (**35**) by thermolysis of **26** gave rise to **36**, mainly *via* metalation of the diamido ligand of **35** (Figure 1-13). When **36** was

treated with PMe_3 , **34** was produced by trapping **35** with phosphine. Small amounts of **36** were also formed *via* γ -abstraction of the diamido ligand of **26** (see Vaughan *et. al.*⁴² for a more detailed mechanistic analysis). Reactivity of the molybdenum alkylidene (**33**) remains largely unexplored.²⁷

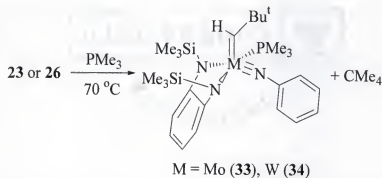


Figure 1-12. Formation of molybdenum and tungsten alkylidene adducts

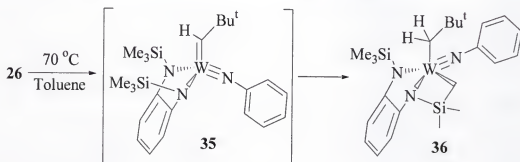


Figure 1-13. Formation and reactivity of metallacycle **36**

The β -hydrogen-containing dialkyl complexes of tungsten are stable and have been synthesized in a fashion analogous to **24-29**.⁴³ In general, coordinatively unsaturated β -hydrogen-containing complexes decompose by β -abstraction or elimination. The stability of these alkyl complexes is therefore surprising. Addition of PMe_3 to some of these species promoted β -abstraction and the formation of olefin complexes. This behavior is clearly unexpected, as the dissociation of ligands to yield unsaturated species usually induces β -abstraction.^{43, 44, 45}

Molybdenum and tungsten arene and molybdenum olefin complexes. Unlike the tungsten analogues, β -hydrogen-containing molybdenum dialkyl complexes decompose readily at 20°C (room temperature) to yield olefin complexes.⁴⁶ These high-oxidation-state olefin complexes are rare and were hydrogenated in the presence of arenes, forming high-oxidation-state arene complexes (Figure 1-14).⁴⁷ High valent Group 6 arene complexes, with the exception of the tungsten complex mentioned here, are nonexistent; and generation of arene complexes in this way remains a rare process.

We recently synthesized related tungsten arene complexes that showed interesting reactivity with phenylacetylene.⁴⁸ Furthermore, several bis(pyridine) complexes⁴⁹ were generated from this arene complex and were used to activate the carbon-sulfur bond of thiophenes.⁵⁰

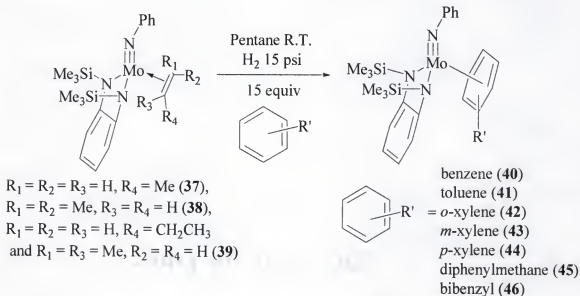


Figure 1-14. Molybdenum olefin complexes and the synthesis of arene complexes

Scope of the Dissertation

The work embodied in this dissertation reports the latest results toward new imido-diamido molybdenum complexes. Chapter 1 is a general introduction to metal

imides and amides. Chapter 2 discusses pyridine, phosphine, phosphite, and Arduengo carbene Lewis base-stabilized imido-diamido complexes and carbon monoxide derivatives. Chapter 3 is devoted to the discussion of dihydrogen complexes generated from the phosphine complexes discussed in Chapter 2. In Chapter 4, imido-diamido butadiene complexes and related reactivity involving the synthesis of alkyne complexes are discussed. The reactions of molybdenum olefin and arene complexes with imines, ketones, aldehydes, and azobenzene are discussed in Chapter 5. Experimental data are recorded in Chapter 6.

In this work, we have taken advantage of the unique ability of our π -loaded imido-diamido system to stabilize interesting and rare molybdenum complexes. In a π -loaded system, the excess π -donors can act as electron sinks, stabilizing high-oxidation-state molecules through *p-d* overlap if necessary. Oftentimes the reactivity observed resembles that of later metals in lower oxidation states. One long-term goal of this project is to take advantage of this π -loaded system to develop species that can replace expensive, later metals in chemical syntheses.

CHAPTER 2

SYNTHESIS OF LEWIS BASE-STABILIZED MOLYBDENUM COMPLEXES: SOURCES OF REACTIVE MOLYBDENUM(IV)

The dissociation of labile Lewis bases from transition metal centers can generate reactive molecules capable of interesting stoichiometric and catalytic reactions that often proceed through oxidative-addition and reductive-elimination pathways.¹ We are interested in exploring this avenue regarding our molybdenum imido-diamido system and have thus prepared a (bis)pyridine complex, phosphine and phosphite complexes, and a coordinatively unsaturated Arduengo carbene complex. In this chapter we report the synthesis, structure, and initial reactivity studies of these complexes. Some of the phosphine complexes reported here react with molecular hydrogen, generating stretched dihydrogen complexes. Chapter 3 is devoted to the synthesis and properties of these novel dihydrogen complexes.

Generation of Imido-Diamido Pyridine Complexes

Synthesis and Characterization of $[\text{Mo}(\text{NPh})(\text{Py})_2(o\text{-(Me}_3\text{SiN)}_2\text{C}_6\text{H}_4)]$ (**47**)

Adding excess pyridine to a stirring pentane solution of olefin complex **37** or **38** resulted in the precipitation of $[\text{Mo}(\text{NPh})(\text{Py})_2(o\text{-(Me}_3\text{SiN)}_2\text{C}_6\text{H}_4)]$ (**47**) as a purple solid that was isolated by filtration in high yield (Scheme 2-1).⁵¹ The ^1H NMR spectrum of **47** displays a significant broadening of the pyridine protons in the 2 and 6 positions at 20°C. At low temperature (-20°C), two distinct doublet resonances are observed in the ^1H NMR spectrum for these protons: one for the two protons *syn* to the imido group and the second for two protons *anti* to the imido functionality. The proton resonances corresponding to

the pyridine ligand protons in the 2 and 6 positions, 3 and 5 positions, and 4 position are labeled 2-6, 3-5, and 4, respectively, in the expanded ^1H NMR spectrum shown in Figure 2-2. These observations are consistent with the slow rotation of the pyridine rings about the Mo-N bond on the NMR time scale at -20°C .

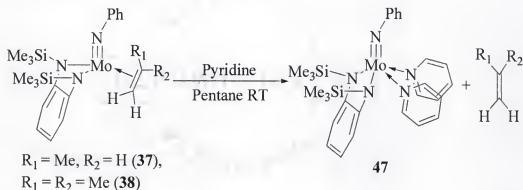


Figure 2-1. Synthesis of $[\text{Mo}(\text{NPh})(\text{Py})_2(o\text{-(Me}_3\text{SiN)}_2\text{C}_6\text{H}_4)]$ (**47**)

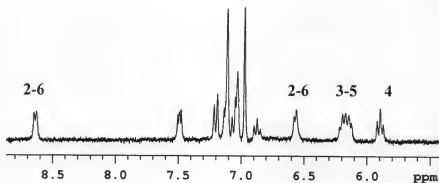


Figure 2-2. Enlarged region of the ^1H NMR spectrum of **47** at -20°C

An X-ray structural analysis was carried out on a single crystal of **47** grown at 20°C by layering a saturated toluene solution of **47** with pentane. The crystal data and details of the structure refinement are summarized in Table 2-1. A thermal ellipsoid plot of **47** is shown in Figure 2-3 with selected bond lengths and angles. The solid-state structure reveals a square pyramidal geometry about the molybdenum atom, with the imido ligand in the apical position. The Mo-N(4) and N(5) bond lengths of $2.1247(16)$ Å and

2.1460(16) Å, respectively, are consistent with Mo(IV)-pyridine Lewis acid-base interactions. The Mo-N(1) bond length of 1.7476(14) Å and the C(1)-N(1)-Mo angle of 166.35(13)° are typical values for molybdenum imido triple-bond interactions.^{11,27,47}

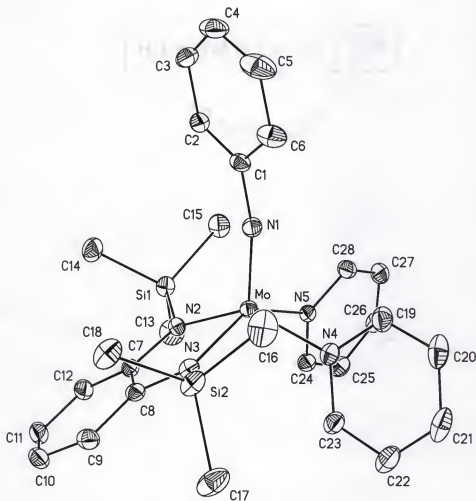


Figure 2-3. Thermal ellipsoid plot of **47** (50% probability thermal ellipsoids). Selected bond lengths (Å) and angles (°): Mo-N(1) 1.7476(14), Mo-N(2) 2.0779(16), Mo-N(3) 2.0637(16), Mo-N(4) 2.1247(16), Mo-N(5) 2.1460(16), C(1)-N(1)-Mo 166.35(13), N(3)-Mo-N(4) 88.22(6), N(5)-Mo-N(4) 80.43(6), N(2)-Mo-N(5) 88.72(6), N(2)-Mo-N(3) 78.30(6).

The space-filling model of **47**, generated from the X-ray study, reveals a sterically congested area around the pyridine ligands due to the presence of the SiMe₃ groups (Figure 2-4). This steric crowding hinders the rotation of these ligands.

Table 2-1. X-ray data^a for crystal structures **19**, **47**, and **48**

	19	47	48
Chemical formula	C ₂₀ H ₃₃ N ₃ MoSi ₂	C ₂₈ H ₃₇ N ₅ MoSi ₂	C ₂₉ H ₃₇ N ₅ MoOSi ₂
Formula weight	467.61	595.75	623.76
Crystal system	Monoclinic	Orthorhombic	Monoclinic
Space group	<i>P2₁/n</i>	<i>Pna2₁</i>	<i>C2/c</i>
$\mu(\text{Mo-K}\alpha)$ (mm ⁻¹)	0.652	0.547	0.542
<i>a</i> (Å)	10.3212(4)	15.5947(8)	16.2857(8)
<i>b</i> (Å)	18.0052(7)	10.3170(5)	16.9169(8)
<i>c</i> (Å)	13.3662(5)	18.4572(9)	22.086(1)
β (°)	103.774(2)	-	94.578(1)
<i>V_c</i> (Å ³)	2412.5(2)	2969.6(3)	6065.3(5)
<i>Z</i>	4	4	8
Θ_{max} °	27.50	27.49	27.50
Total reflections	21116	19478	21646
Uniq. reflections	5508	6777	6965
<i>R</i> (int)	0.0300	0.0272	0.0930
<i>R</i> ₁ [<i>I</i> ≥ 2σ(<i>I</i>) data] ^b	0.0221	0.0218	0.0475
w <i>R</i> ₂ (all data) ^c	0.0609	0.0530	0.1198
Larg. diff. peak, hole	0.380, -0.336	0.231, -0.222	0.474, -0.637

^aObtained with monochromatic Mo K α radiation ($\lambda = 0.71073$ Å) at 173 K. ^b $R_1 = \sum |F_o| - |F_c| / \sum |F_o|$. ^c $wR_2 = \{\sum [w(F_o^2 - F_c^2)^2] / \sum [w(F_o^2)^2]\}^{1/2}$.

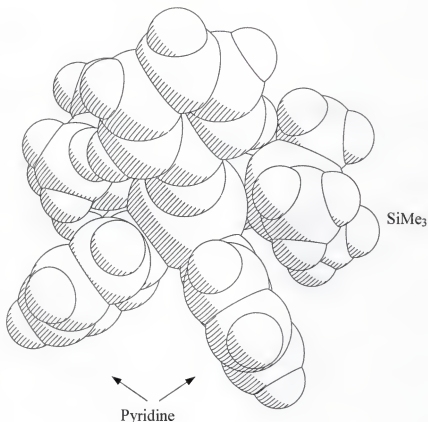


Figure 2-4. Space-filling model of **47**. Steric crowding hinders pyridine ligand rotation

Metal d^2 vs. d^0 Electronic Configuration and Diamido Ligand Folding

Although the synthesis of dialkyl complexes **19-23** has been reported,²⁷ X-ray structural studies on these compounds were not carried out at that time. We are interested in the solid-state structures of these complexes, and an X-ray study was carried out on a single crystal of **19** grown in a pentane solution at -30°C . The thermal ellipsoid plot of **19** is shown in Figure 2-5. The crystal data and details of the structure refinement are summarized in Table 2-1. The Mo-C(19) and Mo-C(20) bond lengths of 2.1911(19) Å and 2.2041(19) Å, respectively, are within the range expected for metal-carbon single bonds. The Mo-N(2) and Mo-N(3) bond lengths of 2.0117(14) Å and 2.0182(14) Å, respectively, also fall within the expected range. The Mo-N(1) bond length of 1.7204(14)

Å and the C(1)-N(1)-Mo angle of $171.66(13)^\circ$ are consistent with a metal-nitrogen triple-bond interaction.

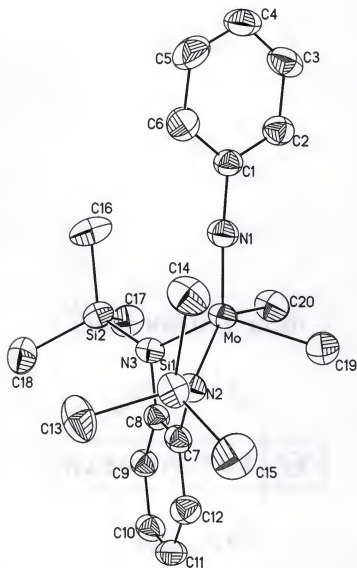


Figure 2-5. Thermal ellipsoid plot of **19** (50% probability thermal ellipsoids). Selected bond lengths (Å) and angles ($^\circ$): Mo-N(1) 1.7204(14), Mo-N(2) 2.0117(14), Mo-N(3) 2.0182(14), Mo-C(20) 2.2041(19), Mo-C(19) 2.1911(19), C(1)-N(1)-Mo 171.66(13), N(2)-Mo-N(3) 82.73(5), N(2)-Mo-C(19) 84.86(7), N(3)-Mo-C(20) 85.85(7), C(20)-Mo-C(19) 79.49(8).

There is a significant difference between the structures of the d^0 and d^2 analogues involving bonding of the diamide as born out by comparison of the solid-state structures of **19** (d^0) and **47** (d^2). In **47** the C_6H_4 ring, the diamido nitrogens (N(2) and N(3)), and

the metal center are nearly co-planar. This co-planarity is no longer present in **19**, and there is an angle of 45.6° between the planes defined by the C_6H_4 ring and the N(3), Mo, and N(2) atoms, as depicted in Figure 2-6. This structural feature is referred to in the literature as “ligand folding”, and the above-mentioned angle for **19** is called the fold-angle.

Recent density functional theory (DFT) studies attribute ligand folding to π -donation from the NSiMe₃ lone pairs to an appropriate metal-based atomic orbital at the d^0 metal-center for **19** and similar compounds.⁵² In these structures, the diamido nitrogen atoms remain sp^2 hybridized, and in order to achieve effective p - d overlap, the diamido ligand must take on the folded configuration. This bonding situation, which may simply be described as a 3 orbital $4e^-$ interaction (Figure 2-7), contributes to the π -loading of this molybdenum system. In contrast, there is no ligand folding in **47** (d^2) in order to avoid a filled-filled interaction between the p and d orbitals (the fold-angle for **47** is 4.5°). The lack of ligand folding places the SiMe₃ groups in proximity to the pyridine rings, hindering their rotation as mentioned in the previous section. The term π -loaded applies well to **47** for there are too many ligand π -donors and not enough metal-based acceptors.

We have explored the structure in compounds **19** and **47** theoretically using DFT in order to gain more insight into the bonding interactions in these compounds. DFT calculations were performed using the Gaussian 98W program package (see Chapter 6 for more details).⁵³ The model systems consist of the structures shown in Figure 2-8. Steric effects of the ligand set were investigated by varying the substitution pattern at the diamido nitrogen. The optimized geometries were visualized with gOpenMol, and results

for cases **19a**, **19b**, and **19c** are shown in Figure 2-9.^{54,55} Model system **19c** is the most accurate for reproducing the experimental structure of **19**. The fold-angle increases in the order **19a** (18.5°), **19b** (26.0°), **19c** (40.3°) (since there is no C₆H₄ moiety in the model system, the N=C=N plane of the diamide was used to calculate the fold-angle). This increase in angle can be attributed to the increase in the steric component of the diamido ligand in going from model system **19a** to **19c**. These initial results indicate that attempts to directly correlate ligand fold-angle to bond order should be avoided.

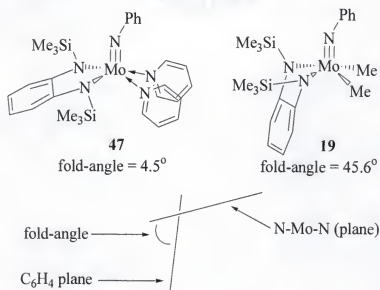


Figure 2-6. Diamido ligand folding in molybdenum imido-diamido complexes

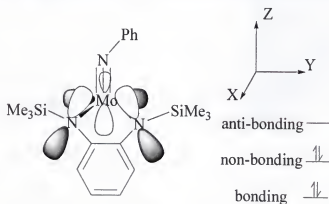


Figure 2-7. Ligand-folding and a general 3 orbital 4e⁻ interaction

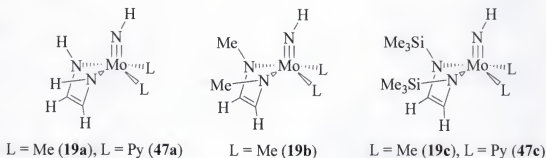


Figure 2-8. Model systems for DFT studies on **19** and **47**

The MOs involved in the 3 orbital $4e^-$ interaction (Figure 2-7) for **19c** have been identified. The MO involved in the metal-diamide bonding interaction is the HOMO of **19c**, represented graphically in Figure 2-10.^{54,55} This MO is best described as interacting metal (predominately $d_{x^2-y^2}$ and d_{yz}) and diamido nitrogen p_y and p_z atomic orbitals. The lowest unoccupied molecular orbital (LUMO) of **19c** corresponds to the anti-bonding MO for this 3 orbital $4e^-$ interaction as presented in Figure 2-7 (Figure 2-10). The nonbonding MO, as depicted in Figure 2-7, has been lowered in energy due to other interactions and is the HOMO-3 of **19c** shown in Figure 2-10.

In contrast to the d^0 system, the HOMO-1 orbital in **47c**, which is predominately of $d_{x^2-y^2}$ character, best represents the lone-pair d electrons on the metal-center. This MO is represented graphically in Figure 2-11. The LUMO of **47c** is localized on the pyridine ligands as shown in Figure 2-11.

Synthesis and Characterization of $[\text{Mo}(\text{NPh})\text{trans}(\text{Py})_2(\text{CO})(o\text{-(Me}_3\text{SiN)}_2\text{C}_6\text{H}_4)]$ (**48**)

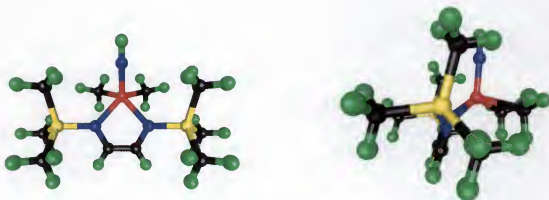
Exposure of a toluene solution of **47** to dry carbon monoxide gas (ca. 15 psi) resulted in the formation of the six-coordinate complex $[(\text{Mo}(\text{NPh})\text{-trans-(Py)}_2(\text{CO})(o\text{-(Me}_3\text{SiN)}_2\text{C}_6\text{H}_4)]$ (**48**) (Figure 2-12). An X-ray crystallographic study was carried out on single crystals of **48** grown from a concentrated toluene solution. The thermal



19a, fold-angle = 18.5°

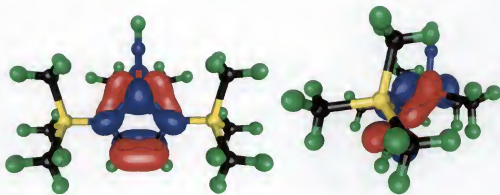
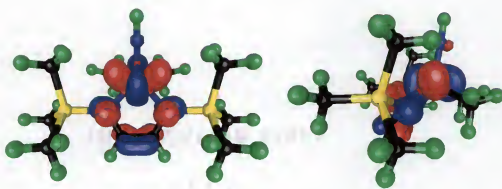
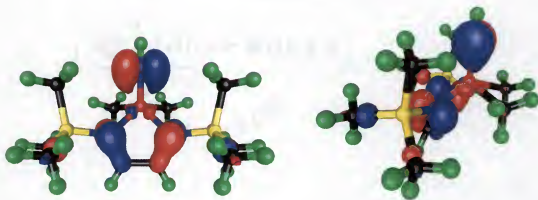


19b, fold-angle = 26.0°



19c, fold-angle = 40.3°

Figure 2-9. Optimized geometries for **19a**, **19b**, and **19c**, emphasizing ligand folding

HOMO of **19c**LUMO of **19c**HOMO-3 of **19c**Figure 2-10. Important MO interactions for **19c**

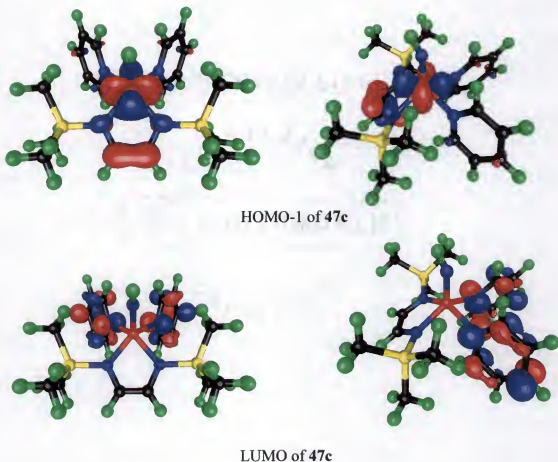


Figure 2-11. Important MO interaction for 47c

ellipsoid plot of 48 is shown in Figure 2-13 along with selected bond lengths and angles.

The crystal data and details of the structure refinement are summarized in Table 2-1.

Complex 48 adopts a distorted octahedral geometry. The Mo-N(1) bond length of 1.778(3) Å and the C(1)-N(1)-Mo angle of 162.5(3)° are consistent with a molybdenum-nitrogen triple-bond interaction. The Mo-N(4) and N(5) bond lengths of 2.207(3) Å and 2.217(3) Å, respectively, are within the expected range for a six-coordinate molybdenum pyridine adduct. An important feature in 48 is the *trans* geometry adopted by the two pyridine ligands as well as the *trans* arrangement of one amide and the carbonyl ligand, presumably a result of combined steric and electronic

effects. For example, this *trans* arrangement of amido and CO ligand allows for a 3 orbital $4e^-$ interaction between the filled amido p orbital, the appropriate metal d orbital, and the CO π^* orbital. Furthermore, the *trans* orientation of the pyridine ligands keeps them away from each other and away from the steric bulk of the SiMe_3 groups.

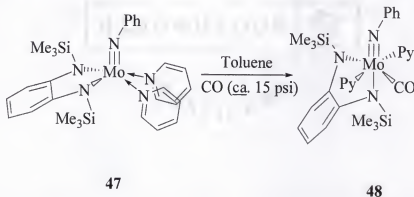


Figure 2-12. Synthesis of $[(\text{Mo}(\text{NPh})\text{trans}(\text{Py})_2(\text{CO})(o\text{-(Me}_3\text{SiN)}_2\text{C}_6\text{H}_4)]$ (**48**), Py = pyridine

Two resonances for the inequivalent SiMe_3 groups are observed at 0.32 ppm and 0.37 ppm in the ^1H NMR spectrum of **48**, consistent with the solid-state structure. The equivalency of the pyridine protons in the 2 and 6 positions in the ^1H NMR spectrum at 20°C indicate that rotation about the pyridine molybdenum bond is not hindered at this temperature on the NMR time scale in this six-coordinate complex. This is interesting when compared to the hindered rotation of the pyridine rings in five-coordinate **47** and is an unusual example of a coordinatively saturated system (**48**) being less sterically hindered than an unsaturated system (**47**). A stretching frequency of 1913 cm^{-1} in the IR spectrum of **48** has been assigned to the CO ligand (free carbon monoxide has a C-O stretch at 2143 cm^{-1}), indicating a considerable amount of back bonding from the metal to the carbon monoxide ligand.

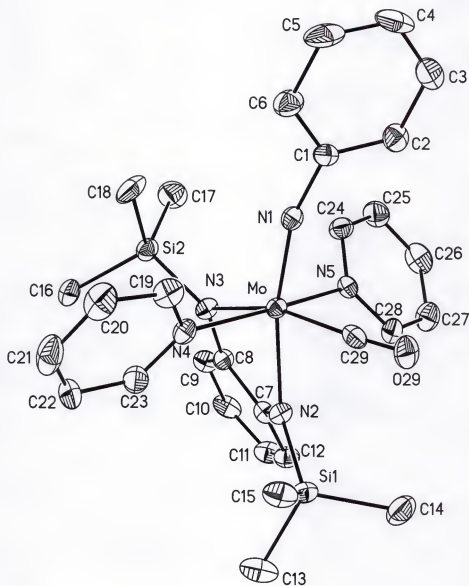


Figure 2-13. Thermal ellipsoid plot of **48** (50% probability thermal ellipsoids). Selected bond lengths (Å) and angles (°): Mo-N(1) 1.778(3), Mo-N(2) 2.128(3), Mo-N(3) 2.136(3), Mo-N(4) 2.207(3), Mo-N(5) 2.217(3), Mo-C(29) 1.993(5), C(29)-O(29) 1.158(5), O(29)-C(29)-Mo 175.2(4), N(4)-Mo-N(5) 169.52(12), N(2)-Mo-N(3) 78.10(13), C(1)-N(1)-Mo 162.5(3).

C-N Activation of an Amido Ligand: Synthesis of Imido-Bridged **49** from **47**

Monomeric **47** is stable at 20°C in the solid-state for extended periods. However, when heated to 80°C in toluene, **47** converted cleanly to bimetallic **49** with loss of pyridine in 2 h (Figure 2-14).⁵¹ This air sensitive, diamagnetic complex is thermally stable in solution for extended periods, even at the temperature required for synthesis. A single crystal of **49** was grown from a pentane/dichloromethane solution at -30°C. Compound **49** crystallizes with two molecules of dichloromethane. An X-ray diffraction study shows that **49** contains two molybdenum atoms bridged by two phenyl imido groups as well as a $\text{Me}_3\text{SiN-C}_6\text{H}_4$ ligand (Figure 2-15). This unusual $\text{Me}_3\text{SiN-C}_6\text{H}_4$ group is apparently formed by cleavage of one NSiMe_3 group from an $o\text{-(Me}_3\text{SiN)}_2\text{C}_6\text{H}_4$ ligand. The NSiMe_3 group that was cleaved remains as an additional terminal imido ligand on one of the molybdenum atoms. The formal oxidation state at each metal center is best described as Mo(V). The Mo(1)-Mo(2) distance of 2.5669(4) Å, although short for a Mo-Mo single bond, indicates the existence of a metal-metal bond and accounts for the observed diamagnetism of **49**.^{56,57} Four upfield resonances, assigned to the four inequivalent Me_3Si groups, are observed in the ^1H NMR spectrum of **49**, consistent with the structure as determined by X-ray crystallography. The crystal data and details of the structure refinement for **49** are summarized in Table 2-2.

The unusual aromatic C-N bond cleavage reaction that is observed during the pyrolysis of **47** is presumably driven by the formation of the Mo-N triple bond and demonstrates the reactivity of the Mo(IV) moiety towards oxidation. Reactions providing a straightforward example of C-N single-bond activation, a most desirable transformation, are rare.⁵⁸ The metal-mediated rupture of C-N bonds is, for the most part, limited to strained amines⁵⁹ or amidines.⁶⁰ Activation of nonactivated substrates such as

aniline⁶¹ and the ring opening of pyridine⁶² have been observed with highly reactive, trivalent, Group 5 metal complexes. A slight variation on this theme involves the recently reported C-N bond cleavage reactivity of a Nb(II) cluster upon ligand replacement by anionic amides.⁶³ An observation related to this reaction type, made in 1985 by Chisholm,⁶⁴ involved the isolation of a carbide/imide cluster that may have arisen *via* degradation of an amido ligand.

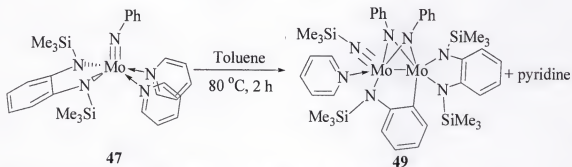


Figure 2-14. C-N activation of the $o\text{-(Me}_3\text{SiN)}_2\text{C}_6\text{H}_4$ ligand in **47**

Generation of Imido-Diamido P(OMe)_3 Adducts

Synthesis and Characterization of $[\text{Mo(NPh)(P(OMe)}_3)_3(o\text{-(Me}_3\text{SiN)}_2\text{C}_6\text{H}_4)]$ (**50**)

From a pentane solution of olefin complex **37** or **38** treated with 4.0 equiv of P(OMe)_3 precipitated a red-brown powder of $[\text{Mo(NPh)(P(OMe)}_3)_3(o\text{-(Me}_3\text{SiN)}_2\text{C}_6\text{H}_4)]$ (**50**), which was isolated in high yield (Figure 2-16). A single crystal X-ray study was carried out on a suitable crystal of **50** grown from a toluene/pentane solution at low temperature. The crystal data and details of the structure refinement are summarized in Table 2-2. In the thermal ellipsoid plot of **50**, the geometry about molybdenum is best described as a distorted octahedron, and the olefin from the starting material has been displaced by three trimethyl phosphite ligands (Figure 2-17). The phosphite ligands take up a meridional bonding motif, and the Mo-P(1), Mo-P(2), and Mo-P(3) bond lengths of 2.5090(8) Å, 2.4509(8) Å, and 2.4972 Å, respectively, are as expected for a complex of

this nature. The molybdenum imido interaction is consistent with a metal-nitrogen triple bond.

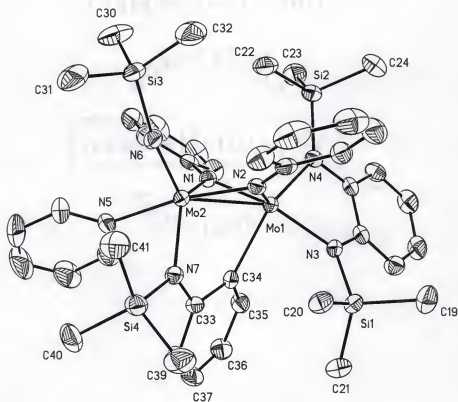


Figure 2-15. Thermal ellipsoid plot of **49** (50% probability thermal ellipsoids). The solvating dichloromethane molecules have been omitted for clarity. Selected bond lengths (Å) and angles (°): Mo(1)-Mo(2) 2.5669(4), Mo(1)-C(34) 2.179(3), Mo(2)-N(7) 2.047(2), Mo(2)-N(6) 1.745(2), Mo(2)-N(5) 2.285(3), Mo(1)-N(1) 1.955(2), Mo(1)-N(2) 1.866(2), Mo(2)-N(1) 2.007(2), Mo(2)-N(2) 2.061(2), Mo(1)-N(1)-Mo(2) 80.74(9), Mo(1)-N(2)-Mo(2) 81.48(9), Mo(2)-N(6)-Si(3) 170.50(17).

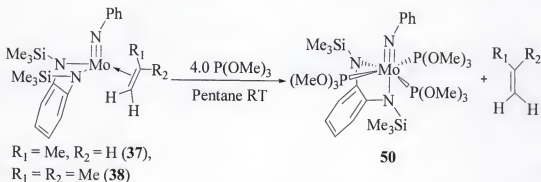


Figure 2-16. Synthesis of $[\text{Mo}(\text{NPh})(\text{P}(\text{OMe})_3)_3(o\text{-(Me}_3\text{SiN)}_2\text{C}_6\text{H}_4)]$ (**50**)

Although the SiMe_3 groups of **50** are inequivalent in the solid-state, only one SiMe_3 resonance is observed for these protons in the ^1H NMR spectrum from 20°C (0.62 ppm, C_7D_8) to -70°C . A high degree of fluxionality in solution, most likely involving phosphite dissociation and exchange, could be responsible for the formation of a five-coordinate complex where the SiMe_3 groups are equivalent, accounting for this observation. In the (bis)pyridine complex (**47**), steric interactions hinder the rotation of the pyridine ligands about the Mo-N bonds. The steric interactions in **50** should help encourage phosphite exchange and, in this way, generate a coordinatively unsaturated metal center. Steric interactions such as this one will become a recurring theme throughout this chapter.

The phosphite complex is rather unstable and begins to decompose in solution at 20°C within hours. Compound **50** even decomposes in the solid-state at -30°C over months. The decomposition product was isolated as an air and thermally sensitive, black, toluene-insoluble powder. The thermal sensitivity and the insolubility of this compound have made it very difficult to characterize. We have hypothesized that this compound may be an oligomeric species with the formula $[\text{Mo}(\text{NPh})(\text{o}-(\text{Me}_3\text{SiN})_2\text{C}_6\text{H}_4)]_x$, but have no solid evidence with which to substantiate this claim other than a ^1H NMR spectrum.⁴⁶ This unknown material will be henceforth referred to as **X**.

Synthesis and Characterization of $[\text{Mo}(\text{NPh})(\text{P}(\text{OMe})_3)_2\text{CO}(\text{o}-(\text{Me}_3\text{SiN})_2\text{C}_6\text{H}_4)]$ (**51**)

When freshly generated **50** was dissolved in a minimum amount of toluene and treated with CO gas (ca. 15 psi), $[\text{Mo}(\text{NPh})(\text{P}(\text{OMe})_3)_2\text{CO}(\text{o}-(\text{Me}_3\text{SiN})_2\text{C}_6\text{H}_4)]$ (**51**) formed and was isolated in excellent yield. Single crystals of **51** were grown from a toluene solution, and an X-ray study was carried out on a suitable crystal. The crystal data and details of the structure refinement are summarized in Table 2-2. The thermal

ellipsoid plot of **51** is shown in Figure 2-18. The overall geometry around the metal is distorted octahedral, and the structure type is similar to that of **48**. In this instance, the phosphite ligands are mutually *trans*, presumably for the same reasons discussed for the pyridine ligands in **48**.

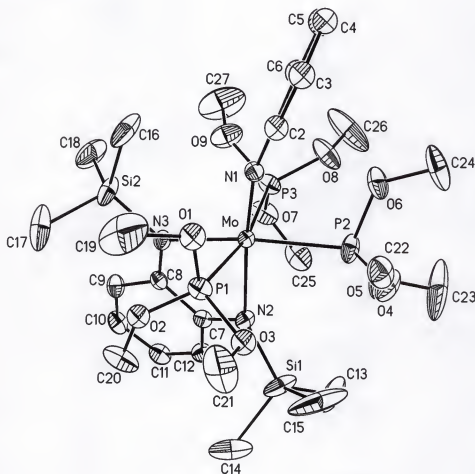


Figure 2-17. Thermal ellipsoid plot of **50** (50% probability thermal ellipsoids). Selected bond lengths (Å) and angles (°): Mo-N(1) 1.771(2), Mo-N(2) 2.161(2), Mo-N(3) 2.190(2), Mo-P(1) 2.5090(8), Mo-P(2) 2.4509(8), Mo-P(3) 2.4972(8), N(1)-Mo-N(2) 174.40, C(1)-N(1)-Mo 163.2(3), N(3)-Mo-P(2) 165.99(6), P(3)-Mo-P(1) 168.10(3).

The ^1H and ^{13}C NMR spectra of **51** are highly fluxional at 20°C (C_7D_8). In the ^1H NMR spectrum at 20°C, a single resonance is observed for the SiMe_3 groups at 0.66 ppm along with a doublet resonance at 3.09 ppm ($^3J_{\text{P-H}} = 6.5$ Hz) for the P(OMe)_3 ligands. At

low temperature (-50°C , C_7D_8), two resonances are observed for the SiMe_3 groups at 0.66 ppm and 0.75 ppm in the ^1H NMR spectrum. Phosphite dissociation from **51** at 20°C could produce a five-coordinate species with equivalent SiMe_3 groups, accounting for this behavior.

The coalescence of the SiMe_3 peaks in the ^1H NMR spectrum takes place at 5°C . The activation energy for this process can be calculated using the simple two-site exchange equation shown in Equation 2-1, where N is Avogadro's number, T_c is the temperature of coalescence, and $\delta\nu$ is the maximum chemical shift difference between the two resonances in question.⁶⁵ Using Equation 2-1 a value of 58.73 KJ/mol (14.04 Kcal/mol) is calculated for this process, where $\delta\nu = 24$ Hz.

$$\Delta G^\ddagger / RT_c = \ln (\sqrt{2} (R / \pi N h)) + \ln (T_c / \delta\nu) \quad \text{Equation 2-1}$$

A peak at 1959 cm^{-1} corresponding to the carbonyl ligand stretch was observed in the IR spectrum of **51**. The carbonyl stretching frequency for **51** is 46 cm^{-1} higher than that for **48**, implying a stronger CO bond in **51**. This is not surprising as the phosphite ligands are weaker Lewis bases than pyridine, and **51** will therefore have less electron density at the metal center available for back bonding to the carbonyl ligand.

Generation of Imido-Diamido PMe_3 Adducts

Synthesis and Characterization of $[\text{Mo}(\text{NPh})(\text{PMe}_3)_3(o\text{-(Me}_3\text{SiN)}_2\text{C}_6\text{H}_4)]$ (**52**)

The $[\text{Mo}(\text{NPh})(\text{PMe}_3)_3(o\text{-(Me}_3\text{SiN)}_2\text{C}_6\text{H}_4)]$ (**52**) complex was synthesized by Dr. Carlos Ortiz, a previous graduate student, through a route identical to that used in the preparation of **50**.⁶⁶ The results of the X-ray crystal structure study on this complex are included here, as they are relevant to structural discussions in this chapter. The thermal ellipsoid plot of **52** is shown in Figure 2-19 along with selected bond lengths and angles.

The overall geometry is distorted octahedral and similar to that of **50**. The bond lengths and angles associated with the phenyl imido group are as expected for a metal-imido triple-bond interaction (Mo-N(1) 1.7851(14) Å, C(1)-N(1)-Mo 169.77(13)°). The rest of the bond lengths are unexceptional in that they all fall within the expected range. There is, however, a significant difference of approximately 0.1 Å between the Mo-N(2) and Mo-N(3) bond lengths, 2.2325(14) Å and 2.1408(14) Å respectively, in this complex. Elongation of Mo-N(2) has been attributed to a filled-filled interaction between a nitrogen (N(2) in **52**) *p* orbital and a metal *d* orbital of appropriate symmetry. This filled-filled interaction is presumably alleviated in **48** due to the π -accepting carbonyl ligand, and the corresponding molybdenum nitrogen amide bond lengths in **48** differ by approximately 0.01 Å. However, such arguments should be made with caution as steric effects may also have an impact on bond length. Consider, for example, complex **53** an analogue to **52** where a SiMe₃ group has been replaced with a proton (Figure 2-20). In **53** the Mo-N(3) bond length (2.0873(16)Å) is 0.05 Å shorter than the corresponding length in **52** (2.1408(14)Å), presumably due to loss of steric clout upon replacing SiMe₃ with H. The origin of complex **53** will be discussed in-depth in Chapter 3. The X-ray crystal study of **53** was first reported by Dr. Carlos Ortiz. It is included here for the purposes of this discussion.⁶⁶

Synthesis and Characterization of [Mo(NPh)(PMe₃)₂CO(*o*-(Me₃SiN)₂C₆H₄)] (**54**)

Exposure of a toluene solution of **52** to dry carbon monoxide gas (ca. 15 psi) resulted in the formation of the six-coordinate complex [(Mo(NPh)(PMe₃)₂(CO) (*o*-(Me₃SiN)₂C₆H₄)] (**54**) (Figure 2-21). The structure of **54** has been assigned by ¹H,

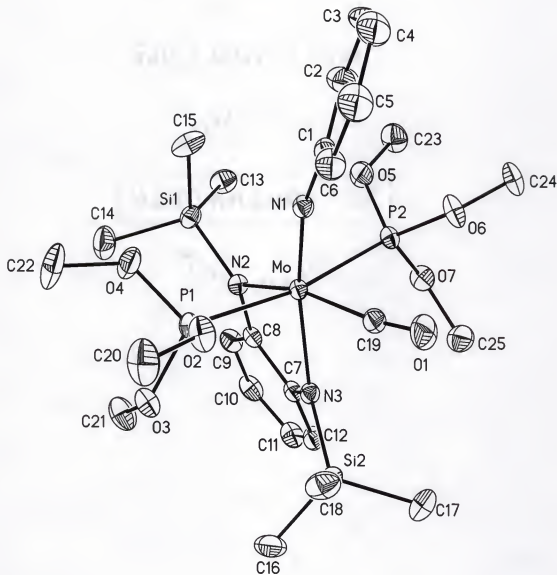


Figure 2-18. Thermal ellipsoid plot of **51** (50% probability thermal ellipsoids). Selected bond lengths (Å) and angles (°): Mo-N(1) 1.7882(13), Mo-N(2) 2.1566(12), Mo-N(3) 2.1242(13), Mo-C(19) 2.0112(16), Mo-P(1) 2.5291(4), Mo-P(2) 2.4784(4), O(1)-C(19) 1.145(2), N(1)-Mo-N(3) 166.33(5), N(2)-Mo-C(19) 162.00(6), P(1)-Mo-P(2) 170.451(15), C(1)-N(1)-Mo 161.78(12).

Table 2-2. X-ray data^a for crystal structures 49, 50, and 51

	49	50	51
Chemical formula	C ₄₁ H ₅₉ N ₇ Mo ₂ Si ₄ ·2CH ₂ Cl ₂	C ₂₇ H ₅₄ N ₃ MoO ₉ P ₃ Si ₂	C ₂₅ H ₄₅ N ₃ MoO ₇ P ₂ Si ₂
Formula weight	1124.04	809.76	713.70
Crystal system	Monoclinic	Triclinic	Monoclinic
Space group	<i>P</i> 2 ₁ / <i>n</i>	<i>P</i> $\bar{1}$	<i>P</i> 2 ₁ / <i>c</i>
$\mu(\text{Mo-K}\alpha)$ (mm ⁻¹)	0.805	0.578	0.581
<i>a</i> (Å)	14.4655(8)	10.1800(5)	17.2665(6)
<i>b</i> (Å)	23.572(1)	10.4700(5)	11.3438(4)
<i>c</i> (Å)	15.9891(9)	18.6036(9)	18.3306(7)
α (°)	-	91.681(2)	-
β (°)	104.390(1)	92.692(2)	104.640(2)
γ (°)	-	104.317(2)	-
<i>V_c</i> (Å ³)	5280.8(5)	1917.4(2)	3473.8(2)
<i>Z</i>	4	2	4
Θ_{max} °	27.50	27.50	27.50
Total reflections	37951	17160	30213
Uniq. reflections	12085	8561	7876
<i>R</i> (int)	0.0512	0.0298	0.0328
<i>R</i> ₁ [<i>I</i> ≥ 2σ(<i>I</i>) data] ^b	0.0384	0.0416	0.0222
w <i>R</i> ₂ (all data) ^c	0.0930	0.1021	0.0641
Larg. diff. peak, hole	0.807, -0.694	1.063, -0.864	0.326, -0.360

^aObtained with monochromatic Mo K α radiation ($\lambda = 0.71073$ Å) at 173 K. ^b $R_1 = \sum |F_o| - |F_c| / \sum |F_o|$. ^c $wR_2 = \{\sum [w(F_o^2 - F_c^2)^2] / \sum [w(F_o^2)^2]\}^{1/2}$.

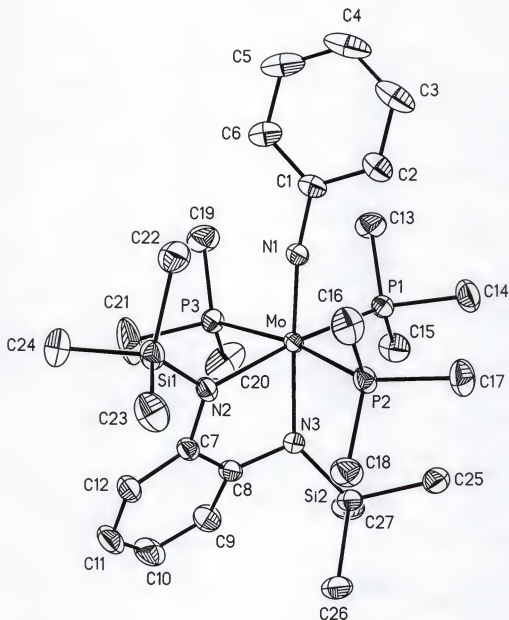


Figure 2-19. Thermal ellipsoid plot of **52** (50% probability thermal ellipsoids). Selected bond lengths (Å) and angles (°): Mo-N(1) 1.7851(14), Mo-N(2) 2.2325(14), Mo-N(3) 2.1408(14), Mo-P(1) 2.5280(5), Mo-P(2) 2.5461(5), Mo-P(3) 2.5534(5), C(1)-N(1)-Mo 169.77(13), N(1)-Mo-N(3) 176.91(6), P(3)-Mo-P(2) 169.383(16), N(2)-Mo-P(1) 171.381(4).

^{13}C , and ^{31}P NMR spectroscopy and is consistent with that shown in Figure 2-21. At 20°C two resonances are observed for the inequivalent SiMe_3 groups at 0.51 ppm and 0.60 ppm in the ^1H NMR spectrum. One broad resonance at -15.2 ppm is observed for the equivalent phosphines in the $^{31}\text{P}\{^1\text{H}\}$ spectrum of **54** at 20°C and the carbonyl carbon resonates at 260.2 ppm in the ^{13}C NMR spectrum at that temperature. The carbonyl stretch in the IR spectrum of **54** is observed at 1925 cm^{-1} . The electron density at the metal center, determined primarily by the PMe_3 ligands, is thus somewhere between that in **47** and **51**.

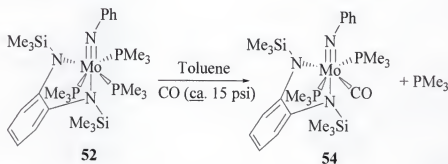


Figure 2-21. Synthesis of $[(\text{Mo}(\text{NPh})(\text{PMe}_3)_2(\text{CO})(o\text{-(Me}_3\text{SiN)}_2\text{C}_6\text{H}_4)]$ (**54**)

Generation of Imido-Diamido PMe_2Ph Adducts

Synthesis and Characterization of $[\text{Mo}(\text{NPh})(\text{PMe}_2\text{Ph})_2(o\text{-(Me}_3\text{SiN)}_2\text{C}_6\text{H}_4)]$ (**55**)

The olefin fragment in complexes **37** and **38** was displaced with 2.0 equiv of PMe_2Ph . The product in this instance was the bis(phosphine) complex $[\text{Mo}(\text{NPh})(\text{PMe}_2\text{Ph})_2(o\text{-(Me}_3\text{SiN)}_2\text{C}_6\text{H}_4)]$ (**55**) that precipitated from solution as a green solid, and was isolated by filtration (Figure 2-22). Single crystals of **55** were grown from a concentrated toluene solution at low temperature. An X-ray study was carried out on a suitable crystal, and the thermal ellipsoid plot of **55** is shown in Figure 2-23. The relevant details of the structure refinement are summarized in Table 2-3.

The geometry about the molybdenum in **55** is best described as distorted square pyramidal. The atoms N(2), N(3), P(2) and N(1) make up the base of the square pyramid, as defined by the two biggest metal-centered angles in the molecule, N(1)-Mo(1)-N(3) 151.03(8)° and N(2)-Mo(1)-P(2) 164.67(5)°. The remaining P(1) occupies the apical position.

The formulation of the molecule as a bis(phosphine) complex is also supported by integration of the SiMe_3 and PMe_2Ph resonances in the ^1H NMR spectrum of **55**. The structure of complex **55** is fluxional in solution, and one resonance is observed for both SiMe_3 groups at 0.45 ppm along with one resonance for the two PMe_2Ph ligands at 0.94 ppm (br) in the ^1H NMR spectrum (-65°C, C_7H_8).

When **55** was generated by treatment of an olefin complex with 2.0 equiv PMe_2Ph , **X** was simultaneously formed in small amounts. Using 4.0 equiv PMe_2Ph helped discourage, but did not completely eliminate the formation of **X**. Complex **55** was, however, stable when stored for months at -30°C under an inert atmosphere.

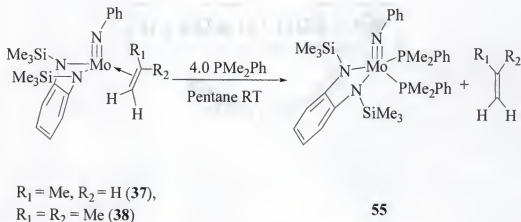


Figure 2-22. Synthesis of $[\text{Mo}(\text{NPh})(\text{PMe}_2\text{Ph})_2(o\text{-(Me}_3\text{SiN)}_2\text{C}_6\text{H}_4)]$ (**55**)

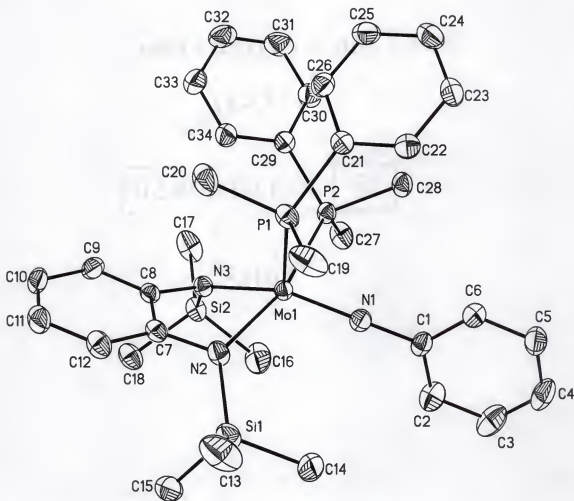


Figure 2-23. Thermal ellipsoid plot of **55** (50% probability thermal ellipsoids). Selected bond lengths (Å) and angles (°): Mo(1)-N(1) 1.768(2), Mo(1)-P(1) 2.3968(6), Mo(1)-P(2) 2.5113(6), Mo(1)-N(2) 2.174(2), Mo(1)-N(3) 2.073(2), N(1)-Mo(1)-N(3) 151.03(8), N(1)-Mo(1)-N(2) 107.33(8), N(3)-Mo(1)-P(1) 114.38(5), N(2)-Mo(1)-P(2) 164.67(5), C(1)-N(1)-Mo(1) 168.89(17), N(3)-Mo(1)-N(2) 77.15(7), N(1)-Mo(1)-P(1) 94.55(6), N(2)-Mo(1)-P(1) 86.60(5), N(1)-Mo(1)-P(2) 87.73(6), N(3)-Mo(1)-P(2) 88.30(5), P(1)-Mo(1)-P(2) 95.20(2). Complex **55** crystallized with two molecules in the asymmetric unit and only one is shown here.

Synthesis and Characterization of $[\text{Mo}(\text{NPh})(\text{PMe}_2\text{Ph})_2\text{CO}(o\text{-(Me}_3\text{SiN)}_2\text{C}_6\text{H}_4)]$ (**56**)

When the coordinatively unsaturated **55** reacted with CO gas (ca. 15 psi), the carbonyl adduct $[\text{Mo}(\text{NPh})(\text{PMe}_2\text{Ph})_2\text{CO}(o\text{-(Me}_3\text{SiN)}_2\text{C}_6\text{H}_4)]$ (**56**) formed and was isolated as a red/purple solid (Figure 2-24). Two resonances are observed for the

inequivalent SiMe_3 groups in the ^1H NMR spectrum of **56** at 0.19 ppm and 0.55 ppm (C_6D_6 , 20°C). Only one resonance is observed for the four PMe_2Ph ligand methyl groups at 1.20 ppm in the ^1H NMR spectrum (C_6D_6 , 20°C). A very broad resonance is observed in the ^{31}P NMR spectrum at -7.0 ppm for the PMe_2Ph phosphorus group. Based on these observations, a phosphine exchange pathway at 20°C can account for the equivalent PMe_2Ph methyl groups. A carbonyl stretching frequency of 1921 cm^{-1} is observed in the IR spectrum of **56**. This frequency is slightly lower than that of complex **54** (1925 cm^{-1}), and is surprising in that PMe_2Ph is slightly more electron withdrawing than PMe_3 . We would therefore expect the stretching frequency for **56** to be higher than that for **54**.

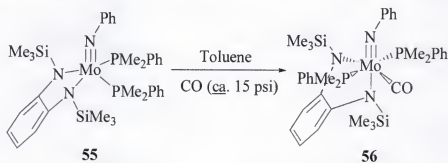


Figure 2-24. Synthesis of $[\text{Mo}(\text{NPh})(\text{PMe}_2\text{Ph})_2\text{CO}(o\text{-(Me}_3\text{SiN)}_2\text{C}_6\text{H}_4)]$ (**56**)

Synthesis and Characterization of $[\text{Mo}(\text{NPh})(\text{DMPE})(o\text{-(Me}_3\text{SiN)}_2\text{C}_6\text{H}_4)\text{-}\mu\text{-(DMPE)Mo}(\text{NPh})(\text{DMPE})(o\text{-(Me}_3\text{SiN)}_2\text{C}_6\text{H}_4)]$ (57**)**

When a pentane solution of olefin complex **37** or **38** was treated with 3.0 equiv of DMPE (1,2-bis(dimethylphosphino)ethane), dimeric $[\text{Mo}(\text{NPh})(\text{DMPE})(o\text{-(Me}_3\text{SiN)}_2\text{C}_6\text{H}_4)\text{-}\mu\text{-(DMPE)Mo}(\text{NPh})(\text{DMPE})(o\text{-(Me}_3\text{SiN)}_2\text{C}_6\text{H}_4)]$ (**57**) precipitated from solution as a red powder and was isolated by filtration (Figure 2-25). The dimeric nature of **57** was confirmed by a single crystal X-ray study. The thermal ellipsoid plot **57** is shown in Figure 2-26 with selected bond lengths and angles. The details of the structure refinement are summarized in Table 2-3. The metal-centers Mo and MoA are

related by an inversion center. The geometry at Mo in **57** is best described as distorted octahedral and is very similar to that in **50** and **52**. The phosphorus atoms are coordinated to the Mo center in a meridional array, also similar to what is observed for complexes **50** and **52**. The smallest metal-centered angles are the P(2)-Mo-P(1) and N(2)-Mo-N(3) angles of 78.170(15)° and 77.67(5)°, respectively. The acuteness of these angles can be attributed to the chelating nature of the ligands. All other bond lengths and angles are unexceptional.

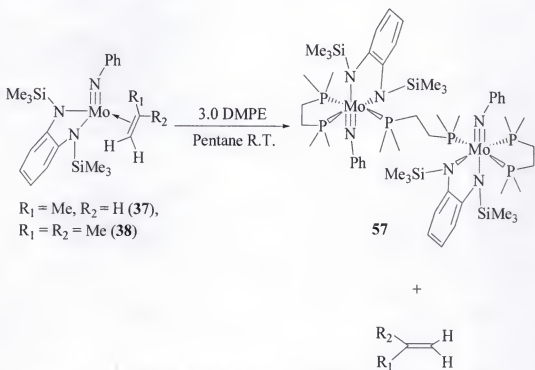


Figure 2-25. Synthesis of $[\text{Mo}(\text{NPh})(\text{DMPE})(o\text{-(Me}_3\text{SiN)}_2\text{C}_6\text{H}_4)\text{-}\mu\text{-(DMPE)}\text{Mo}(\text{NPh})(\text{DMPE})(o\text{-(Me}_3\text{SiN)}_2\text{C}_6\text{H}_4)]$ (**57**)

Complex **57** reacts with carbon monoxide gas giving a mixture of products by ^1H NMR spectroscopy. A CO stretch appears at 1927 cm^{-1} in the IR spectrum of the crude reaction product. This confirms the presence of a metal carbonyl, however the exact nature of the coordination environment about the metal-center is not known at this time.

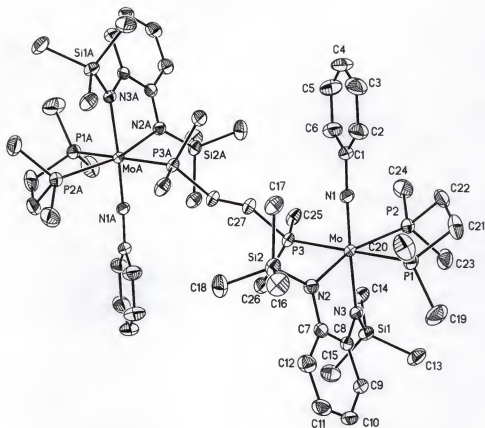


Figure 2-26. Thermal ellipsoid plot of **57** (50% probability thermal ellipsoids). Selected bond lengths (Å) and angles (°): Mo-N(1) 1.7914(12), Mo-P(1) 2.4890(4), Mo-P(2), 2.4887(4), Mo-P(3) 2.5710(4), Mo-N(2) 2.2061(12), Mo-N(3) 2.1422(12), C(1)-N(1)-Mo 171.89(12), N(1)-Mo-N(3) 174.94(5), P(2)-Mo-P(1) 78.170(15), N(2)-Mo-N(3) 77.67(5), P(2)-Mo-N(2) 162.68(3), P(1)-Mo-P(3) 175.229(14). All atoms labeled A are symmetry related to non A labeled atoms by a center of inversion.

Generation of an Imido-Diamido Arduengo Carbene (Imidazol-2-Ylidene) Adduct

Stable and isolable imidazol-2-ylidenes were first discovered by Arduengo in 1991.⁶⁷ These carbenes display an uncanny ability to coordinate to transition metals through σ -donation from the carbene to the metal, and back bonding to the carbene is negligible. Transition metals modified with imidazol-2-ylidene ligands have recently found widespread use in catalytic transformations such as the Heck coupling reaction, hydrogenation and hydroformylation of olefins, hydrosilation, olefin metathesis, copolymerization of ethylene and CO, and polymerization of alkynes. Some recent

reviews have thoroughly treated this subject matter.^{68,69,70} Our molybdenum imido-diamido fragment can stabilize Schrock-type carbene complex **33**. We were interested in exploring the structure of an imidazol-2-ylidene derivative of our imido-diamido system. To this day only carbene complexes of low-valent molybdenum in octahedral geometries have been described in the literature.^{68,71} We have been able to synthesize a complex of this type, and the synthesis and initial structural studies will be discussed here. This is both the first instance of a molybdenum imidazol-2-ylidene complex with a tetrahedral-like structure and the first instance of a molybdenum (IV) imidazol-2-ylidene complex.

When a benzene solution of **55** was treated with 1.0 equiv of imidazol-2-ylidene **58** (IMes) [Mo(NPh)IMes(*o*-(Me₃SiN)₂C₆H₄)] (**59**) formed in high yield as determined by ¹H NMR spectroscopy (Figure 2-27). Although complex **59** was also generated by treatment of **52** with **58** the crude reaction product was not as pure as when **55** was used as the starting material. Single crystals of **59** grew from C₆D₆ NMR samples generated by treatment of **52** and **55** with **58**, and a single crystal X-ray study was carried out on an appropriate crystal. The thermal ellipsoid plot of **59** and selected bond lengths and angles are presented in Figure 2-28. The details of the structure refinement are summarized in Table 2-3.

One interesting feature of **59** is the lack of phosphine coordination. The IMes ligand is a strong σ -donor and bulky enough to displace and inhibit phosphine coordination. The geometry at the metal-center is best described as distorted tetrahedral. The largest deviation from the ideal tetrahedral angle of 109.5° involves the metal centered angle N(2)-Mo(1)-N(3) of 78.77(10)°. The chelating nature of the diamido

ligand is responsible for the acuteness of this angle. The C(1)-N(1)-Mo(1) angle of $161.6(2)^\circ$ and the N(1)-Mo(1) bond length of $1.740(3) \text{ \AA}$ agree well with a metal-nitrogen triple-bond interaction. The metal carbene (Mo(1)-C(19)) bond length of $2.178(3) \text{ \AA}$ in **59** is approximately 0.10 \AA shorter than in octahedral molybdenum (0) analogues and is similar to that of Fisher carbene $(\text{CO})_5\text{Mo}=\text{C}(\text{OR})\text{SiPh}_3$ ($2.15(2) \text{ \AA}$).⁷² While the metal to carbene bond lengths of **59** and $(\text{CO})_5\text{Mo}=\text{C}(\text{OR})\text{SiPh}_3$ are similar, we believe that the short molybdenum to carbene length in **59** is a result of the high oxidation state and the distorted tetrahedral geometry and not a result of substantial back bonding.

Complex **59** is paramagnetic as revealed by ^1H NMR spectroscopy. All protons in **59** are represented by broad singlets *via* ^1H NMR spectroscopy, and the number of peaks and relative integration are consistent with the structure of **59** reported here. The tentative assignment of the ^1H NMR spectrum is included in the experimental section.

We attribute the paramagnetic nature of **59** to a very small energy difference between the two lowest energy *d* orbitals, allowing for thermal population of both orbitals at 20°C giving a paramagnetic complex. Magnetic susceptibility measurements will shed some light on this situation.

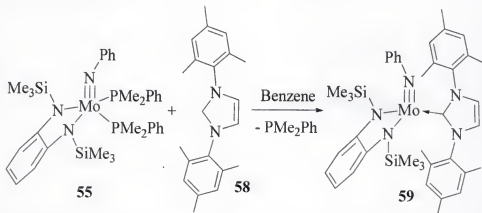


Figure 2-27. Synthesis of $[\text{Mo}(\text{NPh})\text{IMes}(o\text{-(Me}_3\text{SiN)}_2\text{C}_6\text{H}_4)]$ (**59**)

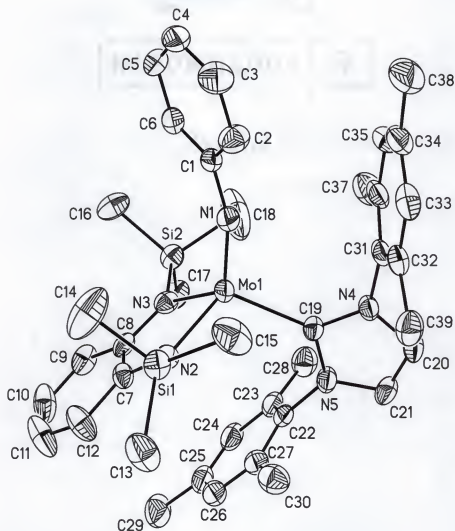


Figure 2-28. Thermal ellipsoid plot of **59** (50% probability thermal ellipsoids). Selected bond lengths (Å) and angles (°): Mo(1)-C(19) 2.178(3), Mo(1)-N(1) 1.740(3), Mo(1)-N(2) 2.074(2), Mo(1)-N(3) 2.031(3), C(19)-N(4) 1.371(4), C(19)-N(5) 1.369(4), C(20)-C(21) 1.334(4), N(1)-Mo(1)-N(3) 119.45(11), N(1)-Mo(1)-N(2) 116.41(11), N(2)-Mo(1)-N(3) 78.77(10), N(1)-Mo(1)-C(19) 107.31(11), N(3)-Mo(1)-C(19) 123.51(11), N(2)-Mo(1)-C(19) 108.02(11). Complex **59** crystallized with two molecules in the asymmetric unit and only one is shown here.

Table 2-3. X-ray data^a for crystal structures **55**, **57**, and **59**

	55	57	59
Chemical formula	C ₃₄ H ₄₉ N ₃ MoP ₂ Si ₂	C ₅₄ H ₁₀₂ N ₆ Mo ₂ P ₆ Si ₄	C ₃₉ H ₄₈ N ₅ MoSi ₂
Formula weight	713.82	1325.48	738.94
Crystal system	Monoclinic	Monoclinic	Orthorhombic
Space group	<i>P</i> 2 ₁ / <i>n</i>	<i>P</i> 2 ₁ / <i>n</i>	<i>Pbca</i>
$\mu(\text{Mo-K}\alpha)$ (mm ⁻¹)	0.539	0.626	0.433
<i>a</i> (Å)	26.355(2)	10.9359(4)	18.3689(8)
<i>b</i> (Å)	10.3180(7)	16.6758(7)	21.069(2)
<i>c</i> (Å)	27.297(2)	18.8773(8)	40.047(2)
β (°)	100.475(2)	102.930(2)	-
<i>V_c</i> (Å ³)	7299.4(9)	3355.3(2)	15499(2)
<i>Z</i>	8	2	16
Θ_{max} °	27.50	27.50	27.03
Total reflections	63955	29611	110986
Uniq. reflections	16703	7668	15985
<i>R</i> (int)	0.0447	0.0317	0.0812
<i>R</i> ₁ [<i>I</i> ≥ 2σ(<i>I</i>) data] ^b	0.0312	0.0210	0.0425
w <i>R</i> ₂ (all data) ^c	0.0756	0.0542	0.1016
Larg. diff. peak, hole	0.387, -0.407	0.323, -0.412	0.963, -0.935

^aObtained with monochromatic Mo K α radiation ($\lambda = 0.71073$ Å) at 173 K. ^b $R_1 = \sum |F_o| - |F_c| / \sum |F_o|$. ^c $wR_2 = \{\sum [w(F_o^2 - F_c^2)^2] / \sum [w(F_o^2)^2]\}^{1/2}$.

Summary

The isolation of molybdenum imido-diamido adducts of pyridine, PMe₃, PMe₂Ph, P(OMe₃)₃, DMPE, and IMes have been discussed. Through the study of these compounds a general theme involving steric crowding at the metal center was mentioned as was that concerning π -loading.

The DFT study on complex **19** revealed the nature of the diamido ligand folding in this d^0 system. In contrast, DFT studies showed that the absence of ligand folding in complex **47** was due to a lack of empty d metal orbitals available for bonding. An interesting effect of this lack of folding is the hindered rotation of the pyridine rings. Complex **47** is also unique when compared to the tris complexes **50**, **52**, **53**, and **57**. From a steric stand-point, we have no concrete explanation as to why bis and not tris coordination of pyridine is preferred.

The structures of complexes **50**, **52**, **53**, and **57** are very similar. All phosphorus-based ligands bind to molybdenum in a meridional fashion, and the coordination sphere of each is best described as distorted octahedral. Complex **57** stands out in this group, for the two metal centers in the dimer are linked by a DMPE moiety.

Complexes **55** and **59** highlight the steric interactions in this system. The PMe_2Ph ligand used in the preparation of **55** has a larger cone angle⁷³ (cone angle (θ°) PMe_2Ph = 122) than the phosphine or phosphites used in the preparations of **50**, **52**, **53**, and **57** (θ° PMe_3 = 118, θ° $\text{P}(\text{OMe})_3$ = 107, θ° DMPE = 107). This larger cone angle accounts for the bis coordination of PMe_2Ph in **55**. Sterically, the IMes ligand in complex **59** is often compared with $\text{P}(\text{Cy})_3$ (Cy = cyclohexyl, θ° $\text{P}(\text{Cy})_3$ = 170). The large steric cloud of IMes is responsible for the displacement of all phosphines from the starting material in the preparation of **59**.

Initial reactivity of complexes **47**, **50**, **52**, and **55** with carbon monoxide gas was outlined, and a summary of these complexes and appropriate CO stretching frequencies are included in Figure 2-29. The next chapter discusses the reactivity of these adducts

with dihydrogen gas. Hopefully, the complexes discussed in this chapter will find uses in other bond activation reactions in the near future.

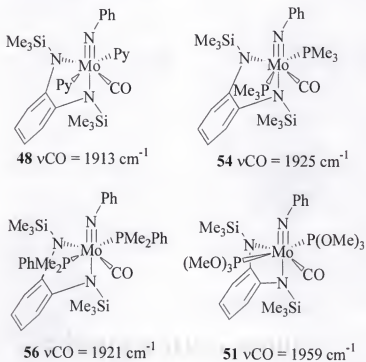


Figure 2-29. Carbon monoxide complexes and ν_{CO} (cm^{-1})

CHAPTER 3

SYNTHESIS AND REACTIVITY OF A MOLYBDENUM IMIDO-DIAMIDO STRETCHED DIHYDROGEN COMPLEX

The first literature report to describe the isolation of a dihydrogen complex (referred to as $\eta^2\text{-H}_2$ or H_2 complexes) was put forth by Gregory J. Kubas in 1984.⁷⁴ Since this date, over 350 stable H_2 complexes have been synthesized and characterized, and roughly 100 additional reported examples are either thermally unstable, transient species, or are proposed to contain H_2 ligands. Dihydrogen complexes of every metal from vanadium to platinum have been reported, and an example of a europium complex is known. Most complexes are coordinatively saturated and are cationic in nature. Several review articles have been written on the subject over the years.^{75,76,77,78,79,80,81} The most recent treatment of this area has taken the form of an excellent book written by Kubas.⁸²

Dihydrogen complexes are important species in metal-mediated catalysis, as they represent "arrested" states along the path to dihydrogen bond-breaking or oxidative addition of the dihydrogen molecule. Metal-bound dihydrogen also displays unique chemical and physical properties, can be electrophilic or superacidic, and may exist in a stretched or an unstretched mode.⁷⁵⁻⁸¹ The unique properties displayed by dihydrogen upon binding to a metal center are a result of the metal-hydrogen bonding interaction.

Bonding in H_2 complexes involves σ -donation from the H-H σ -bond to the metal and back bonding of electron density from a filled metal d orbital to the H-H σ^* orbital (Figure 3-1). The back bonding interaction is primarily responsible for elongating the

H-H bond in an H_2 complex. The oxidative addition process can be arrested at various stages through variation of the metal and ligands, producing complexes with different H-H distances (d_{HH}). In general, true H_2 complexes have $d_{HH} = 0.8 \text{ \AA}$ - 0.9 \AA and stretched (elongated) H_2 complexes have $d_{HH} = 1.0 \text{ \AA}$ - 1.6 \AA . In comparison, the d_{HH} in free dihydrogen is 0.74 \AA while in metal dihydride species $d_{HH} > 1.6 \text{ \AA}$.⁸²

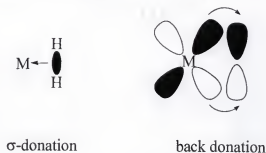


Figure 3-1. General bonding in H_2 complexes

Characterization of Dihydrogen Complexes

Characterization of H_2 complexes is primarily carried out by measuring d_{HH} in related complexes. This value can be measured experimentally by diffraction methods, solid state NMR spectroscopy, and solution NMR spectroscopy. We will briefly discuss solution NMR methods here as it pertains to later discussions in this chapter. In general, d_{MH} (metal-hydrogen distance) are not measured for several reasons. There are no general NMR spectroscopy techniques that can be used to measure this value. X-ray diffraction techniques produce large uncertainties in d_{MH} and are of limited use. There are not enough d_{MH} distances determined by neutron diffraction to draw useful correlations. Finally, d_{MH} cannot be easily used to determine the degree of H-H activation in complexes with different metals because of differences in van der Waals radii.

Solution NMR Spectroscopy: d_{HH} and $^1J_{H-D}$

The single most important spectroscopic parameter involved in the characterization of an H_2 complex is $^1J_{H-D}$ for the HD isotopomer of the H_2 complex. Classical dihydrides do not show any significant $^1J_{H-D}$ because there is no H-D bond present. In an H-D complex, there is still H-D bonding, and an H-D coupling constant can be measured by 1H NMR spectroscopy. In general, the longer the H-D bond, the smaller the $^1J_{H-D}$. The value of $^1J_{H-D}$, determined by solution NMR spectroscopy, can be correlated to d_{HH} in the solid state by using the empirical relationships developed by Morris⁸³ and Heinekey⁸⁴ (Equations 3-1 and 3-2, respectively).

$$d_{HH} = 1.42 - 0.0167(J_{H-D})\text{\AA} \quad [\text{Morris}] \quad \text{Equation 3-1}$$

$$d_{HH} = 1.44 - 0.0168(J_{H-D}) \quad [\text{Heinekey}] \quad \text{Equation 3-2}$$

These relationships were created using d_{HH} from neutron diffraction and solid-state NMR measurements for complexes where J_{H-D} was known. A plot of d_{HH} vs. $^1J_{H-D}$ gave a straight line with little deviation. Therefore, if $^1J_{H-D}$ for any H-D complex is known, d_{HH} can be calculated from the above relationships. The results obtained using Equations 3-1 or 3-2 do not usually differ significantly. Equations 3-1 and 3-2 will be used to characterize H_2 complexes in this chapter to verify this statement.

Solution NMR Spectroscopy: d_{HH} and NMR Relaxation Time (T_1)

Measuring the minimum value of the relaxation time ($T_{1(\min)}$) for the H nuclei of the H_2 ligand can provide a reasonable estimate of d_{HH} . The dipolar relaxation of one H of the H_2 ligand by its neighbor is the dominant contribution to T_1 for H_2 complexes and is generally < 50 ms, whereas T_1 for hydrides is $\gg 100$ ms. Furthermore, T_1 is proportional to d_{HH}^6 , and dipole-dipole relaxation theory states that T_1 varies with temperature and goes through a minimum at $T_{1(\min)}$. Crabtree and Hamilton have shown that at $T_{1(\min)}$, the

value of d_{HH} can be determined.^{85,86} When using this approach, the researcher must be aware that contributions to relaxation from other sources, such as proton-containing ligands^{87,88} and metals with high gyromagnetic ratios (Co, Re, and Mn),⁸⁹ can complicate the interpretation of d_{HH} from $T_{1(\text{min})}$. Another area of concern involves the effects of the rotational motion of the H_2 ligand on d_{HH} . This rotational motion is described as H_2 ligand rotation being slower or faster than molecular tumbling, and can affect dipolar relaxation. Morris has addressed this and proposed two equations for the calculation of d_{HH} from $T_{1(\text{min})}$, one for slow rotation of H_2 (Equation 3-3) and one for fast rotation of H_2 , where ν is the spectrometer frequency (Equation 3-4).⁹⁰ Equation 3-3 will be used in the characterization of the H_2 complexes discussed in this manuscript.

$$d_{\text{HH}} = 5.81 [T_{1(\text{min})}/\nu]^{(1/6)} \quad \text{Equation 3-3 (slow rotation)}$$

$$d_{\text{HH}} = 4.61 [T_{1(\text{min})}/\nu]^{(1/6)} \quad \text{Equation 3-4 (fast rotation)}$$

Molybdenum Imido-Diamido Stretched Dihydrogen Complexes

The adducts presented in Chapter 2 were generated in order to explore their potential for the oxidative addition of small molecules. Our initial interest in this area has focused on the reactivity of these adducts with molecular hydrogen. Along these lines, we have synthesized phosphine-stabilized H_2 complexes from **52** and **55**.⁹¹ Of the various H_2 complexes known, none, to our knowledge, contain metal-ligand multiple bonds, and few contain amide functionalities.⁹² Furthermore, these are rare examples of H_2 complexes in nominal d^2 configurations. Our initial studies concerning the synthesis and characterization of these unique H_2 complexes are reported herein.

Characterization of [Mo(NPh)(PMe₃)₂(H₂)(*o*-(Me₃SiN)₂C₆H₄)] (60)

Exposure of a cold (-10°C), toluene-*d*₈ solution of [Mo(NPh)(PMe₃)₃(*o*-(Me₃SiN)₂C₆H₄)] (**52**) to an atmosphere of molecular hydrogen (ca. 1 atm) resulted in a rapid color change from purple to green. The ¹H and ³¹P NMR spectra of this solution indicate that **52** and the H₂ complex [Mo(NPh)(PMe₃)₂(H₂)(*o*-(Me₃SiN)₂C₆H₄)] (**60**) were present in solution in a 1:3 ratio at -50°C (Figure 3-2). When allowed to warm to 30°C, **60** underwent an additional transformation to give a purple solution of [Mo(NPh)(PMe₃)₃(*o*-(Me₃SiN)(NH)C₆H₄)] (**53**) over a 1 h period. Thus, the net reaction of **52** with H₂ is addition of H₂ across the Si-N bond of the diamide ligand. This addition is, to our knowledge, unprecedented in the literature.

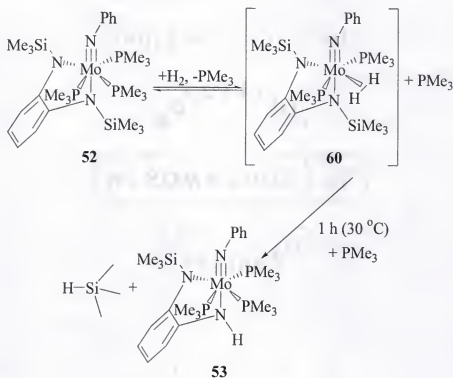


Figure 3-2. Generation and reactivity of H₂ complex **60**

Dihydrogen complex **60** is stable for days under an atmosphere of molecular hydrogen (1 atm) at -20°C but will convert to **53** at this temperature over a period of

several weeks. Attempted isolation of **60** by concentration of toluene solutions *in vacuo* resulted in isolation of the starting material (**52**). Although efforts to scavenge PMe_3 with tris(pentafluorophenyl)borane⁹³ were successful, **60** remained reactive under these conditions, generating HSiMe_3 and unidentified metal-containing products. Presumably lack of phosphine in solution compromises the formation of **53**, and the (bis)phosphine analogue of **53** is not stable under these conditions. Complex **60** can be observed in degassed (H_2 free), phosphine-scavenged solutions by ^1H NMR spectroscopy, but it decomposes rapidly.

The conversion of **60** to **53** is shown as an irreversible step in Figure 3-2. This was confirmed by reaction of the deuterated analogue of **53** (**53 D**) with HSiMe_3 (Figure 3-3). At 20°C no H/D exchange was observed between the N-D and Si-H sites by ^1H NMR spectroscopy, demonstrating that this step is irreversible.

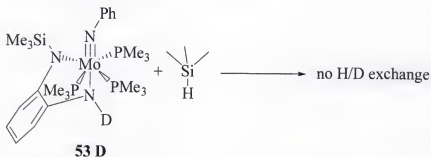


Figure 3-3. No H/D exchange between N-D and Si-H sites at 20°C

A characteristic resonance in the ^1H NMR spectrum of **60** is a broad triplet at 3.59 ppm ($^2J_{\text{P-H}} = 28$ Hz, C_7D_8 , -20°C) (Figure 3-4). The dramatically different chemical shift of these protons relative to the hydride protons of the tungsten analogue, $[\text{W}(\text{NPh})(\text{PMe}_3)_2\text{H}_2(o-(\text{Me}_3\text{SiN})_2\text{C}_6\text{H}_4)]$,⁹⁴ (9.26 ppm, br, t, $^2J_{\text{P-H}} = 40$ Hz, 18°C , C_6D_6) prompted us to investigate the metal-hydrogen interaction in more detail.

The H-D isotopomer of **60**, **60D**, was generated in order to determine d_{HH} from $^1J_{\text{H-D}}$ as discussed above. The isotopomer (**60D**) displays both coupling with phosphorous (t, 1:2:1, $^2J_{\text{P-H}} = 28$ Hz) and deuterium (t, 1:1:1, $^1J_{\text{H-D}} = 15$ Hz, C_7D_8 , -20°C) (Figure 3-4). Using the $^1J_{\text{H-D}}$ of 15 Hz in Equation 3-1 gives a value of 1.17 Å for d_{HH} , which is typical of a stretched- H_2 complex. A comparable value of 1.19 Å is calculated using Equation 3-2.

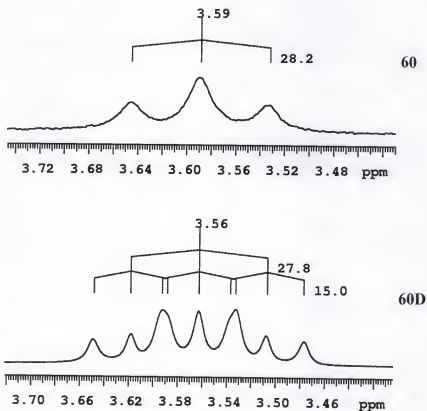


Figure 3-4. Spectra (^1H NMR) of the H_2 and H-D ligands of **60** and **60D** (-20°C)

The determination of d_{HH} using a $T_{1(\text{min})}$ analysis is consistent with d_{HH} as determined *via* $^1J_{\text{H-D}}$. A plot of T_1 vs. temperature for **60** yields a $T_{1(\text{min})}$ of approximately 36.99 ms, which is normal for an H_2 complex (Figure 3-5). Using Equation 3-3, a value of 1.19 Å for d_{HH} is calculated. Due to the good agreement between d_{HH} , as determined

by $^1J_{\text{H-D}}$, and $T_{1(\text{min})}$, the H_2 ligand in **60** is most likely slowly rotating and is significantly stretched.

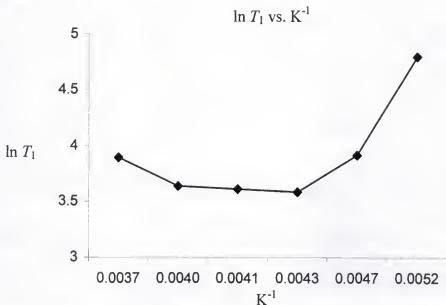


Figure 3-5. Relaxation time vs. temperature plot for **60**, $\ln T_1$ vs. K^{-1}

Two mechanisms can be proposed to account for the transformation of **60** to **53**. These mechanisms will be presented separately. Both mechanisms will be presented with H-H(D) as the reactive molecule in order to represent reactions with H_2 and H-D gas (**D** will be written in bold for this discussion only). The **D** will always be placed in the nonbridging position, as is expected from zero point energy arguments.⁹⁵ In the first mechanism, HSiMe_3 is eliminated giving bent-imido **62** (Figure 3-6). The bent imido can be converted to **53** by H(D) migration and coordination of PMe_3 . The direct elimination of HSiMe_3 can proceed through the five-centered transition state **61**.

In the second mechanism (Figure 3-7), initial proton migration to an amide, through a four-centered transition state (**63**), gives rise to **64**. Elimination of H(D)SiMe_3 then takes place through another four-centered species (**65**) ultimately giving **53**.

When **52** is treated with deuterium hydride gas (H-D), an uneven distribution of H and D is observed in the products, as shown in Figure 3-8. The H atoms prefer the N site

Figure 3-6. Potential mechanism for the formation of **53**

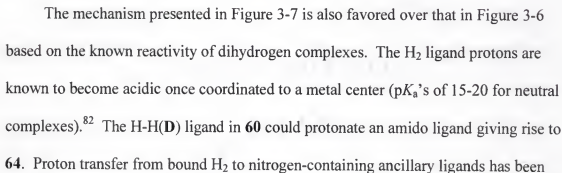


Figure 3-6. Potential mechanism for the formation of **53**

proposed in the literature.^{92,97} Elimination of H(D)SiMe_3 can then occur as shown in Figure 3-7. The mechanism shown in Figure 3-6 involves the formation of the bent-imido species **62**. Although bent imides are known, this species should be of high energy and thus it is not very favorable.

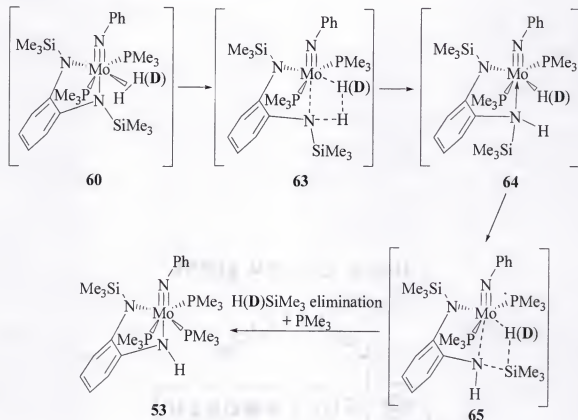


Figure 3-7. Potential mechanism for the formation of **53**

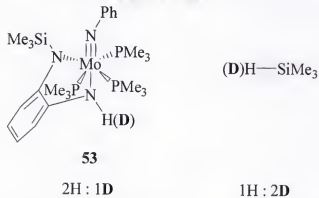


Figure 3-8. H and D do not partition equally between N and Si sites

Characterization of $[\text{Mo}(\text{NPh})(\text{PMe}_2\text{Ph})_2(\text{H}_2)(o\text{-(Me}_3\text{SiN)}_2\text{C}_6\text{H}_4)]$ (**66**)

Complex **55** reacted with dihydrogen gas to give $[\text{Mo}(\text{NPh})(\text{PMe}_2\text{Ph})_2(\text{H}_2)(o\text{-(Me}_3\text{SiN)}_2\text{C}_6\text{H}_4)]$ (**66**) (Figure 3-9). At 20°C, **66** converted to **67** with loss of HSiMe_3 . This reactivity is similar to that observed with H_2 complex **60**. The main difference between the formation of **60** and **66** involves the phosphine starting materials. The formation of **60** from **52** involves initial loss of PMe_3 , and at -50°C an equilibrium between **52** and **60** exists. Generation of **66** does not require loss of phosphine from **55**, as **55** is already coordinatively unsaturated. Furthermore, in reactions where **55** was treated with H_2 , **66** was observed as the only metal species in solution by ^1H and ^{31}P NMR spectroscopy.

The expanded region of the H_2 and H-D ligand resonances in the ^1H NMR spectra of **66** and its H-D isotopomer, **66D**, are shown in Figure 3-10 (C_7D_8 , -20°C). The H_2 ligand resonance for **66** appears as a very broad triplet centered at 3.46 ppm in the ^1H NMR spectrum. A broad, five-line resonance is observed for the H-D ligand of **66D**, centered at 3.46 ppm. The isotopomer (**66D**) displays both coupling to phosphorous (t, 1:2:1, $^2J_{\text{P-H}} = 21$ Hz) and deuterium (t, 1:1:1, $^1J_{\text{H-D}} = 21$ Hz, C_7D_8 , -20°C) (Figure 3-10). The identical $^2J_{\text{P-H}}$ and $^1J_{\text{H-D}}$ for **66D** produce the 1:3:4:3:1 multiplet observed in the ^1H NMR spectrum. Using Equation 3-1, a d_{IH} value of 1.07 Å is found for **66**, and a value of 1.09 Å is calculated using Equation 3-2.

A $T_{1(\text{min})}$ analysis of **66** gives a d_{IH} value of 1.10 Å (Figure 3-11). This value is in excellent agreement with the value found through use of $^1J_{\text{H-D}}$, indicating that the H_2 ligand is slowly rotating.

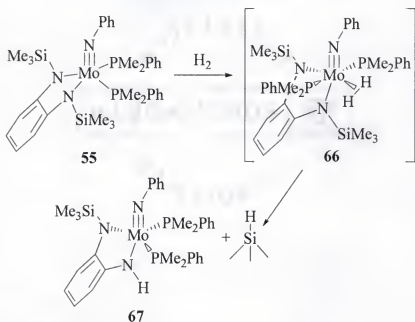


Figure 3-9. Generation and reactivity of H_2 complex **66**

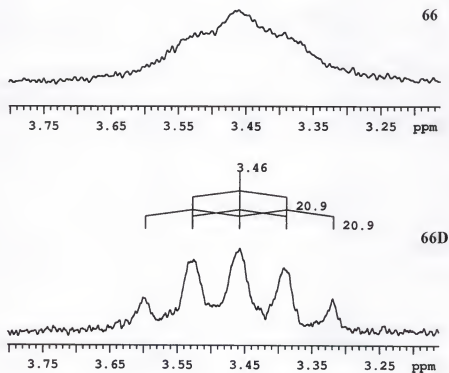


Figure 3-10. Spectra (^1H NMR) of the H_2 and H-D ligands of **66** and **66D** (-20°C)

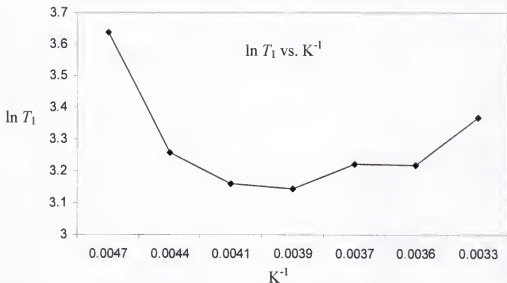


Figure 3-11. Relaxation time vs. temperature plot for **66**, $\ln T_1$ vs. K^{-1}

Bonding in Molybdenum Imido-Diamido Stretched Dihydrogen Complexes

A general bonding scenario for H_2 complexes **60** and **66** is shown in Figure 3-12. The π^* MOs involved with metal-imido anti-bonding are shown at the highest energy in Figure 3-12. The bonding combinations of these MOs are much lower in energy. The metal- H_2 interaction is shown at an intermediate energy. This interaction involves back bonding from the metal d_{xy} atomic orbital to the $H_2 \sigma^*$ atomic orbital. The back bonding interaction is primarily responsible for lengthening the H-H bond due to population of the $H_2 \sigma^*$ atomic orbital. If this is true, increasing back bonding by increasing the electron density at the metal center should lengthen the H-H bond.

The d_{HH} of 1.19 Å for **60** is longer than the d_{HH} of 1.09 Å for **66** (using Equation 3-2). This difference in bond length reflects the difference in electron density at the metal center. Since PMe_2Ph is less electron donating than PMe_3 , d_{HH} in **66** should be shorter than d_{HH} in **60**, as there is less back bonding to the $H_2 \sigma^*$ orbital in **66**.

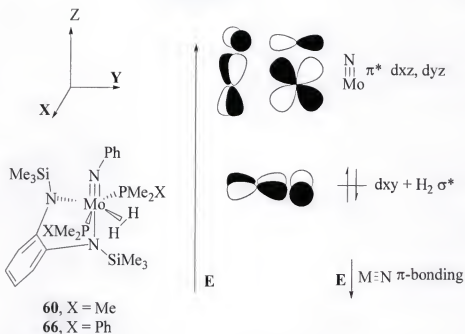


Figure 3-12. Bonding scenario for H_2 complexes **60** and **66**

Reaction of **50** and **57** with Dihydrogen Gas

When samples of **50** and **57** were treated with H_2 gas in NMR tubes (C_6D_6) no initial change in the sample composition was observed by ^1H NMR spectroscopy. The samples did react with H_2 gas over 1 week, in each case generating HSiMe_3 and metal complex (Figure 3-13). We have not fully characterized the metal-containing species **68** or **69** but have assigned tentative structures because of the similarities in ^1H NMR spectra with **53** and **67**. Presumably, the less electron donating phosphite ligands in **50** hinder formation of significant amounts of H_2 complex in solution when **50** is treated with H_2 gas. We propose that small concentrations of H_2 complex exist in solution, allowing for formation of HSiMe_3 and **68** after one week of reaction time.

Small concentrations of H_2 complex must also be present in solution when **57** is treated with H_2 gas in order to account for the formation of HSiMe_3 . The *cis* coordination of the DMPE ligand may inhibit the large-scale formation of a species with

trans phosphines capable of coordinating H_2 . A possible H_2 complex of this system could be the "arm off" complex (**70**) shown in Figure 3-14. The chelate effect of DMPE would certainly curtail the formation of large amounts of **70**.

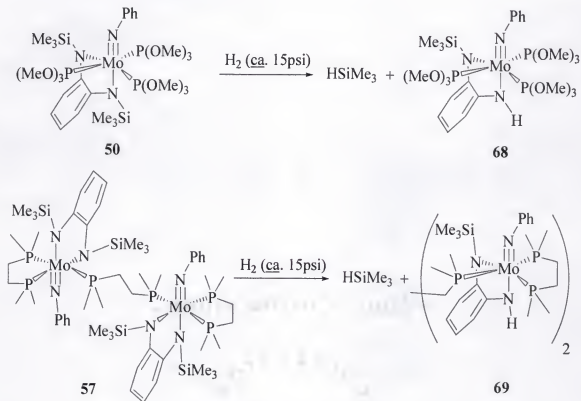


Figure 3-13. Reaction of **50** and **57** with Dihydrogen Gas

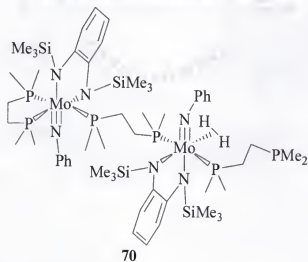


Figure 3-14. Possible H_2 complex in the DMPE system

Reaction of **52** with Phenylsilane and Diphenylsilane

Complex **52** reacted with phenylsilane and diphenylsilane in C_6D_6 . The major products of these reactions at $20^\circ C$ are cyclic silyl amines **71** and **72** (Figure 3-15). The metal-containing products in these reactions have not yet been identified. The structures of compounds **71** and **72** have been tentatively assigned using the following data. Cyclic **71** has been isolated and characterized by 1H NMR and mass spectroscopy. We propose that **72** exists based on 1H NMR data only. Further experiments to positively identify these materials, especially **72**, will be required.

When **52** reacted with H_3SiPh at low temperature ($-30^\circ C$), **72** formed along with a substantial amount of the dihydrogen complex **60**. Complex **60** decomposed to **53** and $HSiMe_3$ when left to stand at $20^\circ C$. The exact nature of the mechanism that generates **60** in this fashion is not known. A dehydrocoupling pathway does not seem to be active, as the expected silicon-based dehydrocoupling products (for example: $PhSi(H)_2Si(H)_2Ph$) are not observed by 1H NMR.⁹⁶

Presumably, thermodynamics drives the formation of **72** when **52** is treated with H_3SiPh at $20^\circ C$. In contrast, low temperatures favor the formation of **60**, the kinetic product of this reaction sequence. Very small amounts of $HSiMe_3$ and **53** are observed in the reaction mixture after treatment of **52** with H_2SiPh_2 at $20^\circ C$. This reaction must be explored at lower temperature in the future.

Summary

Reactions of molybdenum imido-diamido phosphine adducts of PMe_3 (**52**) and PMe_2Ph (**55**) with CO gas were discussed in Chapter 2. In the case of **52** CO displaces PMe_3 to give a carbonyl complex, whereas CO coordinates to coordinatively unsaturated **55** to give the appropriate metal carbonyl. In this chapter we report that the phosphine

complexes **52** and **55** react with dihydrogen gas to give stretched dihydrogen complexes **60** and **66**, respectively. The formation of **60** from **52** is interesting in that a PMe_3 ligand is displaced from the metal center by a much weaker H_2 ligand. Steric crowding around the metal center may help influence PMe_3 dissociation from **52**, allowing for the generation of a (bis)phosphine complex that can coordinate H_2 . Displacement of phosphine by H_2 is a rare process, and to our knowledge, only one other example has been reported in the literature.⁸²

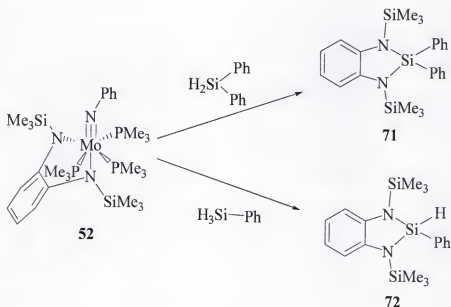


Figure 3-15. Generation of cyclic **71** and **72**

We also discuss the reactivity of the dihydrogen complexes **60** and **66**. These reactions proceed by formal addition of H_2 across the N-Si bond, liberating HSiMe_3 and giving metal complexes **53** and **67**. While proton transfer from H_2 ligands to amido and amine ligands has been proposed in the literature^{92,97} and may play a role in the mechanism of this reaction, elimination of H-SiMe_3 from a metal center in this way is, to our knowledge, unprecedented.

Preliminary results concerning the reaction of **52** with H_2SiPh_2 and H_3SiPh are reported here. Future efforts toward characterization of several products are required. In the interim, we propose that thermodynamics drives the formation of **71** and **72** at 20°C . The dihydrogen complex formed when **52** and H_3SiPh react at low temperature is most likely a kinetic product of the system.

CHAPTER 4
SYNTHESIS, CHARACTERIZATION, AND REACTIVITY OF A MOLYBDENUM
(IV), η^1 -BUTADIENE COMPLEX AND η^2 -ALKYNE COMPLEXES

Early Transition Metal Butadiene Complexes

Low valent zirconium (0) butadiene complexes with bidentate phosphine ligands were among the first well-characterized examples of Group 4 metal butadiene complexes.⁹⁸ The well-known, higher valent, base-free zirconocene butadiene complexes were independently synthesized by both Erker⁹⁹ and Nakamura¹⁰⁰ (Figure 4-1). Among the striking structural characteristics of these complexes is the ability of the butadiene fragment to coordinate to the metallocene core in *cis* and *trans*-modes and the dynamic envelope shift isomerization process associated with the *cis*-coordination mode.⁹⁹⁻¹⁰¹

The structure and bonding of *cis*-butadiene complexes can vary between two extremes, the π^2 and the σ^2 , π -designations (Figure 4-2).^{95,100} The bonding in π^2 complexes is best described as donation of butadiene π -electron density to the metal center. A number of π^2 complexes have been characterized by X-ray crystallography, and in these compounds the butadiene C-C bond lengths are very similar. In σ^2 , π -type complexes, the butadiene ligand is considered a dianionic dialkyl, a result of considerable back bonding. Solid-state structural studies have shown that the C(1)-C(2) and C(3)-C(4) bond lengths are considerably longer than the C(2)-C(3) bond in σ^2 , π -complexes (Figure 4-2). The substitution of the butadiene ligand and the identity and electronic structure of the metal play a large role in dictating which structure type will be adopted. To date there are several examples of structurally characterized Group 4 and 5 *cis*¹⁰¹ and

*trans*¹⁰²-butadiene metal complexes, with the *cisoid* conformation being the most common.

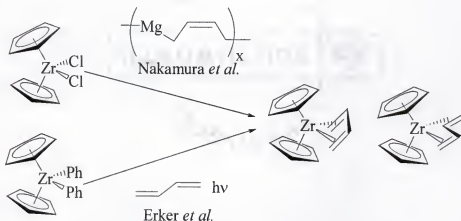


Figure 4-1. Synthesis of zirconocene butadiene complexes

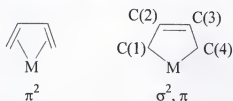


Figure 4-2. Possible π^2 and σ^2, π structures for *cis*-butadiene complexes

Characteristic reactivity of Group 4 and 5 butadiene complexes involves reactions with unsaturated substrates such as carbonyl compounds, nitriles, and alkynes.¹⁰³ This reactivity is typified by $\text{Cp}_2\text{Zr}(\text{butadiene})$ where C-C coupling of the unsaturated substrate with a terminal butadiene carbon results in metallacyclic complexes (Figure 4-3). In some cases, the interconversion of these metallacyclic compounds can be observed experimentally. The metallacycles are generally stable, and hydrolysis protocols are required to free useful acyclic organic products from the metal center. In sharp contrast, later transition metals (Groups 9 and 10) catalyze the intermolecular 4+2 cycloaddition of nonactivated substrates,¹⁰⁴ while related transition metal-catalyzed

cycloisomerization reactions constitute a rapidly developing area of research.¹⁰⁵ Recent developments involving Group 4 butadiene complexes involve their applications as catalysts in olefin polymerization reactions.¹⁰⁶

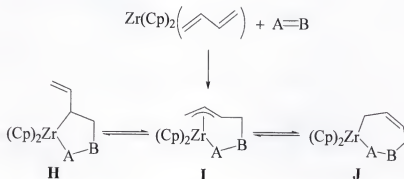


Figure 4-3. Reactivity of $\text{Cp}_2\text{Zr}(\text{butadiene})$ with a representative unsaturated substrate

Reports concerning the synthesis and characterization of high valent Group 6 transition metal butadiene complexes are not as common as those of the earlier Groups.¹⁰⁷ Furthermore, reactivity of these Group 6 butadiene complexes differs from the well-explored reaction chemistry associated with the Group 4 and 5 butadiene complexes and the catalytic cycloisomerization reactions of the later metals.¹⁰⁷

Molybdenum Imido-Diamido Butadiene Complexes

We have recently prepared a butadiene complex of our molybdenum imido-diamido system. The synthesis, structural characterization, and reactivity of this monomeric, diamagnetic, molybdenum (IV)-*cis*-butadiene complex, $[(\text{Mo}(\text{NPh})-\eta^4-(\text{H}_2\text{C}=\text{CHCH}=\text{CH}_2)(o-(\text{Me}_3\text{SiN})_2\text{C}_6\text{H}_4)]$ (**73**) is discussed below.¹⁰⁸ To our knowledge, this is the first report of a molybdenum complex of this nature. While structurally similar to other molybdenum butadiene complexes, the reactivity of **73** departs from these showing similarities to both early and late transition metal reactivity.

The synthesis of a related imido-diamido methylvinyl ketone (MVK) complex is also discussed here.

Synthesis and Characterization of η^4 -Butadiene Complex

$[(\text{Mo}(\text{NPh})-\eta^4-(\text{H}_2\text{C}=\text{CHCH}=\text{CH}_2)(o-(\text{Me}_3\text{SiN})_2\text{C}_6\text{H}_4)]$ (**73**)

Treatment of a pentane solution of **37** or **38** with molecular butadiene gave the η^4 -*cis*-butadiene complex $[(\text{Mo}(\text{NPh})-\eta^4-(\text{H}_2\text{C}=\text{CHCH}=\text{CH}_2)(o-(\text{Me}_3\text{SiN})_2\text{C}_6\text{H}_4)]$ (**73**) in good yield (Figure 4-4). Decomposition of **73** occurred within 4 h at 20°C, affording an intractable mixture, as determined by ^1H NMR spectroscopy. When kept at -30 °C in the solid-state, **73** did not decompose appreciably over several months, as noted by ^1H NMR spectroscopy. An X-ray crystallographic study was carried out on a single crystal of **73** grown from a -30°C solution of pentane/methylene chloride. The crystal data and details of the structure refinement are summarized in Table 4-1.

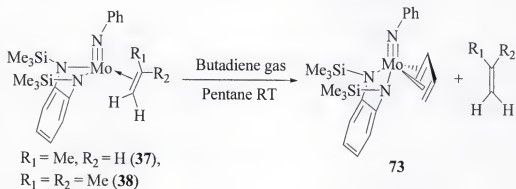


Figure 4-4. Synthesis of $[(\text{Mo}(\text{NPh})-\eta^4-(\text{H}_2\text{C}=\text{CHCH}=\text{CH}_2)(o-(\text{Me}_3\text{SiN})_2\text{C}_6\text{H}_4)]$ (**73**)

The butadiene complex crystallizes in a monoclinic unit cell with one molecule of methylene chloride. The molecular structure of **73**, accompanied by selected bond lengths and angles, is shown in Figure 4-5. The butadiene fragment clearly adopts a *cis*-arrangement when bound to the metal center. The metal to terminal butadiene carbon distances of 2.254(3) Å (Mo-C(19)) and 2.257(2) Å (Mo-C(22)) and the Mo-C(20) and

Mo-C(21) bond lengths of 2.336(2) Å and 2.355(2) Å, respectively, support a π^2 , η^4 -butadiene bonding motif for **73**. Other molybdenum butadiene complexes adopt similar bonding modes.¹⁰⁷ Within the butadiene fragment, the similar C(19)-C(20), C(20)-C(21), and C(21)-C(22) bond lengths of 1.401(4) Å, 1.397(4) Å, and 1.405(4) Å, respectively, also support a π^2 , η^4 -bonding mode for **73**. The Mo-N(1) length of 1.7517(19) Å is typical of a Mo-N triple-bond interaction and is comparable to the Mo-N(1) lengths in similar complexes (see Chapter 2).^{11,27,47}

It is common practice to use the $^1J_{C-H}$ coupling constants to determine the relative degree of sp^2 - sp^3 hybridization of the coordinated diene carbons in metal butadiene complexes. By determining the relative degree of hybridization of the diene carbon atoms, the structure, in terms of butadiene bonding, can be assigned a position somewhere between the two extremes π^2 or σ^2 , π . Using Newton's semi-empirical rule,¹⁰⁹ it is possible to calculate the % *s* character of carbon atoms in the dienes and hence the hybridization. The value of *n* for the carbons at diene termini reaches 2.8-2.9 (132-128 Hz) when the molecule adopts a σ^2 , π -type structure while the value is in the range of 2.1-2.3 (165-154 Hz) in the case of a π^2 -complex.¹¹⁰ We have assigned the observed triplet in the ^{13}C NMR spectrum of **73** at 75.0 ppm to the terminal butadiene carbons, and the observed $^1J_{C-H}$ 158 Hz coupling constant is in good agreement with the formulation of **73** as a π^2 -butadiene complex. In light of these results regarding **73**, the formal oxidation state at the metal center is best represented by Mo(IV).

Analogous tungsten imido-diamido complexes have been prepared in our laboratories.¹¹¹ These complexes are better described as adopting the σ^2 , π -butadiene bonding mode. This trend has been observed for Group 4 butadiene species where

zirconium complexes prefer π^2 -type bonding, while hafnium complexes prefer σ^2 , π type bonding. This is as expected and follows the general trend that metal-carbon σ -bonds of third row transition metal complexes are stronger than the corresponding bonds in the isostructural second row complexes.^{100(b),112}

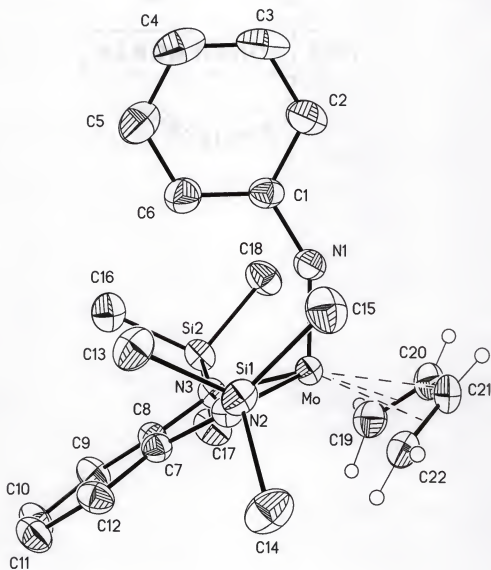


Figure 4-5. Thermal ellipsoid plot of **73** (50% probability thermal ellipsoids). Selected bond lengths (Å) and angles (°): Mo-N(1) 1.7517(19), Mo-N(2) 2.0556(17), Mo-N(3) 2.0536(18), Mo-C(19) 2.254(3), Mo-C(20) 2.336(2), Mo-C(21) 2.355(2), Mo-C(22) 2.257(2), C(19)-C(20) 1.401(4), C(20)-C(21) 1.397(4), C(21)-C(22) 1.405(4), C(19)-C(20)-C(21) 124.4(2), C(20)-C(21)-C(22) 123.3(2), C(1)-N(1)-Mo 147.27(17), N(3)-Mo-N(2) 78.24(7).

Table 4-1. X-ray data^a for crystal structures 73, 74, and 78

	73	74	78
Chemical formula	C ₂₂ H ₃₃ N ₃ MoSi ₂ ·CH ₂ Cl ₂	C ₂₆ H ₃₉ N ₃ MoSi ₂	C ₂₂ H ₃₃ N ₃ MoSi ₂
Formula weight	576.56	545.72	507.63
Crystal system	Monoclinic	Monoclinic	Monoclinic
Space group	<i>P</i> 2 ₁ / <i>n</i>	<i>P</i> 2 ₁ / <i>c</i>	<i>P</i> 2 ₁ / <i>n</i>
μ(Mo-Kα) (mm ⁻¹)	0.775	0.590	0.641
<i>a</i> (Å)	11.9736(6)	16.031(1)	10.0648(5)
<i>b</i> (Å)	15.8844(8)	10.0300(8)	17.0457(9)
<i>c</i> (Å)	14.5066(7)	16.906(1)	14.4866(8)
β (°)	95.324(1)	93.351(1)	90.371(1)
<i>V</i> _c (Å ³)	2747.2(2)	2713.7(4)	2485.3(2)
<i>Z</i>	4	4	4
Θ _{max} °	27.50	27.50	27.50
Total reflections	16414	19246	16938
Uniq. reflections	6282	6216	5672
<i>R</i> (int)	0.0434	0.0638	0.0250
<i>R</i> ₁ [<i>I</i> ≥ 2σ(<i>I</i>) data] ^b	0.0307	0.0356	0.0228
w <i>R</i> ₂ (all data) ^c	0.0815	0.0947	0.0616
Larg. diff. peak, hole	0.365, -0.425	0.582, -0.672	0.339, -0.291

^aObtained with monochromatic Mo Kα radiation (λ = 0.71073 Å) at 173 K. ^b*R*₁ = Σ|*F*_o - *F*_c|/Σ|*F*_o|. ^cw*R*₂ = {Σ[w(*F*_o² - *F*_c²)²/Σw(*F*_o²)]^{1/2}.

Reactivity of [(Mo(NPh)- η^4 -(H₂C=CHCH=CH₂)(*o*-(Me₃SiN)₂C₆H₄)] (73) with 2-Butyne

The reactivity of **73** with 1.0 or 2.0 equiv of 2-butyne was explored. Proton NMR spectra of these reaction mixtures revealed the formation of two intermediates that disappeared within 30 min at 20°C, giving rise to the final products, as outlined in Figure 4-6. Reaction of **73** with 1.0 equiv of 2-butyne afforded the molybdenum 2,3-dimethyl-1,3-cyclohexadiene complex (**74**), as determined by ¹H NMR spectroscopy, while reaction with 2.0 equiv of 2-butyne gave 1,2-dimethyl-1,4-cyclohexadiene and the molybdenum η^2 -alkyne complex, [(Mo(NPh)- η^2 -(MeCCMe)(*o*-(Me₃SiN)₂C₆H₄)] (**75**), according to ¹H NMR spectroscopy (this alkyne complex has been synthesized independently, *vide infra*). Complex **74** was prepared independently by treatment of **38** with excess 1,2-dimethyl-1,4-cyclohexadiene (Figure 4-6). In addition, the 2,3-dimethyl-1,3-cyclohexadiene ligand in **74** was not displaced by 2-butyne at room temperature, as observed by ¹H NMR spectroscopy.

The identity of **74** was confirmed by X-ray crystal structure analysis, and the thermal ellipsoid plot is shown in Figure 4-7. The crystal data and details of the structure refinement are summarized in Table 4-1. In **74** the metal is bound to the 2,3-dimethyl-1,3-cyclohexadiene in an η^4 -mode reminiscent of **73**. The C-C distances between C(21)-C(20), C(20)-C(19), and C(19)-C(24) in **74** (1.418(3) Å, 1.418(3) Å, and 1.405(3) Å respectively), as well as the metal-carbon bond lengths, are similar to the corresponding distances in **73**. The Mo-N(1) distance of 1.7686(18) Å is consistent with a molybdenum nitrogen triple-bond interaction. The Mo-N(2) and N(3) amide distances of 2.0561(18) Å and 2.0492(17) Å, respectively, are within the range expected for Mo-N single bonds.^{27,46,51,56,91} Complex **74** is stable in solution at 20°C for weeks. We attribute

the difference in stabilities between **73** and **74** in part to steric crowding around the metal center in **74**.

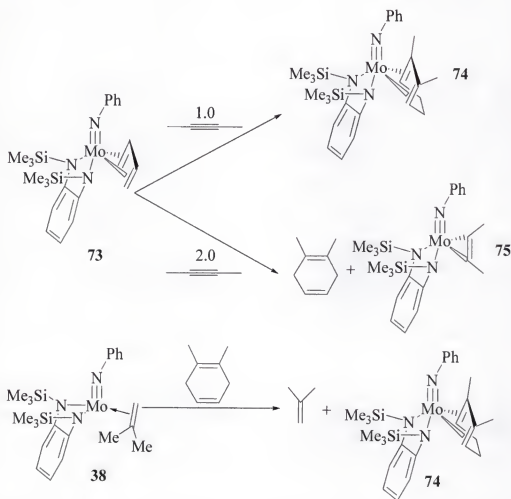


Figure 4-6. Reactivity of $[(\text{Mo}(\text{NPh})-\eta^4\text{-(H}_2\text{C=CHCH=CH}_2\text{)}(o\text{-(Me}_3\text{SiN)}_2\text{C}_6\text{H}_4)]$ (**73**) with 2-butyne

When **73** was treated with 1.0 equiv of 2-butyne at -20°C , the accumulation of two metal-containing species was observed by ^1H NMR spectroscopy over 24 h. These species are the fleeting intermediates observed during this reaction at 20°C and are stable at -20°C for extended periods (over 2 days). An array of two-dimensional NMR spectroscopic techniques was used to elucidate the structures of these intermediates. The intermediates consist of two isomeric complexes present in a 4:1 ratio. The major

intermediate has been characterized as [*syn*-(Mo(NPh)(C(Me)=C(Me)CH₂CHCHCH₂)(*o*-(Me₃SiN)₂C₆H₄)] (**76a**), a *syn*- η^3 -allyl metallacyclic system.

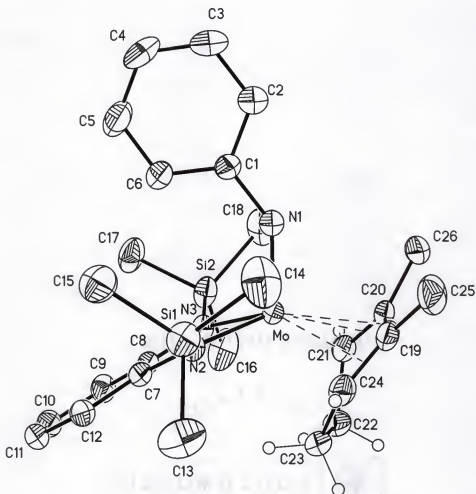


Figure 4-7. Thermal ellipsoid plot of **74** (50% probability thermal ellipsoids). Selected bond lengths (Å) and angles (°): Mo-N(1) 1.7686(18), Mo-N(2) 2.0561(18), Mo-N(3) 2.0492(17), Mo-C(21) 2.258(2), Mo-C(20) 2.342(2), Mo-C(19) 2.402(2), Mo-C(24) 2.274(2), C(21)-C(20) 1.418(3), C(20)-C(19) 1.418(3), C(24)-C(19) 1.405(3), C(24)-C(23) 1.518(3), C(23)-C(22) 1.542(3), C(22)-C(21) 1.525(3), C(1)-N(1)-Mo 142.47(16).

The results of the structural elucidation study are presented in Figure 4-8. The metallacycle H_a-C and H_b-C ¹J_{C-H} of ca. 160 Hz are consistent with an sp² hybridization of the carbon resonance at 76.8 ppm. This along with the lack of resolved coupling between H_a and H_b, support the existence of an η^3 -allyl functionality. The chemical

shifts of the remaining allyl proton and carbon nuclei also support the allyl fragment in **76a**. The sequence of the protons which display multiplets was seen in the DQCOSY spectrum. NOe's between the methyl at 1.58 ppm and the methylene protons at 2.59 ppm and 2.67 ppm identified it as the one proximal to the methylene group. The protonated carbons were assigned to the corresponding protons using a GHMQC spectrum. The GHMBC spectrum displayed long-range couplings between the quaternary carbons at 177.5 ppm and 154.7 ppm and the protons of both the methylene and the methyl groups, which confirm the metallacycle fragment. The relative sizes of the nOe's place H_b, H_d, and H_e on one side of the ring and H_a, H_c, and H_f on the other side. In **76a** H_a, H_c, and H_f showed nOe's to aromatic proton H_g. We state that H_g is an *ortho* phenyl imido proton and not a phenylene proton because in the DQCOSY spectrum they displayed a phenyl coupling pattern (7.15 ppm (H_g) - 6.98 ppm - 6.79 ppm). Therefore H_c occupies a *syn* relationship with respect to the phenyl imido group. This intermediate metallacyclic π -allyl system most likely arises from C-C coupling at the conjugated diene terminus.

The minor species also consists of a metallacyclic π -allyl system, [*anti*-(Mo(NPh)(C(Me)=C(Me)CH₂CHCHCH₂)(*o*-(Me₃SiN)₂C₆H₄))] (**76b**), that is very similar to **76a** (Figure 4-9). Metallacycle **76b** differs from **76a** in that in **76b** the central allyl proton H_c is *anti* with respect to the phenyl imido group as revealed by the nOe's between H_g at 7.19 ppm and H_a, H_d, and H_f. The details of the structural elucidation of **76b** are similar to those of **76a**, however the low concentration of **76b** in solution prevented the assignment of the ¹³C chemical shifts of the metallacycle fragment from the GHMQC and GHMBC spectra. The NOESY spectrum did not display any chemical exchange peaks between **76a** and **76b** at -20 °C.

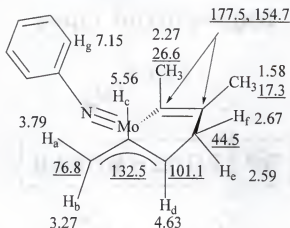


Figure 4-8. Structure of intermediate (**76a**), showing selected carbon (underlined) and proton chemical shifts, assigned by NMR spectroscopy. The diamido ligand has been omitted for clarity.

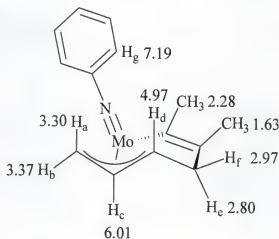


Figure 4-9. Structure of intermediate (**76b**), showing selected proton chemical shifts, assigned by NMR spectroscopy. The diamido ligand has been omitted for clarity.

There has been extensive mechanistic work by Erker *et al.* and Nakamura *et al.* on the reactivity of Group 4 metallocene derivatives of 1,3-butadienes with unsaturated substrates. The pathway favored for such reactions involves coupling of the unsaturated moiety with one of the diene double bonds, producing a 2-vinylmetallacyclopentane species (**H**) (Figure 4-3). This species can then isomerize as shown in Figure 4-3.

It thus seems reasonable to propose that **73** reacts with 2-butyne to give **76e**, which does not accumulate to any detectable levels by ^1H NMR spectroscopy (Figure 4-10). Intermediate **76e** rapidly rearranges, affording **76a** and **76b**, which can be observed at low temperature. At 20°C **76a**, **76b**, or some combination of the two most likely rearrange to form **76f**, which rapidly generates **76g** via reductive elimination. Isomerization of **76g** ultimately results in the formation of **74**. The production of **74** from treatment of olefin complex **38** with excess 1,2-dimethyl-1,4-cyclohexadiene (Figure 4-6) gives evidence supporting the formation of **76g** in the proposed mechanism.

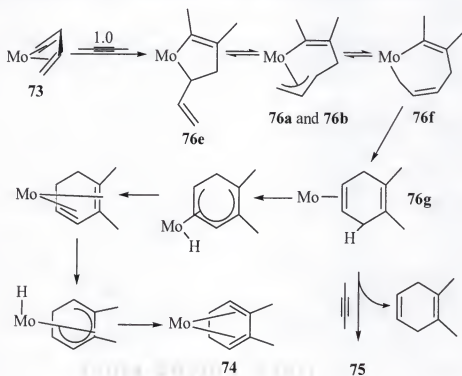


Figure 4-10. Proposed mechanism for reaction of **73** with 2-butyne. Ancillary ligands have been omitted for clarity.

The difference in product distribution when 2.0 equiv of 2-butyne reacts with **73** is consistent with the proposed mechanism in Figure 4-10. Excess 2-butyne competes for the metal center with the 1,2-dimethyl-1,4-cyclohexadiene ligand in **76g**, liberating free

1,2-dimethyl-1,4-cyclohexadiene and forming **75** as the metal-containing product. In the absence of excess 2-butyne isomerization of **76g** to **74** occurs.

Reactivity of [(Mo(NPh)- η^4 -(H₂C=CHCH=CH₂)(*o*-(Me₃SiN)₂C₆H₄)] (73**) with Acetone: Formation of [(Mo(NPh)(CH₂CH=CHCH₂C(Me)₂O)(*o*-(Me₃SiN)₂C₆H₄)] (**77**)**

When a green C₆D₆ solution of **73** was treated with 1.0 equiv of acetone, a red solution containing **77** was generated (Figure 4-11). Organometallic, metallacycle **77** was characterized by an array of NMR spectroscopic techniques, including GHMBC, GHMQC, TOCSY, NOESY, and COSY. The results of the structural elucidation are shown in Figure 4-12.

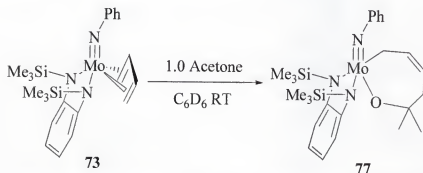


Figure 4-11. Formation of [(Mo(NPh)(CH₂CH=CHCH₂C(Me)₂O)(*o*-(Me₃SiN)₂C₆H₄)] (**77**)

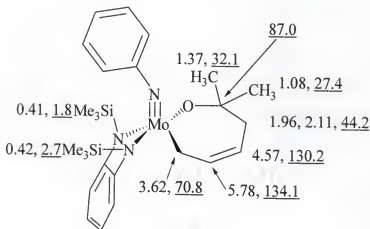


Figure 4-12. Proposed structure for **77** showing selected carbon (underlined) and proton chemical shifts, assigned by NMR spectroscopy

Exchange peaks are observed between the methyl groups at 1.08 ppm and 1.37 ppm in the NOESY spectrum of **77** at 25°C, corresponding to a dynamic process that exchanges these methyl group environments. Furthermore, at 25°C there are two resonances corresponding to inequivalent SiMe₃ groups in the ¹H NMR spectrum of **77** at 0.41 ppm and 0.42 ppm. At 60°C these resonances have coalesced, and the ΔG^\ddagger for this process is approximately 74.37 KJ/mol (17.77 Kcal/mol), using Equation 2-1.

The epimerization process shown in Figure 4-13 could account for this behavior. In Figure 4-13 the square pyramidal enantiomers, **77a** and **77d**, can interconvert through a Berry pseudorotation mechanism involving the trigonal bipyramidal intermediates **77b** and **77c**. This process clearly exchanges the methyl groups labeled Me_a and Me_b in Figure 4-13. At 25°C the epimerization process could be slow enough on the NMR time scale as to allow observation of two SiMe₃ resonances in the ¹H NMR spectrum. If at 60°C the epimerization process is fast on the NMR timescale, then only one SiMe₃ resonance will be observed by ¹H NMR spectroscopy. Different dynamic NMR properties have been observed for similar early-metal complexes.^{102(c)}

Synthesis and Characterization of η^4 -MVK Complex [(Mo(NPh)- η^4 -(O=C(Me)CH=CH₂)(*o*-(Me₃SiN)₂C₆H₄)] (78**)**

The coordination chemistry of Group 6 metals with acyclic conjugated dienes other than butadiene, more specifically α , β -unsaturated carbonyl compounds, is a topic under current investigation in the scientific community. Recent developments in this area involve the synthesis of a tris methylacrylate molybdenum complex, [Mo(H₂C=CHCOOMe)₃(PMe₃)], where two methylacrylate groups bind to the metal through both C=C and C=O functionalities as η^4 -1-oxa-1,3-diene ligands while the third associates with the metal through the C=C double bond.¹¹³ A series of related compounds was reported by

Schmidt *et al.*,¹¹⁴ and a molybdenum/tungsten (II) hydrotris(pyrazolyl)borate system that binds to α , β -unsaturated aldehydes in η^1 and η^2 -modes through the carbonyl moiety only is also known.¹¹⁵ The synthesis and crystal structure of a thermally stable, base-free, monomeric molybdenum (IV) *cis*- η^4 -methyl vinyl ketone complex, $[(\text{Mo}(\text{NPh})-\eta^4-(\text{O}=\text{C}(\text{Me})\text{CH}=\text{CH}_2)(o-(\text{Me}_3\text{SiN})_2\text{C}_6\text{H}_4)]$ (**78**), is discussed below.

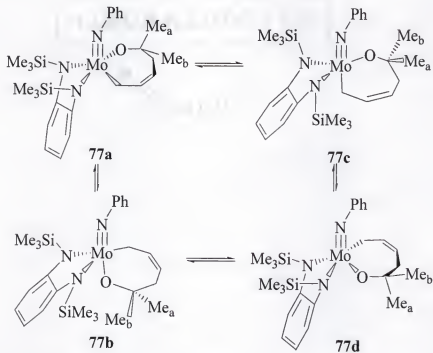


Figure 4-13. Possible methyl group exchange pathway

Pentane solutions of **37** or **38** reacted with 1.0 equiv of MVK affording **78** in high yield. Complex **78** was isolated by removal of the pentane solvent under reduced pressure and could be recrystallized from a concentrated toluene/pentane solution at -30°C .

An X-ray crystallographic study on a single crystal of **78** was carried out. The thermal ellipsoid plot of **78** is shown in Figure 4-14 and is accompanied by selected bond lengths and angles. The crystal data and details of the structure refinement are summarized in Table 4-1. The Mo-N(1) bond length of $1.7607(14)$ Å is consistent with a

metal-nitrogen triple bond. The Mo-O(1) bond is slightly longer (ca. 0.1 Å) than a Mo-O single bond, while the remaining Mo-MVK carbon contacts (Mo-C(19) 2.3666(17) Å, Mo-C(20) 2.3702(18) Å, and Mo-C(21) 2.2149(19) Å) are similar in length to analogous Mo-carbon bond lengths in butadiene complex **73**, supporting considerable η^4 -1-oxa-1,3-diene character in **78**. The formal oxidation state at the metal center is thus best described as Mo(IV), and the ^1H NMR spectrum of **78** is consistent with the solid-state structure.



Figure 4-14. Thermal ellipsoid plot of **78** (50% probability thermal ellipsoids). Selected bond lengths (Å), angles (°), and torsion angles (°): Mo-O(1) 2.0492(11), Mo-C(19) 2.3666(17), Mo-C(20) 2.3702(18), Mo-C(21) 2.2149(19), O(1)-C(19) 1.324(2), C(19)-C(20) 1.390(3), C(21)-C(20) 1.414(3), Mo-N(1) 1.7607(14), Mo-N(3) 2.0107(14), Mo-N(2) 2.0452(14), O(1)-C(19)-C(20) 118.02(17), C(19)-C(20)-C(21) 123.09(19), O(1)-C(19)-C(22) 119.38(18), C(20)-C(19)-C(22) 123.27(19), C(1)-N(1)-Mo 143.40(12), O(1)-C(19)-C(20)-C(21) 4.3(3).

Summary

The synthesis and reactivity of molybdenum butadiene complex **73** has been discussed. Structurally this complex is similar to other molybdenum butadiene complexes. Reactivity wise, this complex shows parallels with earlier metals, forming transient η^3 -allyl metallacycles when treated with 2-butyne and metallacyclic **77** when treated with acetone. While this reactivity places **73** in a group with earlier metal butadiene complexes, the C-C bond-forming reaction that occurs during the formation of **74** is more akin to the reactivity of later metals. Thus, complex **73** occupies a unique position among other known transition metal butadiene complexes.

Early Transition Metal Alkyne Complexes

The study of early transition metal complexes of alkynes has been a mainstay of organometallic chemistry for many years.¹¹⁶ In general, alkyne complexes are generated by ligand displacement reactions or by reduction of a metal halide species in the presence of the appropriate alkyne. An important development in this area was the discovery that η^2 -alkyne ligands have the ability to act as 2 or 4 electron donor ligands and that ^{13}C NMR spectroscopy could be used to determine the electron donating character of the alkyne ligand.¹¹⁷

The simple bonding scenario for a transition metal alkyne complex is shown in Figure 4-15. Both acetylene π -bonding MOs can interact with metal-based orbitals through σ and π -donation interactions if the metal orbitals are available for bonding. Back bonding (π -acceptance) interactions are often common in alkyne complexes, and when such contributions to bonding are significant, the metallacyclopentadiene structure is a good description of the net alkyne-metal interaction (Figure 4-15). The δ -interaction

shown in Figure 4-15 does not contribute much to the overall bonding picture, for it is a weak interaction. While an extensive foray into the synthesis and characterization of Group 6 alkyne complexes has been made over the years, base-free, high-valent examples of such are rare entities in the literature.

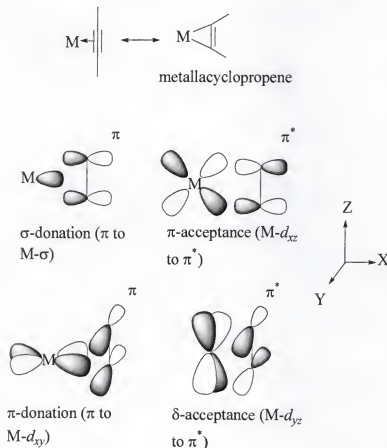


Figure 4-15. Bonding in transition metal alkyne complexes

Synthesis and Characterization of Molybdenum Imido-Diamido Alkyne Complexes
 $[(Mo(NPh)-\eta^2-(RCCR)(o-(Me_3SiN)_2C_6H_4)]$ ($R = Me$ (**75**), Ph (**79**), $SiMe_3$ (**80**))

We have recently prepared base-free molybdenum (IV) alkyne complexes of the type $[(Mo(NPh)-\eta^2-(RCCR)(o-(Me_3SiN)_2C_6H_4)]$ ($R = Me$ (**75**), Ph (**79**), $SiMe_3$ (**80**)) (Figure 4-16). These complexes were prepared by treating pentane solutions of **37** or **38** with the appropriate alkyne, followed by removal of solvent under reduced pressure. The alkyne reactants effectively displace the bound olefin of **37** or **38** with complete

conversion to products within 15 min at 20°C. The ^1H NMR spectra of **75**, **79**, and **80** are consistent with monomeric alkyne complexes. The carbons of the alkyne fragment coordinated to the metal in **75**, **79**, and **80** resonate at 181 ppm, 180 ppm, and 205 ppm, respectively, in the ^{13}C NMR spectra, suggesting that the alkyne ligands are acting as 3-4 electron donor ligands.¹¹⁷ Compounds **79** and **80** are air sensitive but stable in solution and in the solid-state. In contrast, **75** is highly unstable and decomposes in solution at -40°C overnight.

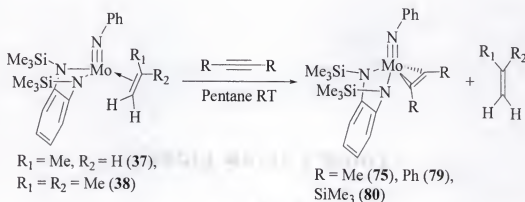


Figure 4-16. Synthesis of $[(\text{Mo}(\text{NPh})-\eta^2-(\text{RCCR})(o-(\text{Me}_3\text{SiN})_2\text{C}_6\text{H}_4)]$ ($\text{R} = \text{Me}$ (**75**), Ph (**79**), SiMe_3 (**80**))

Single crystal X-ray analyses were carried out on single crystals of **75** (Figure 4-17) and **80** (Figure 4-18). The crystal data and details of the structure refinement are summarized in Table 4-2. Both **75** and **80** adopt square pyramidal geometries where the imido groups occupy the apical positions. The metal imido interactions (**75**: Mo-N(1) 1.7511(17) Å, **80**: Mo-N(1) 1.745(2) Å) are consistent with metal-nitrogen triple bonds, and the molybdenum amide contacts are consistent with metal-nitrogen single-bond interactions.^{27,46,51,56,91}

The Mo-C(20) and Mo-C(21) bond lengths of 2.056(2) Å and 2.052(2) Å for **75**, respectively, are consistent with Mo-C single bonds and the C(20)-C(21) bond length of

1.297(3) Å is close to the generally accepted value of 1.34 Å for a C-C double bond.¹¹⁸ Pronounced back bonding is responsible for the lengthening of this alkyne bond, and the structure of **75** is thus best described as having a strong contribution from a metallacyclopentene structure (Figure 4-17). The alkyne ligand can be considered as a dianionic ligand, and the formal oxidation state of the metal would be best described as Mo(VI). Similar structural parameters have been reported for high-valent Group 4 alkyne complexes¹¹⁹ and for isostructural tungsten complexes made in our laboratories.¹¹¹

Similar arguments apply to the solid-state structure of **80**. The C(19)-C(20) bond length of 1.305(4) Å in **80** is very close to the C(20)-C(21) length of 1.297(3) Å in **75**. Complex **80** is thus also best described by the metallacyclopentene structure (Figure 4-18). The unique bonding interactions in these complexes are currently being studied theoretically through DFT analysis and these results will be published in due course.

Reaction of [(Mo(NPh)-η²-(PhCCPh)(*o*-(Me₃SiN)₂C₆H₄)] (79**) with *tert*-Butyl Isocyanide**

When a sample of **79** was treated with 1.0 equiv of Bu¹NC, a new metal-containing complex formed, as observed by ¹H NMR spectroscopy. This complex was not fully characterized, but we have assigned it a preliminary structure (**81**, Figure 4-19), which is consistent with the ¹H NMR spectrum (selected ¹H NMR for **81** (C₆D₆, 18 °C): δ 4.05 (br, C=C(Ph)*H*), 2.58 (d, 14 Hz, metallacycle methylene C-*H*), 1.73 (d, 14 Hz, metallacycle methylene C-*H*)). Complex **81** converted to **82** over the course of several weeks (Figure 4-19). Complex **82** was characterized by NMR spectroscopy, and the structural assignment is shown in Figure 4-20. The chemical shift of the imino-acyl carbon is atypical and approximately 60 ppm upfield from where expected. This shift could possibly be explained by the unusual metallacyclic nature of **82**.

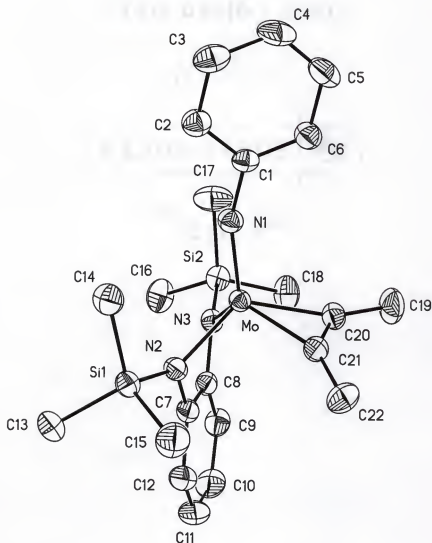


Figure 4-17. Thermal ellipsoid plot of **75** (50% probability thermal ellipsoids). Selected bond lengths (Å) and angles (°): Mo-N(1) 1.7511(17), Mo-N(2) 2.0314(16), Mo-N(3) 2.0014(16), Mo-C(20) 2.056(2), Mo-C(21) 2.052(2), C(20)-C(21) 1.297(3), C(20)-C(21)-C(22) 140.2(2), C(21)-C(20)-C(19) 137.3(2), C(1)-N(1)-Mo 159.22(15), N(3)-Mo-N(2) 84.41(7), N(3)-Mo-C(20) 100.89(7), N(2)-Mo-C(21) 93.90(7).

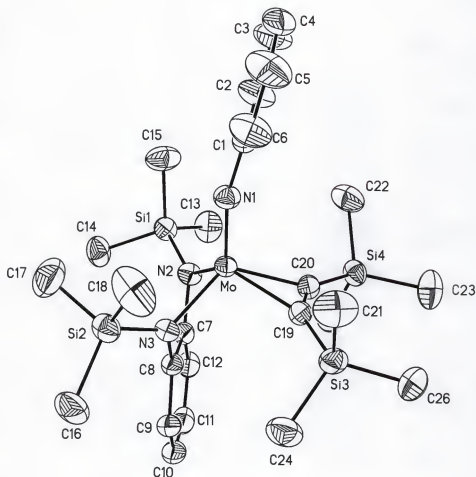


Figure 4-18. Thermal ellipsoid plot of **80** (50% probability thermal ellipsoids). Selected bond lengths (Å) and angles (°): Mo-N(1) 1.745(2), Mo-N(2) 2.022(2), Mo-N(3) 2.009(2), Mo-C(20) 2.079(3), Mo-C(19) 2.078(3), C(19)-C(20) 1.305(4), C(20)-C(19)-Si(3) 147.2(2), C(19)-C(20)-Si(4) 148.6(2), C(1)-N(1)-Mo 164.6(2), N(2)-Mo-N(3) 84.51(9), N(2)-Mo-C(20) 98.96(10), N(3)-Mo-C(19) 96.62(10). Complex **80** crystallized with two molecules in the asymmetric unit and only one is shown here.

Table 4-2. X-ray data^a for crystal structures **75** and **80**

	75	80
Chemical formula	C ₂₂ H ₃₃ N ₃ MoSi ₂	C ₂₆ H ₄₅ N ₃ MoSi ₄
Formula weight	491.63	607.95
Crystal system	Triclinic	Triclinic
Space group	$P\bar{1}$	$P\bar{1}$
$\mu(\text{Mo-K}\alpha)$ (mm ⁻¹)	0.632	0.555
a (Å)	10.7483(5)	12.9348(7)
b (Å)	10.8358(6)	14.2840(7)
c (Å)	12.3049(6)	19.643(1)
α	77.788(1)	79.211(1)
β (°)	64.377(1)	70.947(1)
γ	77.812(1)	89.995(1)
V_c (Å ³)	1251.2(1)	3362.6(3)
Z	2	4
Θ_{max} °	27.50	27.50
Total reflections	8547	22991
Uniq. reflections	5542	15040
$R(\text{int})$	0.0357	0.0505
R_1 [$I \geq 2\sigma(I)$ data] ^b	0.0275	0.0426
wR_2 (all data) ^c	0.0742	0.1233
Larg. diff. peak, hole	0.377, -0.366	0.499, -0.579

^aObtained with monochromatic Mo K α radiation ($\lambda = 0.71073$ Å) at 173 K. ^b $R_1 = \sum |F_o| - |F_c| / \sum |F_o|$. ^c $wR_2 = \{\sum [w(F_o^2 - F_c^2)^2] / \sum [w(F_o^2)^2]\}^{1/2}$.

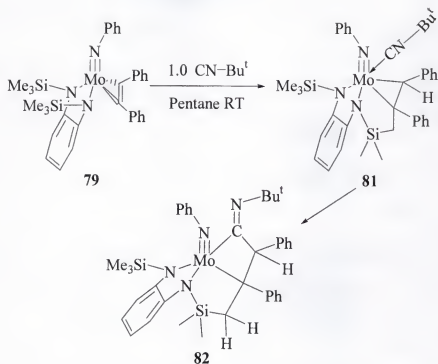


Figure 4-19. Reaction of $[(\text{Mo}(\text{NPh})-\eta^2-(\text{PhCCPh})(o-(\text{Me}_3\text{SiN})_2\text{C}_6\text{H}_4)]$ (**79**) with Bu^tNC : formation of **82**

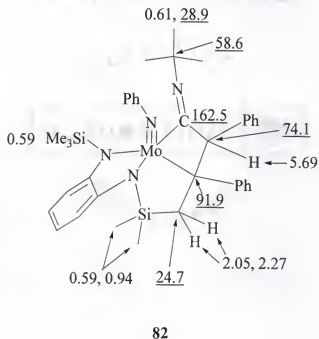


Figure 4-20. Proposed structure of **82** showing selected carbon (underlined) and proton chemical shifts, assigned by NMR spectroscopy

We have no concrete evidence for a possible mechanism but propose that C-H activation of the SiMe_3 ligand is an important step in the reaction and could be responsible for generating a species such as **79a** (Figure 4-21). Intermediate **79a** could come about by insertion of diphenyl acetylene into a metal hydride produced by C-H activation of the SiMe_3 methyl group. A γ -abstraction process could also be responsible for the formation of **79a**. The exact role of Bu^tNC in this reaction is unknown, but it most likely promotes C-H activation. Related Lewis base promoted α , β , and γ -abstraction processes have been observed with the analogous tungsten system, as discussed in Chapter 1.⁴²⁻⁴⁵ Reductive elimination from **79a** would result in the formation of **81**, and insertion of Bu^tNC into the metallacyclopropane function of **81** can give **82**. Full characterization of **81** and **82** will contribute to the formulation of a more complete mechanism.

Summary

To our knowledge, reports of other metal imido-diamido alkyne complexes are nonexistent. The disubstituted alkyne complexes **75**, **79**, and **80** have interesting bonding properties, a result of the π -loaded system. A detailed DFT study aimed at understanding the bonding in these complexes is underway in our group, as are reactions involving monosubstituted and unsymmetrically disubstituted alkyne reactants. Initial reactivity studies have shown that complex **79** is a reactive species. We hope to further develop this chemistry in the future.

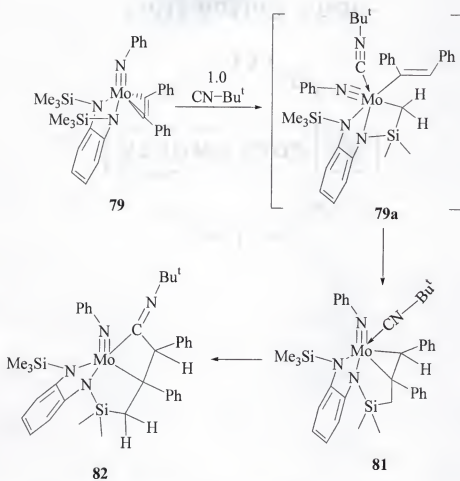


Figure 4-21. Proposed mechanism for the formation of **82**

CHAPTER 5
REACTIVITY OF MOLYBDENUM OLEFIN AND ARENE COMPLEXES WITH
UNSATURATED SUBSTRATES

**Reaction of Molybdenum Olefin Complexes with Imines: The Synthesis of
Molybdenum Imido-Diamido η^2 -Imine Complexes**

Current synthetic methodologies affording η^2 -imine complexes (azametallacyclopropanes) consist of C-H activation from methylmetallocene amides,^{120,121} rearrangements of iminoacyl complexes,^{5,122} reaction between $\text{Cp}^*_2\text{ZrH}_2$ and ArNC ,¹²³ reduction of a low-valent complex with phosphazene,¹²⁴ and various *in situ* methods of η^2 -imine complex formation.¹²⁵ Isolation and characterization of η^2 -imine complexes generated by direct reaction of imines with metal reductants has, for the most part, been unsuccessful, and although two recent reports detail the isolation and characterization of ytterbium¹²⁵ and tantalum¹²⁶ η^2 -imine complexes via such direct methods, examples with other early metals are, to our knowledge, nonexistent. We report herein structural characterization and direct synthesis of molybdenum (IV) η^2 -imine complexes obtained by treatment of the molybdenum (IV) olefin complex, **38**, with appropriate aldimines and ketimines. Furthermore, aldimine reductive coupling products are isolated for less sterically demanding aldimines.

Reaction of the aryl amine derived aldimine $\text{PhN}=\text{C}(\text{H})\text{Ar}$ ($\text{Ar} = \text{C}_6\text{H}_4\text{-}p\text{-OMe}$) and ketimine $\text{PhN}=\text{C}(\text{Me})\text{Ph}$ with **38** afforded the η^2 -imine complexes $[\text{Mo}(\text{NPh})\text{-}\eta^2\text{-PhN}=\text{C}(\text{H})\text{Ar}(o\text{-(Me}_3\text{SiN)}_2\text{C}_6\text{H}_4)]$ ($\text{Ar} = \text{C}_6\text{H}_4\text{-}p\text{-OMe}$) (**83**) and $[\text{Mo}(\text{NPh})\text{-}\eta^2\text{-PhN}=\text{C}(\text{Me})\text{Ph}(o\text{-(Me}_3\text{SiN)}_2\text{C}_6\text{H}_4)]$ (**84**) as green crystals in 70% isolated yield (Figure

5-1). The molecular structure of **84** was determined by an X-ray crystallographic study, and selected bond distances and angles for **84** are shown in Figure 5-2. The crystal data and details of the structure refinement are summarized in Table 5-1.

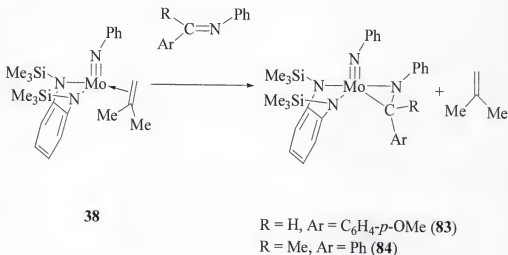


Figure 5-1. Synthesis of η^2 -imine complexes **83** and **84**

Complex **84** adopts a five-coordinate square pyramidal geometry with the imido ligand occupying the apical position. The short imido Mo(1)-N(3) bond length of 1.736(2) Å is typical of a Mo-N triple-bond interaction.^{11,27,47,51} The Mo(1)-N-(4), Mo(1)-N(2), and Mo(1)-N(1) bond lengths of 1.944(2) Å, 2.009(2) Å, and 1.996(2) Å, respectively, are all consistent with Mo-N single bonds.^{27,46,51,56,91} The C(31)-centered bond angles of the imine fragment are all less than 120° and support a considerable amount of azametallacyclopropane character in **84**, as does the N(4)-C(31) bond length of 1.414(3) Å.¹²⁷ The imine fragment C-N bond length for **84** is similar to the related bond length of 1.421(7) Å for the azatitanacyclopropane complex [Ti(OAr)₂(Bu^tNCCH₂Ph) (Py-*p*-Ph)] (Ar = 2,6-di-*tert*-butylphenyl),^{122(b)} but much longer than that of the zirconium azametallacyclopropane complex [Cp₂Zr(PhC(H)NPh)(thf)] (1.375(7) Å).^{120(b)}

Table 5-1. X-ray data^a for crystal structures **84**, **85**, and **88**

	84	85	88
Chemical formula	C ₃₂ H ₄₀ N ₄ MoSi ₂	C ₃₈ H ₅₃ N ₅ MoO ₂ Si ₂	C ₂₅ H ₄₁ N ₃ MoOSi ₂
Formula weight	632.80	763.97	551.73
Crystal system	Monoclinic	Monoclinic	Triclinic
Space group	<i>P</i> 2 ₁ / <i>c</i>	<i>P</i> 2 ₁	<i>P</i> $\bar{1}$
$\mu(\text{Mo-K}\alpha)$ (mm ⁻¹)	0.509	0.440	0.569
<i>a</i> (Å)	9.8565(5)	9.9600(5)	9.8841(7)
<i>b</i> (Å)	18.8443(8)	19.0705(9)	11.2646(7)
<i>c</i> (Å)	17.9089(8)	10.2628(5)	14.766(1)
α	-	-	101.370(1)
β (°)	104.6520(10)	97.351(1)	96.272(1)
γ	-	-	115.921(1)
<i>V_c</i> (Å ³)	3218.2(3)	1933.2(2)	1413.6(2) Å
<i>Z</i>	4	2	2
Θ_{max} °	26.50	27.49	27.50
Total reflections	6495	13886	9474
Uniq. reflections	6495	8413	6236
<i>R</i> (int)	na	0.0437	0.0620
<i>R</i> ₁ [<i>I</i> ≥ 2σ(<i>I</i>) data] ^b	0.0431	0.0420	0.0380
w <i>R</i> ₂ (all data) ^c	0.0831	0.0843	0.1090
Larg. diff. peak, hole	0.348, -0.404	0.345, -0.413	0.481, -0.789

^aObtained with monochromatic Mo K α radiation ($\lambda = 0.71073$ Å) at 173 K. ^b $R_1 = \sum |F_o| - |F_c| / \sum |F_o|$. ^c $wR_2 = \{\sum [w(F_o^2 - F_c^2)^2] / \sum [w(F_o^2)^2]\}^{1/2}$.

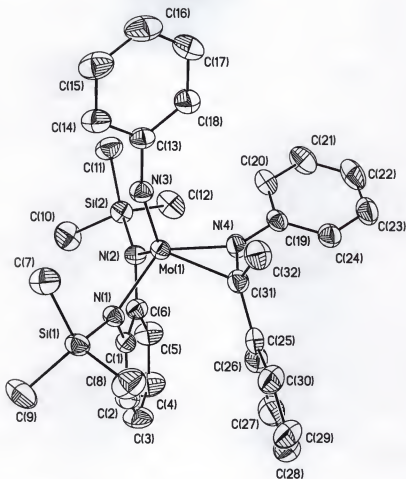


Figure 5-2. Thermal ellipsoid plot of **84** (40% probability thermal ellipsoids). Selected bond lengths (Å) and angles (°): Mo(1)-N(1) 1.996(2), Mo(1)-N(2) 2.009(2), Mo(1)-N(3) 1.736(2), Mo(1)-N(4) 1.944(2), Mo(1)-C(31) 2.200(3), N(3)-C(13) 1.409(3), N(4)-C(31) 1.414(3), C(31)-C(32) 1.518(4), Mo(1)-N(3)-C(13) 163.0(2), N(2)-Mo(1)-N(1) 85.28(9), N(4)-Mo(1)-C(31) 39.29(9), N(2)-Mo(1)-N(4) 100.09(9), N(1)-Mo(1)-C(31) 99.20(9), N(4)-C(31)-Mo(1) 60.55(13), N(4)-C(31)-C(32) 116.9(2), N(4)-C(31)-C(25) 116.6(2), C(32)-C(31)-C(25) 116.2(2).

The ^1H NMR spectra of **83** and **84** are highly fluxional at 20°C. We have carried out variable temperature ^1H NMR studies on **84**. At 20°C considerable broadening of resonances in the aromatic region are observed in the ^1H NMR spectrum. These resonances become well defined, 1.0 proton peaks at -65°C. We propose that the fluxionality observed is a result of the hindered rotation of the phenyl ring attached to the imine carbon. This hindered rotation can produce inequivalent *ortho*-phenyl protons that

will appear as doublets integrating for 1.0 H in the aromatic region of the ^1H NMR spectrum. We observe one of these doublets at 5.18 ppm ($^3J_{\text{C-H}} = 8.0$ Hz) in the ^1H NMR spectrum. This proton is shifted significantly upfield due to the ring current of the nearby (*o*-(Me_3SiN) $_2\text{C}_6\text{H}_4$) ligand. We have observed similar upfield shifted resonances for the aromatic protons of the styrene fragment for a related styrene complex.⁴⁶ Furthermore, analysis of the space-filling model of **84** shows a sterically congested environment around the phenyl group in question, supporting our claims of hindered phenyl group rotation. Two resonances for the SiMe_3 groups are observed from -65°C to 70°C by ^1H NMR spectroscopy, consistent with our interpretation of the dynamic properties of **84** in solution. The imine methyl resonance is observed as a broad signal at 2.34 ppm in the ^1H NMR spectrum of **84** at 20°C . This broad methyl resonance sharpens considerably at low (-65°C) and high (70°C) temperatures, which is also consistent with our interpretation. The same dynamics are observed for **83** in solution, as observed by variable temperature ^1H NMR spectroscopy.

Complete conversion of **83** to the corresponding organic amine (PhNHCH_2Ar) was observed by ^1H NMR spectroscopy upon exposure of a solution of **83** to an atmosphere of 15 psi. H_2 gas at 20°C over a 1 week period. Unfortunately, no catalytic activity was observed upon treatment of **83** with excess imine under low pressures (ca. 15 psi.) of H_2 gas. Complexes **83** and **84** did not react with acetone, 2-butyne, or diphenyl acetylene as determined by ^1H NMR spectroscopy.

The reaction of aldimines, derived from less hindered primary amines, with **38** afforded molybdenum (VI) imido (bis)diamido complexes **85** and **86** from reductive imine coupling (Figure 5-3). Complexes **85** and **86** were isolated in 75% yield from cold

pentane/toluene solutions. Interestingly, only the *rac*-coupled form of the metal complexes were isolated, as ascertained from ^1H and ^{13}C NMR spectroscopy.

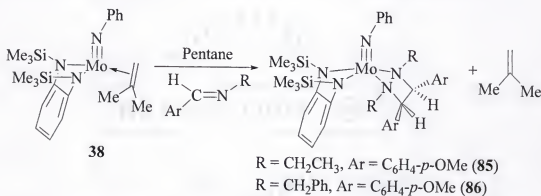


Figure 5-3. Reductive coupling of imines

An X-ray crystallographic study was performed on a single crystal of **85**. The molecular structure and selected bond lengths and angles of **85** are shown in Figure 5-4. The crystal data and details of the structure refinement are summarized in Table 5-1. The overall geometry around molybdenum is extremely distorted and is not best described as trigonal bipyramidal or square pyramidal. Distorted five-coordinate complexes such as this one are best described using a method introduced by Reedijk that relies on calculating a τ -value for the complex in question.¹²⁸ The τ -value can then be used to assign the structure a position between the two extremes in geometry, trigonal bipyramidal and square planar. A τ -value of 0.0 corresponds to a pure square pyramidal structure, while a τ -value of 1.0 corresponds to a true trigonal bipyramid. The τ -value for **85** is 0.47. Thus, the structure of **85** is best described as occupying a position half way between trigonal bipyramidal and square planar. The Mo-N(1) bond length of 1.754(3) Å is consistent with a molybdenum nitrogen triple-bond interaction.^{11,27,47,51} The Mo-N(2), N(3), N(4) and N(5) amide bond lengths of 2.008(3) Å, 2.065(3) Å, 1.996(3) Å, and 2.021(3) Å, respectively, are within the range expected for Mo-N single bonds.^{27,46,51,56,91}

GHMBC and GHMQC spectra. The NMR properties of **86** are similar to those of **85**. The four inequivalent benzyl methylene protons appear as doublets with 15 Hz geminal coupling constants and resonate at 4.51 ppm, 4.64 ppm, 5.45 ppm, and 5.51 ppm in the ^1H NMR spectrum. The β -protons of the newly formed diamide resonant at 4.75 ppm and 4.50 ppm, and although these protons are inequivalent, no coupling is observed at 500 MHz in the ^1H NMR spectrum.

In summary, we have demonstrated that chelate-supported Mo(IV) η^2 -imine complexes are easily prepared via displacement of olefin from **38** upon reaction with N-aryl imines. In contrast, imine reductive coupling products are observed for sterically less demanding imines.

Reaction of Molybdenum Olefin Complexes with Acetone and Aldehydes: The Synthesis of Oxametallacyclopentanes

Transition metal-mediated reductive coupling of a pair of unsaturated molecules can result in the formation of a metallacyclopentane with concomitant formation of a carbon-carbon bond (Figure 5-5). Reactions of this type performed with in situ-generated early metal metallocenes (e.g., Cp_2Ti , Cp_2Zr , and Cp_2Hf) and related reduced metal species have been extensively explored.¹²⁹ Various protocols have been developed for selective metallacycle cleavage, giving rise to an organic product. Although a new organic product is formed, a byproduct metallic species in the wrong oxidation state to effect further reductive coupling is generated during these proteolytic or oxidative cleavage processes. Recent developments in this field that circumvent this problem involve the titanium-catalyzed cyclization of enones mediated by silanes¹³⁰ and titanium-based applications toward the synthesis of γ -butyrolactones.¹³¹

Treatment of the molybdenum olefin complexes discussed above with ketones and aldehydes results in coupling of the metal-olefin fragment and the carbonyl moiety, giving rise to oxametallacyclopentanes (Figure 5-6). The synthesis and characterization of some representative metallacycles are discussed here.

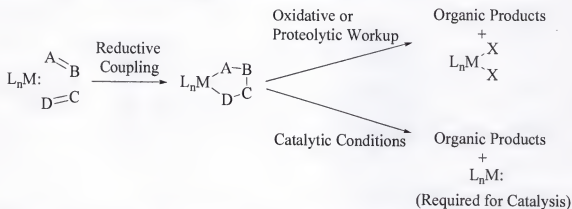


Figure 5-5. General scheme for the reductive coupling of organic molecules

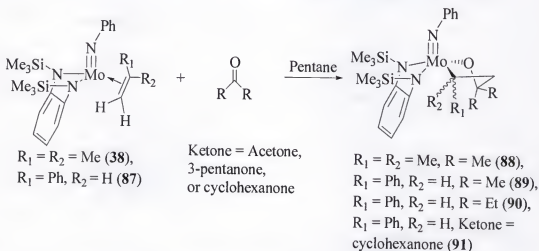


Figure 5-6. Synthesis of oxametallacyclopentanes

Addition of acetone to a solution of **38** in pentane resulted in the exclusive formation of $[(\text{Mo}(\text{NPh})(\text{C}(\text{Me})_2\text{CH}_2\text{C}(\text{Me})_2\text{O})(o\text{-(Me}_3\text{SiN)}_2\text{C}_6\text{H}_4)]$ (**88**), as determined by ^1H and ^{13}C NMR spectroscopy. Single crystals of **88** were grown from cold toluene/pentane solutions.

A single crystal X-ray study of **88** reveals the square pyramidal geometry about molybdenum (Figure 5-7). The crystal data and details of the structure refinement are summarized in Table 5-1. The regioselectivity of this particular reaction, with respect to the formation of the metallacycle, became quite clear upon examination of the thermal ellipsoid plot of **88**. The methylene carbon (C(20)) has taken up position between both tertiary carbons C(19) and C(21). The propensity for molybdenum to form Mo-O bonds, along with the minimization of steric repulsion between the methyl groups of acetone and the isobutene ligand in **38** during the reaction, explain the observed regioselectivity. The Mo-N(1) distance of 1.7348(18) Å is consistent with a metal-nitrogen triple bond and the Mo-N(2) and N(3) amide distances of 2.0513(17) Å and 2.0072(18) Å, respectively, are within the range expected for Mo-N single bonds. The Mo-O(1) distance of 1.9344(15) Å and the Mo-C(19) distance of 2.209(2) Å are both consistent with metal-atom single bonds.¹³²

When acetone was added to a dark green solution of **87** in pentane, the solution turned dark red in color. Concentration of the pentane solution under reduced pressure afforded a red solid. Solution ¹H NMR spectroscopy of this sample confirmed the existence of only one metallacycle-containing product, [(Mo(NPh)(C(H)PhCH₂C(Me)₂O) (*o*-(Me₃SiN)₂C₆H₄)] (**89**). Pure **89** was obtained via recrystallization from pentane at -30°C, and the stereochemistry of **89** was elucidated by NMR spectroscopy (GHMQC, GHMBC, and NOESY). The proposed structure for **89** is illustrated in Figure 5-8, and the proton chemical shifts have been assigned. Complex **89** adopts a five-coordinate square pyramidal geometry very similar to that of **88**. Of interest in **89** is the position of the C(H)Ph fragment, which was once part of the coordinated styrene in **87**. The carbon

atom of this fragment is bound to the molybdenum center, and the phenyl group occupies a *syn* position in reference to the phenyl imido group. Steric constraints during the reaction of **87** with acetone most likely dictate the ultimate configuration of this metallacycle. As **89** is the only diastereomer formed, this reaction does proceed with high diastereomeric excess.

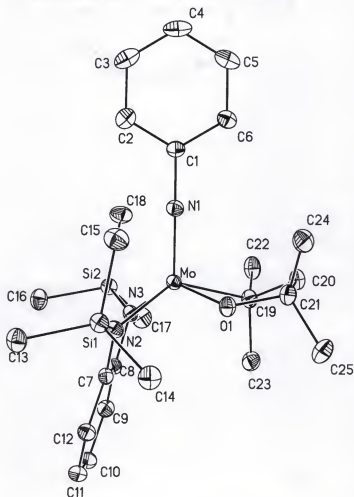


Figure 5-7. Thermal ellipsoid plot of **88** (30% probability thermal ellipsoids). Selected bond lengths (Å) and angles (°): Mo-N(1) 1.7348(18), Mo-O(1) 1.9344(15), Mo-N(3) 2.0072(18), Mo-N(2) 2.0513(17), Mo-C(19) 2.209(2), O(1)-C(21) 1.432(3), C(19)-C(20) 1.541(3), C(20)-C(21) 1.534(3), Mo-C(19)-C(20) 103.80(14), Mo-O(1)-C(21) 122.89(13), C(22)-C(19)-C(23) 109.7(2), C(24)-C(21)-C(25) 109.7(2), C(19)-C(20)-C(21) 111.91(18).

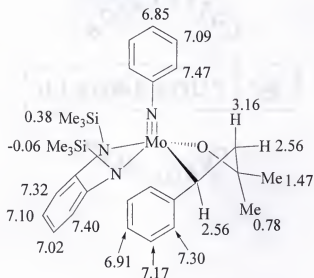


Figure 5-8. Structural assignment of **89** including assigned proton chemical shifts

Compounds **90** and **91** were not fully characterized by NMR spectroscopy in terms of stereochemistry. Their structures are, however, most likely similar to **89**, and the reactions proceed with high diastereomeric selectivity as determined by ^1H NMR spectroscopy.

The reaction of **38** with *p*-anisaldehyde results in the formation of only one metallacyclic product, **92**. Although not yet fully characterized via NMR techniques, only one diastereomer is formed in this particular reaction.

Reaction of **37** or **87** with aldehydes gives rise to oxametallacyclopentanes. The ^1H NMR spectra of these reaction mixtures are complex due to the formation of multiple diastereomers, indicating the low diastereomeric selectivity of reactions between monosubstituted olefin complexes and aldehydes. Because of this low selectivity, these reactions were not investigated further.

Reactivity of Arene Complexes with Acetone

We have observed differing reactivity between arene complexes **40** and **44** with acetone. The benzene complex **40** reacts with acetone affording η^2 -ketone complex **93**

and **94** in a 1:2 ratio (Figure 5-9). Complex **94** most likely arises as a result of a C-H activation pathway. In sharp contrast, reaction of **44** with acetone produces only **93**.

The structures of **93** and **94** have been proposed based on simple ^1H and ^{13}C NMR data. A resonance at 90.5 ppm in the ^{13}C NMR spectrum of **93** is observed at 20°C and has been assigned to the carbon of an η^2 -coordinated acetone moiety. The acetone methyl group protons of **93** are observed as a broad resonance at 1.01 ppm in the ^1H NMR spectrum, and the SiMe_3 protons resonate at 0.49 ppm in the same spectrum. Characteristic resonances in the ^1H NMR spectrum of **94** are the septet at 4.57 ppm (assigned to H_a , $^3J_{\text{C-H}} = 6.0$ Hz) and the two doublets at 0.76 ppm and 1.44 ppm ($^2J_{\text{C-H}} = 12.5$ Hz), assigned to H_b and H_c . The methyl groups that couple to H_a are observed as overlapping doublets at 1.10 ppm ($^3J_{\text{C-H}} = 6.0$ Hz). Complete characterization of these products will be required.

We can only assume that **40** is in equilibrium with a metallated hydride species (**95**), which reacts with acetone giving **94** (Figure 5-10). In contrast, **44** is not in equilibrium with a metallated species due to steric constraints.

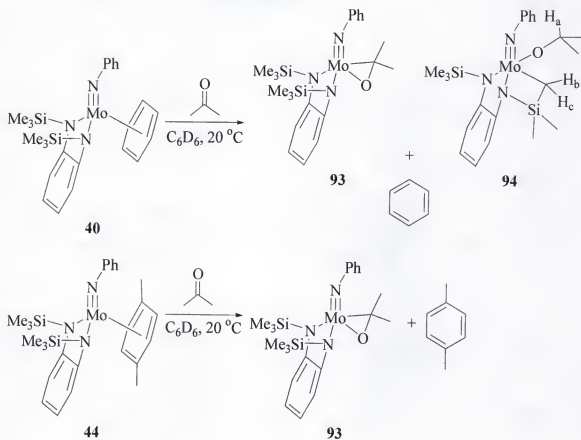


Figure 5-9. Reaction of arene complexes with acetone

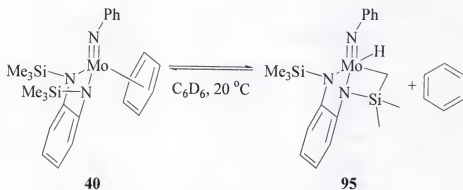


Figure 5-10. Possible equilibrium between an arene complex and a metallated species

CHAPTER 6 EXPERIMENTAL DATA

General Methods

All reactions were conducted under a dry argon atmosphere using standard Schlenk techniques, and all compounds were handled in a nitrogen-filled dry box. All solvents were distilled under nitrogen from sodium or sodium benzophenone ketyl or passed over activated alumina, stored over molecular sieves, and degassed prior to use.

NMR spectra were obtained on a Varian Gemini 300, VXR 300, or Mercury 300 instrument with C_6D_6 , C_7D_8 , or $CDCl_3$ as solvents, as noted, and referenced to residual solvent peaks. A Varian Inova 500 equipped with an indirect detection probe was used as indicated for the GHMQC,¹³³ GHMBC,¹³⁴ and NOESY¹³⁵ experiments. The full X-ray diffraction data for all compounds can be obtained by contacting Dr. Khalil A. Abboud at 352-392-5948.

Density functional theory (DFT) calculations were performed using the Gaussian 98W program package.⁵³ Structures were optimized using Becke's hybrid three-parameter functional (B3LYP). The Los Alamos effective core potential (ECP) plus a standard double-zeta basis set (LANL2DZ) was used to describe the molybdenum and silicon atoms.¹³⁶ Dunning/Huzinaga full double zeta basis set (D95) was used to describe all other atoms.¹³⁶ Using the same level of theory and basis set, vibrational frequency calculations and full population analyses were performed on the stationary points to negate transition structures, to determine thermal/zero-point energies, and to analyze (MOs).^{54,55} Thermochemical information at temperature $T = 298.15$ K and $P =$

1.00 atm was obtained using frequencies without scaling. Single-point energies for each structure were calculated using the B3LYP level of theory and the LANL2DZ basis set, with restricted wave functions again being used for the closed-shell species.

Complex **19** was synthesized according to published procedure, and crystals were grown from a cold toluene/pentane solution.²⁷ The synthesis, details of X-ray structure data, and characterization of **52** and **53** have been reported elsewhere and are included in this Chapter to reflect recent updates.^{66,91} Ligand **58** was synthesized from the imidazolium salt according to standard procedure.⁶⁷ The imidazolium salt was purchased from Strem Chemicals.

Synthesis and Characterization

[Mo(NPh)(Py)₂(*o*-(Me₃SiN)₂C₆H₄)] (**47**)

A representative synthesis of **47**: To a green pentane solution of freshly generated **38** (1.07 g, 2.18 mmol) was added excess pyridine (0.51 g, 6.54 mmol). Upon addition of pyridine, **47** precipitated from solution and was isolated by filtration in 90% yield as a purple powder. ¹H NMR (C₆D₆, 18°C): δ 0.38 (SiMe₃, 18 H), 5.93 (t of t, 7.5 Hz, 1.0 Hz, pyridine *para* protons), 6.19 (t, br, 6.0 Hz, pyridine *meta* protons, 4 H), 6.7 (very br, pyridine *ortho* protons, 2 H), 6.90 (t of t, 7.0 Hz, 1.0 Hz, *para* proton), 7.07 (t of t, 8 Hz, 1 Hz, *meta* protons), 7.12 (m, *o*-(Me₃SiN)₂C₆H₄ protons, 2 H), 7.24 (d, *ortho* protons), 7.51 (m, *o*-(Me₃SiN)₂C₆H₄ protons, 2 H), 8.56 (very br, pyridine *ortho* protons, 2 H). ¹H NMR (C₇D₈, -55°C): δ 0.41 (SiMe₃, 18 H), 5.88 (t, 7 Hz, pyridine *para* protons, 2 H), 6.12 (t, 7 Hz, pyridine *meta* protons, 2 H), 6.18 (t, 7 Hz, pyridine *meta* protons, 2 H), 6.52 (d, 5.5 Hz, pyridine *ortho* protons, 2 H), 6.9-7.2 (ov, m, 7 H), 7.54 (m, *o*-(Me₃SiN)₂C₆H₄ protons, 2 H), 8.64 (d, 5.5 Hz, pyridine *ortho* protons, 2 H). ¹³C{¹H} NMR (C₆D₆, 18°C):

δ 5.0, 117.1, 117.6, 122.7, 123.2, 124.0, 129.0, 130.0, 143.5 (br), 152.7, 160.4. Anal. Calcd for $C_{28}H_{37}N_5MoSi_2$: C, 56.45; H, 6.26; N, 11.76. Found: C, 56.32; H, 6.34; N, 11.53.

[Mo(NPh)*trans*(Py)₂(CO)(*o*-(Me₃SiN)₂C₆H₄)] (48)

To a degassed flask containing a toluene solution of **47** (0.200 g, 0.336 mmol) was added carbon monoxide gas (ca. 15 psi). Concentration of this solution under reduced pressure afforded **48** as a red solid in 89% yield. 1H NMR (C_6D_6 , 20°C): δ 0.32 (SiMe₃, 9 H), 0.37 (SiMe₃, 9 H), 6.30 (t, 6.5 Hz, pyridine *meta* protons, 4 H), 6.54 (t, 7.5 Hz, 2 H), 6.7-7.2 (ov, m, 7 H), 7.40 (d, 7.0 Hz, phenyl imido *ortho* protons, 2 H), 8.69 (d, 5.0 Hz, pyridine *ortho* protons, 4 H). $^{13}C\{^1H\}$ NMR (C_6D_5Br , 18°C): 3.4, 3.7, 114.4, 117.4, 117.8, 119.5, 123.3, 124.6, 128.4, 136.7, 149.6, 151.2, 152.8, 156.0, 268.7, one resonance obscured by solvent. IR: 1913 cm^{-1} .

Imido-Bridged, Bimetallic 49

A toluene solution of **47** (0.200 g, 0.336 mmol) was heated to 90°C in a sealed ampule for 2 h. Concentration of the reaction mixture under reduced pressure afforded **49** as a black solid in 92% yield. 1H NMR (C_6D_6 , 18°C): δ 0.00 (SiMe₃, 9 H), 0.11 (SiMe₃, 9 H), 0.23 (SiMe₃, 9 H), 0.31 (SiMe₃, 9 H), 6.2 (br, 1 H), 6.45 (t, 7.0 Hz, 1 H), 6.6-7.0 (ov, m, 9 H), 7.33 (t, 7.5 Hz, 2 H), 7.6 (m, 2 H), 7.94 (d, 7.5 Hz, 2 H). $^{13}C\{^1H\}$ NMR ($CDCl_3$, 18°C): δ 2.2, 3.0, 3.1, 3.7, 116.8, 118.5, 118.6, 118.7, 118.8, 121.2, 123.0, 123.3, 123.6, 124.4, 126.0, 126.6, 127.4, 128.2, 132.8, 137.5, 150.0, 150.9, 151.8, 152.7, 160.1, 161.0, 169.9.

[Mo(NPh)(P(OMe)₃)₃(*o*-(Me₃SiN)₂C₆H₄)] (50)

A representative synthesis of **47**: To a green pentane solution of freshly generated **38** (0.85 g, 1.72 mmol) was added excess P(OMe)₃ (0.81 mL, 6.88 mmol). Upon addition of P(OMe)₃ red-brown **50** precipitated from solution and was isolated by filtration in 83% yield. Complex **50** is highly unstable and decomposes rapidly in solution and in the solid-state. ¹H NMR (C₆D₆, 18°C): δ 0.62 (SiMe₃, 18 H), 3.20 (d, 10 Hz, P(OMe)₃, 27 H), 6.85 (m, phenyl imido *para* proton), 7.02 (m, 4 H), 7.48 (m, 4 H). ¹³C{¹H} NMR (C₆D₆, 18°C): δ 5.3, 50.7, 117.8, 119.5, 124.6, 125.6, 128.3, 151.5, 157.8. ³¹P{¹H} NMR (C₆D₆, 18°C): 136.0 (br), 196.0 (br).

[Mo(NPh)(P(OMe)₃)₂CO(*o*-(Me₃SiN)₂C₆H₄)] (51)

To a degassed flask containing a toluene solution of **50** (0.800 g) was added carbon monoxide gas (ca. 15 psi). Concentration of this solution under reduced pressure afforded **51** as a red solid in 87% yield. ¹H NMR (C₆D₆, -50°C): δ 0.66 (SiMe₃, 9 H), 0.75 (SiMe₃, 9 H), 3.03 (P(OMe)₃, 18 H), 6.79 (m, 2 H), 7.05 (ov, m, 4 H), 7.44 (d, 8 Hz, 1 H), 7.54 (d, 8 Hz, 2 H). ¹³C{¹H} NMR (C₆D₆, 18°C): δ 4.8 (br), 51.6, 113.7 (br), 119.1 (br), 125.0, 125.8, 129.2, 148.0, 157.3, 250.9. ³¹P{¹H} NMR (C₇D₈, -50°C): δ 131.7. IR: 1959 cm⁻¹.

[Mo(NPh)(PMe₃)₃(*o*-(Me₃SiN)₂C₆H₄)] (52)

To a stirring pentane solution of **37** (1.0 g, 1.83 mmol) was added PMe₃ (0.57 mL, 5.53 mmol). A purple solid precipitated from solution and was isolated by filtration and washed twice with 10 mL of pentane, affording analytically pure **52**. Complex **52** is best stored at -30°C under an inert atmosphere. X-ray quality crystals were grown in toluene at -30°C. ¹H NMR (C₇D₈, -50°C): δ 0.35 (br, SiMe₃, 9 H), 0.61 (br, SiMe₃, 9 H), 0.98 (br,

PMe_3 , 18 H), 1.25 (d, br, 5 Hz, PMe_3 , 9 H), 6.7-7.1 (ov, m, 8 H), 7.47 (d, 8 Hz, 1 H).

$^{31}\text{P}\{^1\text{H}\}$ NMR: -8.9 (t, 5 Hz), -10.6 (br), -11.3 (br). Anal. Calcd for $\text{C}_{27}\text{H}_{54}\text{MoN}_3\text{P}_3\text{Si}_2$: C, 48.71; H, 8.18; N, 6.31. Found: C, 48.54; H, 8.19; N, 8.19.

$\text{Mo}(\text{NPh})(\text{PMe}_3)_3(o\text{-(Me}_3\text{SiN)}(\text{NH})\text{C}_6\text{H}_4)$ (53**)**

A toluene solution of **60** was warmed to 20°C and stirred for 2 h. Solvent was removed from the resulting purple solution under reduced pressure, giving crude **53**, as a solid. Analytically pure **53** was obtained by washing the crude solid with pentane. ^1H NMR (C_7D_8 , -70°C): δ 0.75 (ov, PMe_3 and SiMe_3 , 27 H), 0.98 (d, 7 Hz, PMe_3 , 9 H), 3.84 (d, br, 10 Hz, N-H), 6.7-7.2 (ov, m, 8 H), 7.58 (d, 1 H). $^{13}\text{C}\{^1\text{H}\}$ NMR (C_6D_6 , 20°C): 5.2 (SiMe_3), 19.4 (br, PMe_3), 113.7, 113.8, 116.3, 117.0, 122.4, 125.6, 129.1, 150.0, 152.2, 157.9. $^{31}\text{P}\{^1\text{H}\}$ NMR (C_7D_8 , -70°C): 11.4 (t, 9 Hz), 12.0 (d, 9 Hz). Anal. Calcd for $\text{C}_{24}\text{H}_{46}\text{MoN}_3\text{P}_3\text{Si}$: C, 48.56; H, 7.81; N, 7.08. Found: C, 48.24; H, 7.63; N, 7.37.

$[\text{Mo}(\text{NPh})(\text{PMe}_3)_2\text{CO}(o\text{-(Me}_3\text{SiN)}_2\text{C}_6\text{H}_4)]$ (54**)**

To a degassed flask containing a toluene solution of **52** (0.800 g) was added carbon monoxide gas (ca. 15 psi). Concentration of this solution under reduced pressure afforded **54** as a red solid in 84% yield. ^1H NMR (C_6D_6 , 20°C): δ 0.51 (SiMe_3 , 9 H), 0.60 (SiMe_3 , 9 H), 0.86 (PMe_3 , 18 H), 6.75 (ov, m, 2 H), 6.95 (ov, m, 5 H), 7.10 (d, 8 Hz, 2 H), 7.34 (d, 8 Hz, 1 H). $^{13}\text{C}\{^1\text{H}\}$ NMR (C_6D_6 , 18°C): δ 5.0, 6.3, 16.1, 113.2, 118.2, 118.9, 120.6, 124.2, 124.5, 129.4, 150.2, 152.3, 156.3, 260.2. $^{31}\text{P}\{^1\text{H}\}$ NMR (C_6D_6 , 18°C): δ -15.2. IR: 1925 cm^{-1} .

$[\text{Mo}(\text{NPh})(\text{PMe}_2\text{Ph})_2(o\text{-(Me}_3\text{SiN)}_2\text{C}_6\text{H}_4)]$ (55**)**

A representative synthesis of **55**: To a green pentane solution of freshly generated **37** (1.53 g, 3.18 mmol) was added excess PMe_2Ph (1.76 g, 12.72 mmol). Upon addition

of PMe_2Ph , green **55** precipitated from solution and was isolated by filtration in 65% yield. ^1H NMR (C_6D_6 , -65°C): δ 0.45 (SiMe_3 , 18 H), 0.94 (br, PMe_2Ph , 12 H), 7.0 (ov, m, 17 H), 7.31 (d, 8 Hz, 2 H). Selected $^{13}\text{C}\{^1\text{H}\}$ NMR (C_7D_8 , -65°C): δ 4.9, 119.0, 121.1, 124.3, 125.1, 131 (ov resonances), 138 (ov), 149.9, 159.2. $^{31}\text{P}\{^1\text{H}\}$ NMR (C_6D_6 , 20°C): δ 28.2.

$[\text{Mo}(\text{NPh})(\text{PMe}_2\text{Ph})_2\text{CO}(o\text{-(Me}_3\text{SiN)}_2\text{C}_6\text{H}_4)]$ (56**)**

To a degassed flask containing a toluene solution of **55** (0.800 g) was added carbon monoxide gas (ca. 15 psi). Concentration of this solution under reduced pressure afforded **56** as a red solid in 87% yield. ^1H NMR (C_6D_6 , 20°C): δ 0.19 (SiMe_3 , 9 H), 0.55 (SiMe_3 , 9 H), 1.20 (PMe_2Ph , 12 H), 6.80 (t, 7 Hz, 2 H), 7.0 (ov, m, 15 H), 7.49 (d, 7 Hz, 2 H). $^{13}\text{C}\{^1\text{H}\}$ NMR (C_6D_6 , 20°C): δ 5.0, 5.7, 16.0 (br), 113.3, 118.7, 119.1, 121.2, 123.4, 124.5, 128.8, 129.3, 129.5, 131.2, 150.6, 152.1, 156.7, 261.1, one resonance obscured by solvent. $^{31}\text{P}\{^1\text{H}\}$ NMR (C_6D_6 , 20°C): δ -7.0. IR: 1921 cm^{-1} .

$[\text{Mo}(\text{NPh})(\text{DMPE})(o\text{-(Me}_3\text{SiN)}_2\text{C}_6\text{H}_4)\text{-}\mu\text{-(DMPE)Mo}(\text{NPh})(\text{DMPE})(o\text{-(Me}_3\text{SiN)}_2\text{C}_6\text{H}_4)]$ (57**)**

A representative synthesis of **57**: To a green pentane solution of freshly generated **37** (1.70 g, 3.53 mmol) was added excess DMPE (1.76 g, 10.59 mmol). Upon addition of DMPE, red **57** precipitated from solution and was isolated by filtration in 93% yield. ^1H NMR (C_6D_6 , 20°C): δ 0.46 (SiMe_3 , 36 H), 0.8-1.4 (complex m, DMPE CH_2 and Me , 48 H), 6.75 (d of d, 6.0 Hz, 3.5 Hz, $o\text{-(Me}_3\text{SiN)}_2\text{C}_6\text{H}_4$ protons, 4 H), 6.84 (t, 7.0 Hz, 2 H), 7.0 (ov, m, 8 H), 7.13 (d of d, 6.0 Hz, 3.5 Hz, 4 H). $^{31}\text{P}\{^1\text{H}\}$ NMR (C_6D_6 , 20°C): δ -42.0, 50.0.

[Mo(NPh)IMes(*o*-(Me₃SiN)₂C₆H₄)] (59)

To a C₆D₆ solution of **55** was added 1.0 equiv of imidazol-2-ylidene **58** (IMes). Complex **59** formed in high yield as determined by ¹H NMR spectroscopy. Single crystals of **59** formed in the NMR tube and were isolated for characterization by ¹H NMR spectroscopy and X-ray crystallography. ¹H NMR (C₆D₆, 20°C): δ -38.2 (br, 2 H), -5.01 (2 H), -2.42 (phenyl imido *para* proton), 0.86 (mesityl *Me* protons, 12 H), 3.54 (mesityl *Me* protons, 6 H), 4.48 (br, 2 H), 8.81 (2 H), 10.09 (mesityl protons, 4 H), 17.55 (2 H), 30.00 (SiMe₃, 18 H).

[Mo(NPh)(PMe₃)₂(H₂)(*o*-(Me₃SiN)₂C₆H₄)] (60)

A general synthesis of complex **60**: To a resealable NMR tube was added **52** (0.050 g, 0.075 mmol) in C₇D₈ at 20°C. The solution was frozen and the headspace of the NMR tube was evacuated. The mixture was brought to -10°C and filled with molecular hydrogen (ca. 1 atm). The color of the solution changed from purple to green upon H₂ gas addition. A ratio of 1:3 **60**/**52** was observed by ¹H and ³¹P NMR spectroscopy at -50°C. ¹H NMR (C₇D₈, -30°C): δ 0.66 (SiMe₃, 9 H), 0.73 (SiMe₃, 9 H), 0.79 (virtual triplet, separation 3 Hz, PMe₃), 3.59 (t, br, ²J_{P-H} = 28 Hz, H₂), 6.7-7.4 (ov, m, 8 H), 7.41 (d, 1 H). ¹³C{¹H} NMR (C₇D₈, -50°C): δ 4.6 (SiMe₃, 9 H), 5.8 (SiMe₃, 9 H), 15.4 (t, 11 Hz, PMe₃), 114.1, 116.7, 117.1, 118.4, 123.8, 149.9, 151.8, 155.4, two resonances are obscured by solvent. ³¹P NMR {¹H} (C₇D₈, -30°C): -14.2 (t, br, 28 Hz). ³¹P NMR (C₇D₈, -30°C): δ -14.2. Note that the procedure for the synthesis of **60D** is identical but uses H-D gas.

[Mo(NPh)(PMe₂Ph)₂(H₂)(*o*-(Me₃SiN)₂C₆H₄)] (66)

The synthesis of **66** is identical to that of **60**. ¹H NMR (C₇D₈, -30°C): δ 0.39 (SiMe₃, 9 H), 0.63 (SiMe₃, 9 H), 1.02 (PMe₂Ph, 6 H), 1.09 (PMe₂Ph, 6 H), 3.46 (br, H₂), 6.78 (ov, m, 2 H), 7.0 (ov, m, 16 H), 7.51 (d, 8 Hz, 1 H). ³¹P NMR (C₇D₈, -20°C): δ -5.0 (br). ³¹P{¹H} NMR (C₇D₈, -20°C): δ -5.0. Note that the procedure for the synthesis of **66D** is identical but uses H-D gas.

[Mo(NPh)(PMe₂Ph)₂(*o*-(Me₃SiN)(NH)C₆H₄)] (67)

A toluene solution of **66** was warmed to 20°C and stirred for 2 h. Solvent was removed from the resulting purple solution under reduced pressure, giving crude **67** as a purple solid. ¹H NMR (C₆D₆, 20°C): δ 0.71 (SiMe₃, 9 H), 1.17 (d, 7.0 Hz, PMe₂Ph, 12 H), 5.97 (br, N-H), 7.0 (ov, m, 18 H), 7.75 (m, 1 H).

[Mo(NPh)(P(OMe)₃)₃(*o*-(Me₃SiN)(NH)C₆H₄)] (68)

To a degassed C₆D₆ NMR sample of **50** was added molecular hydrogen at 20°C. After 1 week, **68** was observed in solution by ¹H NMR spectroscopy. ¹H NMR (C₆D₆, 20°C): δ 0.75 (SiMe₃, 9 H), 3.23 (d, 11 Hz, P(OMe)₃, 27 H), 7.0 (ov, m, 6 H), 7.45 (d, 8.0 Hz, 2 H), 7.65 (m, 1 H), N-H resonance not observed.

Synthesis and Characterization of 71

To a 20°C toluene solution of **53** (0.77 g, 1.15 mmol) was added H₂SiPh₂ (0.21 mL, 1.15 mmol). The mixture was stirred overnight and concentrated under reduced pressure. The remaining solid was dissolved in a minimum amount of toluene and cooled to -30°C. Solid **71** precipitated from solution as a white powder and was isolated by filtration. ¹H NMR (C₆D₆, 20°C): δ 0.11 (SiMe₃, 18 H), 6.90 (m, *o*-(Me₃SiN)₂C₆H₄ protons, 2 H), 7.07

(m, *o*-(Me₃SiN)₂C₆H₄ protons, 2 H), 7.14 (ov, m, 7 H), 7.85 (ov, m, 3 H). MS (LSIMS): 432 *m/e*. FW 71 = 432.78.

[(Mo(NPh)-η⁴-(H₂C=CHCH=CH₂))(*o*-(Me₃SiN)₂C₆H₄)] (73)

For a typical procedure, butadiene gas (ca. 15 psi) was added to a degassed flask containing a green solution of **37** (0.42 g, 0.88 mmol) in pentane. The mixture was stirred for 10 min and concentrated *in vacuo* affording **73** as a green solid in 90% yield. Complex **73** decomposes rapidly in solution at 20°C and is best stored as a solid at -30°C under an inert atmosphere. ¹H NMR (C₆D₆, 20°C): δ 0.33 (SiMe₃, 18 H), 0.33 (ov, butadiene protons, 2 H), 4.20 (m, butadiene protons, 2 H), 5.49 (m, butadiene protons, 2 H), 6.7-7.0 (ov, m, 7 H), 7.23 (m, aromatic protons, 2 H). ¹³C {¹H} NMR (C₆D₆, 20°C): δ 4.7, 75.0, 114.7, 117.9, 119.0, 119.4, 127.3, 129.3, 152.8, 158.9. ¹H NMR (C₇D₈, -30°C, assigned via GHMQC, 500 MHz): δ 0.13 (br, m, terminal butadiene protons, 2 H), 0.33 (br, SiMe₃, 18 H), 4.21 (br, m, terminal butadiene protons, 2 H), 5.53 (br, m, internal butadiene protons, 2 H), 6.69 (t, 8.0 Hz, *para* proton), 6.72 (d, 8.0 Hz, *ortho* protons), 6.85 (t, 8.0 Hz, *meta* proton), 6.94 (m, *o*-(Me₃SiN)₂C₆H₄ protons, 2 H), 7.25 (m, *o*-(Me₃SiN)₂C₆H₄ protons, 2 H). ¹³C NMR (C₇D₈, -30°C, assigned via GHMQC and *J*_{CH} in Hz from the gated decoupled ¹³C NMR spectrum): δ 4.2 (q, 122 Hz, SiMe₃), 75.0 (br, t, 158 Hz, butadiene terminal carbon), 114.4 (d, 164 Hz, butadiene internal carbon), 117.3 (d, 147 Hz), 118.3 (d of d, 157 Hz, 8 Hz), 118.7 (d, 162 Hz), 126.9, 128.8, 152.3 (t, 7 Hz), 158.3 (t, 8 Hz). Due to the thermal instability of **73**, elemental analysis was not possible.

[(Mo(NPh)- η^4 -(2,3-dimethyl-1,3-cyclohexadiene)(*o*-(Me₃SiN)₂C₆H₄)] (74)

1,2-Dimethyl-1,4-cyclohexadiene (0.145 g, 1.33 mmol) was added to a stirring solution of **38** (0.660 g, 1.33 mmol) in pentane. This mixture was stirred for 5 days and then concentrated under reduced pressure affording **74** in 76% yield as a green solid. Analytically pure **74** can be obtained by washing the solid with pentane at 20°C. ¹H NMR (C₆D₆, 20°C, 500 MHz, assigned by GHMQC, GHMBC, and NOESY): δ 0.32 (SiMe₃, 18 H), 0.31 (ov, cyclohexadiene methylene protons, 2 H), 1.45 (br, m, cyclohexadiene methylene protons, 2 H), 2.05 (*Me*), 4.59 (br, C=C(H)), 6.68 (*ortho* protons), 6.73 (*para* proton), 6.83 (m, *o*-(Me₃SiN)₂C₆H₄ protons, 2 H), 6.93 (*meta* protons), 7.16 (m, *o*-(Me₃SiN)₂C₆H₄ protons, 2 H). ¹³C NMR (C₆D₆, 20°C, 500 MHz, assigned by GHMQC and GHMBC): δ 3.6 (SiMe₃), 18.4 (CH₂), 22.0 (*Me*), 87.4 (C=C(H)), 117.3 (*o*-(Me₃SiN)₂C₆H₄), 117.6 (*ortho* carbon), 118.2 (*o*-(Me₃SiN)₂C₆H₄), 126.0 (*para* carbon), 126.2 (C=C(H)), 128.7 (*meta* carbon), 153.3 (*ipso*, *o*-(Me₃SiN)₂C₆H₄), 158.7 (*ipso*, phenyl). Anal. Calcd for C₂₆H₃₉MoN₃Si₂: C, 57.22; H, 7.20; N, 7.70. Found: C, 57.08; H, 7.26; N, 7.52.

[(Mo(NPh)- η^4 -(2,3-dimethyl-1,3-cyclohexadiene)(*o*-(Me₃SiN)₂C₆H₄)] (*in situ*) (74)

An NMR tube containing **73** (136.3 mgs, 27.7 mmol) in C₆D₆ was charged with 2-butyne (21.7 μ L, 27.7 mmol) at 20°C. The reaction was complete after 30 min. Complex **74** was observed in the ¹H NMR spectrum of the reaction mixture.

Intermediates [*syn*-(Mo(NPh)(C(Me)=C(Me)CH₂CHCHCH₂)(*o*-(Me₃SiN)₂C₆H₄)] (**76a**) and [*anti*-(Mo(NPh)(C(Me)=C(Me)CH₂CHCHCH₂)(*o*-(Me₃SiN)₂C₆H₄)] (**76b**)

An NMR tube containing **73** (136.3 mgs, 27.7 mmol) in cold C₇D₈ was charged with 2-butyne (21.7 μ L, 27.7 mmol). The mixture was frozen with liquid nitrogen after 1.0 min and placed in a cooled (-20°C) NMR probe. The intermediates accumulated to

detectable levels within hours and were identified by NMR spectroscopy. All NMR spectra (GHMQC, GHMBC, NOESY, DQCOSY, and TOCSY) were acquired at -20°C on an Inova 500. For selected ^1H and ^{13}C NMR data for **76a** and **76b** see Figure 4-8 and Figure 4-9, respectively.

$[(\text{Mo}(\text{NPh})(\text{CH}_2\text{CH}=\text{CHCH}_2\text{C}(\text{Me})_2\text{O})(o\text{-(Me}_3\text{SiN)}_2\text{C}_6\text{H}_4)]$ (77**)**

An NMR tube containing **73** in C_6D_6 was charged with 1.0 equiv of acetone. Complex **77** formed after 30 min and was characterized by NMR spectroscopy. The isolation of complex **77** has not been attempted at this point. For selected NMR data see Figure 4-12.

$[(\text{Mo}(\text{NPh})-\eta^4\text{-(O=C(Me)CH=CH}_2)(o\text{-(Me}_3\text{SiN)}_2\text{C}_6\text{H}_4)]$ (78**)**

MVK (0.136 g, 1.945 mmol) was added to a stirring pentane solution of **38** (0.960 g, 1.945 mmol). Concentration of the pentane solution under reduced pressure afforded solid **78** in 78% yield following crystallization and filtration at -30°C. ^1H NMR (C_6D_6 , 20°C): δ 0.27 (SiMe_3 , 9 H), 0.52 (SiMe_3 , 9 H), 0.86 (d of d, 7.5 Hz, 4.0 Hz, olefinic proton), 2.16 (*Me*), 4.06 ("t", 8 Hz, olefinic proton), 5.21 (d of d, 9.0 Hz, 11.5 Hz, olefinic proton), 6.7-7.2 (ov, m, aromatic protons, 9 H).

$[(\text{Mo}(\text{NPh})-\eta^2\text{-(MeCCMe)})(o\text{-(Me}_3\text{SiN)}_2\text{C}_6\text{H}_4)]$ (75**)**

To a stirring solution of **38** (0.340 g, 6.880 mmol) in pentane was added 2-butyne (0.0373 g, 6.880 mmol). The reaction mixture was stirred for 10 min, and **75** was isolated as a red solid upon concentration of the reaction mixture under reduced pressure (yield 76%). Complex **75** is not stable in solution at 20°C and also decomposes in solution at -30°C overnight. ^1H NMR (C_6D_6 , 20°C): δ 0.45 (SiMe_3 , 18 H), 2.17 (*MeCCMe*, 6 H), 6.9-7.2 (ov, m, 9 H). $^{13}\text{C}\{^1\text{H}\}$ NMR (C_7D_8 , -25°C): δ 1.8, 17.8, 121.9,

123.3, 123.8, 124.1, 157.8, 181.5. Two resonances are overlapping with solvent. Due to the thermal instability of **75**, elemental analysis was not possible.

[(Mo(NPh)- η^2 -(PhCCPh)(*o*-(Me₃SiN)₂C₆H₄)] (79**)**

To a stirring solution of **38** (0.590 g, 1.195 mmol) in pentane was added diphenyl acetylene (0.213 g, 1.195 mmol). The reaction mixture was stirred overnight, and **79** was isolated as a red solid upon concentration of the reaction mixture under reduced pressure (yield 77%). ¹H NMR (C₆D₆, 20°C): δ 0.42 (SiMe₃, 18 H), 6.8-7.4 (ov, m, 19 H).

¹³C{¹H} NMR (C₆D₆, 20°C): δ 2.1, 122.9, 123.6, 124.6, 125.2, 128.5, 128.7, 129.0, 134.1, 139.8, 157.8, 182.0. Anal. Calcd for C₃₂H₃₇MoN₃Si₂: C, 62.42; H, 6.06; N, 6.82. Found: C, 62.11; H, 6.41; N, 6.46.

[(Mo(NPh)- η^2 -(Me₃SiCCSiMe₃)(*o*-(Me₃SiN)₂C₆H₄)] (80**)**

To a stirring solution of **38** (0.910 g, 1.800 mmol) in pentane was added bis(trimethylsilyl)acetylene (0.307 g, 1.800 mmol). The reaction mixture was stirred overnight, and **80** was isolated as a green solid upon concentration of the reaction mixture under reduced pressure (yield 77%). ¹H NMR (C₆D₆, 20°C): δ 0.22 (SiMe₃, 18 H), 0.41 (SiMe₃, 18 H), 6.08 (t of t, 7.0 Hz, 1.0 Hz, phenyl imido *para* proton), 6.9 (m, *o*-(Me₃SiN)₂C₆H₄ protons, 2 H), 7.05 (t, 8.0 Hz, phenyl imido *meta* protons, 2 H), 7.3 (ov, m, *o*-(Me₃SiN)₂C₆H₄ protons and phenyl imido *ortho* protons, 4 H). ¹³C{¹H} NMR (C₆D₆, 20°C): δ 1.1, 2.7, 124.0, 124.2, 124.6, 125.0, 129.2, 135.0, 158.2, 203.4. Anal. Calcd for C₂₆H₄₅MoN₃Si₄: C, 51.37; H, 7.46; N, 6.91. Found: C, 51.13; H, 7.00; N, 7.03.

Reaction of [(Mo(NPh)- η^2 -(PhCCPh)(*o*-(Me₃SiN)₂C₆H₄)] (79**) with *tert*-Butyl Isocyanide: Synthesis and Characterization of **82****

An NMR tube containing **79** in C₆D₆ was charged with 1.0 equiv of Bu^{*t*}NC. Complex **82** formed after several weeks and was characterized by NMR spectroscopy.

The isolation of complex **82** has not been attempted at this point. For selected NMR data see Figure 4-20.

[Mo(NPh)- η^2 -PhN=C(H)Ar(*o*-(Me₃SiN)₂C₆H₄)] (Ar = C₆H₄-*p*-OMe) (83**)**

To a green solution of **38** (0.50 g, 1.05 mmol) in pentane at 20°C was added a pentane solution of PhN=C(H)Ar (Ar = C₆H₄-*p*-OMe) (0.22 g, 1.05 mmol). After stirring for 12 h, the pentane solution was concentrated *in vacuo* and cooled, giving crystals of **83**. ¹H NMR (C₆D₆, 20°C): δ 0.31 (SiMe₃, 9 H), 0.42 (SiMe₃, 9 H), 3.33 (OMe), 4.79 (br, CH), 7.4-6.1 (ov, m, br, Ph, 18 H). ¹H NMR (C₇D₈, -90°C): δ 0.33 (SiMe₃, 9 H), 0.49 (SiMe₃, 9 H), 3.26 (OMe), 4.77 (imine CH), 5.0 (d, br, ³J_{C-H} = 7 Hz, *ortho* H), 6.1 (d, br, ³J_{C-H} = 7 Hz, *ortho* H), 7.5-6.4 (ov, m, Ph, 16 H). ¹³C{¹H} NMR (C₆D₆, 20°C): δ 1.9 (ov, SiMe₃), 55.0 (OMe), 62.2 (br, imine C(H)), 113.7 (ov), 119.3, 120.9, 124.0, 124.5, 124.9, 125.1, 125.5, 125.7, 126.6, 128.8, 129.1, 133.0, 138.4, 153.4, 157.5, one aromatic resonance obscured by solvent. HRMS calcd for [M]: 650.1796 *m/e*. Found (LSIMS): 650.1737 *m/e*. I.R.: 1589 cm⁻¹.

[Mo(NPh)- η^2 -PhN=C(Me)Ph(*o*-(Me₃SiN)₂C₆H₄)] (84**)**

To a green solution of **38** (0.50 g, 1.05 mmol) in pentane at 20°C was added a pentane solution of PhN=C(H)Ar (Ar = C₆H₄-*p*-OMe) (0.20 g, 1.05 mmol). After stirring for 12 h, the pentane solution was concentrated *in vacuo* and cooled, giving crystals of **84**. ¹H NMR (C₆D₆, 20°C): δ 0.34 (SiMe₃), 0.41 (SiMe₃), 2.34 (br, Me), 7.4-6.4 (ov, m, br, Ph, 19 H). ¹H NMR (C₇D₈, -65°C): δ 0.31 (SiMe₃), 0.41 (SiMe₃), 2.55 (Me), 5.18 (d, br, ³J_{C-H} = 8 Hz, *ortho* H), 6.27 (t, ³J_{C-H} = 8 Hz, *para* H), 6.35 (d, ³J_{C-H} = 8 Hz, *ortho* H), 6.61 (t, ³J_{C-H} = 8 Hz, *para* H), 7.4-6.2 (ov, m, Ph, 15 H). ¹³C{¹H} NMR (C₆D₆, 20°C): δ 2.5 (SiMe₃), 2.6 (SiMe₃), 23.3 (Me), 66.6 (br, imine C), 119.6, 121.0, 123.5, 124.1, 124.9,

125.3, 125.4, 125.8, 126.2, 126.8, 127.9, 129.3, 129.6, 134.1, 134.5, 148.7, 151.3, 158.1.
 HRMS calcd for $[M + H]^+$: 635.1925 *m/e*. Found (LSIMS): 635.1854 *m/e*. I.R.: 1580 cm^{-1} .

[Mo(NPh)EtNC(H)ArC(H)ArNEt(*o*-(Me₃SiN)₂C₆H₄)] (Ar = C₆H₄-*p*-OMe) (85)

To a green solution of **38** (0.50 g, 1.05 mmol) in pentane at 20°C was added a pentane solution of EtN=C(H)Ar (Ar = C₆H₄-*p*-OMe) (0.34 g, 2.10 mmol). After stirring for 12 h, the pentane solution was concentrated *in vacuo* and cooled, giving crystals of **85**. ¹H NMR (C₆D₆, 20°C): δ 0.28 (SiMe₃, 9 H), 0.38 (SiMe₃, 9 H), 0.62 (t, ³J_{C-H} = 7 Hz, Me), 0.89 (t, ³J_{C-H} = 7 Hz, Me), 3.26 (d of q, ²J_{C-H} = 13 Hz, ³J_{C-H} = 7 Hz, methylene CH), 3.36 (OMe), 3.38 (OMe), 3.81 (d of q, ²J_{C-H} = 13 Hz, ³J_{C-H} = 7 Hz, methylene CH), 4.01 (d of q, ²J_{C-H} = 13 Hz, ³J_{C-H} = 7 Hz, methylene CH), 4.19 (d of q, ²J_{C-H} = 13 Hz, ³J_{C-H} = 7 Hz, methylene CH), 4.65(NC(H)), 4.88 (NC(H)), 7.6-6.8 (ov, m, Ph, 17 H). ¹³C{¹H} NMR (C₆D₆, 20°C): δ 2.5 (SiMe₃), 3.5 (SiMe₃), 15.8 (Me), 17.3 (Me), 55.3 (OMe), 55.4 (OMe), 58.2 (NC(H)), 59.4 (NC(H)), 83.4 (NCH₂), 85.7 (NCH₂), 114.2, 114.3, 121.6, 123.2, 123.3, 124.5, 126.7, 127.2, 128.9, 129.1, 129.4, 138.1, 138.8, 146.2, 146.3, 156.9, 159.5, 159.7. HRMS Calcd for $[M + H]^+$: 766.2878 *m/e*. Found (LSIMS): 766.2818 *m/e*.

[Mo(NPh)BzNC(H)ArC(H)ArNBz(*o*-(Me₃SiN)₂C₆H₄)] (Ar = C₆H₄-*p*-OMe) (86)

To a green solution of **38** (0.50 g, 1.05 mmol) in pentane at 20°C was added a pentane solution of BzN=C(H)Ar (Ar = C₆H₄-*p*-OMe) (0.47 g, 2.10 mmol). After stirring for 12 h, the pentane solution was concentrated *in vacuo* and cooled, giving crystals of **86**. ¹H NMR (C₆D₆, 20°C, 500MHz): δ 0.26 (SiMe₃, 9 H), 0.39 (SiMe₃, 9 H), 3.35 (OMe), 3.36 (OMe), 4.50 (NC(H)), 4.51 (d, ²J_{C-H} = 15 Hz, benzylic proton), 4.64 (d, ²J_{C-H} = 15 Hz, benzylic proton), 4.75 (NC(H)), 5.45 (d, ²J_{C-H} = 15 Hz, benzylic proton), 5.51

(d, $^2J_{C-H}$ = 15 Hz, benzylic proton), 7.6-6.8 (ov, m, Ph, 27 H). Selected ^{13}C NMR from GHMBC and GHMQC (C_6D_6 , 20°C, 500 MHz): δ 2.1 (SiMe₃), 2.5 (SiMe₃), 54.6 (overlapping OMe), 66.6 (benzylic carbon), 66.8 (benzylic carbon), 80.2 (NC(H)), 81.6 (NC(H)). HRMS calcd for $[M + H]^+$: 890.3184 *m/e*. Found (LSIMS): 890.3157 *m/e*.

[(Mo(NPh)(C(Me)₂CH₂C(Me)₂O)(*o*-(Me₃SiN)₂C₆H₄)] (88)

Acetone (0.037 g, 0.65 mmol) was added to a stirring, green solution of **38** (0.32 g, 0.65 mmol) in 50 mL of pentane at 20°C. The color of the reaction mixture immediately changed from green to purple. The resulting pentane solution was concentrated *in vacuo* and cooled at -30°C for 2 days, affording purple microcrystals that were isolated by filtration and dried *in vacuo*. Additional crops can be crystallized from the mother liquors affording **88** in 78% isolated yield. 1H NMR ($CDCl_3$, 20°C): δ 0.27 (SiMe₃, 9 H), 0.28 (SiMe₃, 9 H), 0.53 (*Me*), 0.95 (*Me*), 1.26 (*Me*), 1.86 (*Me*), 2.08 (d, 13 Hz, C(*H*)), 2.99 (d, 13 Hz, C(*H*)), 6.9-7.4 (aromatic protons, 9 H). $^{13}C\{^1H\}$ NMR ($CDCl_3$, 20°C): δ 0.54, 3.28, 30.8, 31.4, 34.4, 39.5, 67.8, 78.0, 83.8, 119.7, 120.9, 122.0, 125.4, 125.5, 125.8, 128.7, 139.5, 145.7, 156.7. HRMS calcd for $[M + H]^+$: 554.1926 *m/e*. Found (LSIMS): 554.1948 *m/e*.

[(Mo(NPh)(C(H)PhCH₂C(Me)₂O)(*o*-(Me₃SiN)₂C₆H₄)] (89)

Acetone (0.022 g, 0.38 mmol) was added to a stirring, green solution of **87** (0.20 g, 0.38 mmol) in 50 mL of pentane at 20°C. The color of the reaction mixture immediately changed from green to red. The resulting pentane solution was concentrated *in vacuo* and cooled at -30°C for 2 days, affording red microcrystals that were isolated by filtration and dried *in vacuo*. Additional crops can be crystallized from the mother liquors affording **89** in 71% isolated yield. 1H NMR (C_6D_6 , 500MHz, from GHMBC and GHMQC): δ -0.06

(SiMe₃, 9 H), 0.38 (SiMe₃, 9 H), 0.78 (*Me*), 1.47 (*Me*), 2.56 (m, 2 H), 3.16 ("t", 14.5 Hz, 1 H), 6.85 (t of t, 7.5 Hz, 1.0 Hz, N-Ph imido *para* proton), 6.91 (t of t, 7.5 Hz, 1.0 Hz, metallacycle phenyl *para* proton), 7.02 (d of d of d, 8 Hz, 7 Hz, 1.5 Hz, *o*-(Me₃SiN)₂C₆H₄ proton), 7.09 (t, 8 Hz, N-Ph imido *meta* protons), 7.10 (ov, *o*-(Me₃SiN)₂C₆H₄ proton), 7.17 (t, 7.5 Hz, metallacycle phenyl *meta* protons), 7.30 (d of d, 8 Hz, 1 Hz, metallacycle phenyl *ortho* protons), 7.32 (d of d, 8.5 Hz, 1.0 Hz, *o*-(Me₃SiN)₂C₆H₄ proton), 7.40 (d of d, *o*-(Me₃SiN)₂C₆H₄ proton) 7.47 (d of d, 8.5 Hz, 1.0 Hz, N-Ph imido *ortho* protons). ¹³C (C₆D₆, 500MHz, from GHMBC and GHMQC): δ -0.1, 1.0, 28.0, 32.4, 56.2, 76.7, 86.4, 121.2, 123.6, 123.7, 123.8, 124.3, 125.6, 127.6, 128.0, 128.2, 128.9, 133.2, 140.3, 154.0, 156.2. HRMS calcd for [M]⁺: 601.1844 *m/e*. Found (LSIMS): 601.1869.

[(Mo(NPh)(C(H)PhCH₂C(Et)₂O)(*o*-(Me₃SiN)₂C₆H₄)] (90)

To a C₆D₆ solution (0.7 mL) of **87** (0.050 g, 0.092 mmol) in a vial was added 3-pentanone (0.0080 g, 0.092 mmol). The contents of the vial were then transferred to an NMR tube. The reaction was monitored by ¹H NMR for 1 week. Metallacycle **90** was never isolated, and only ¹H NMR has been collected. ¹H NMR (C₆D₆, 20°C): δ -0.05 (SiMe₃, 9 H), 0.42 (SiMe₃, 9 H), 0.62 (t, 7.5 Hz, *Me*), 0.8 (ov, m, methylene C(*H*), 2 H), 1.01 (t, 7.5 Hz, *Me*), 1.15 (m, methylene C(*H*)), 1.78 (m, methylene C(*H*)), 2.64 (m, metallacycle protons, 2 H), 3.11 ("t", 13 Hz, metallacycle proton), 6.8-7.4 (ov, m, 14 H).

[(Mo(NPh)(C(H)PhCH₂C(CH₂)₅O)(*o*-(Me₃SiN)₂C₆H₄)] (91)

Cyclohexanone (0.036 g, 0.37 mmol) was added to a stirring, toluene solution of **87** (0.20 g, 0.37 mmol) at 20°C. Metallacycle **91** was isolated in 75% yield by crystallization from pentane at -30°C followed by filtration. ¹H NMR (CDCl₃, 20°C): δ -0.15 (SiMe₃, 9 H), 0.32 (SiMe₃, 9 H), 0.8-1.8 (ov, m, cyclohexyl protons), 2.37 (d of d,

14 Hz, 5 Hz, metallacycle C(*H*)), 2.53 (d of d, 13 Hz, 5 Hz, metallacycle C(*H*)), 2.85 ("t", 13.5 Hz, metallacycle C(*H*)), 6.9-7.4 (ov, m, aromatic protons). $^{13}\text{C}\{^1\text{H}\}$ NMR (CDCl_3 , 20°C): δ 0.7, 1.2, 23.2, 23.8, 26.4, 37.2, 41.9, 54.8, 75.4, 84.9, 121.4, 123.5, 123.6, 123.9, 124.5, 125.6, 127.4, 127.8, 128.2, 128.9, 133.1, 140.1, 154.5, 156.2. HRMS calcd for $[\text{M} + \text{H}]^+$: 641.2262 *m/e*. Found (LSIMS): 641.2209 *m/e*.

$[(\text{Mo}(\text{NPh})(\text{C}(\text{Me})_2\text{CH}_2\text{C}(\text{H})(\text{C}_6\text{H}_4\text{-}p\text{-OMe})\text{O})(o\text{-(Me}_3\text{SiN)}_2\text{C}_6\text{H}_4)]$ (92)

To a stirring solution of **38** (0.810 g, 1.64 mmol) in pentane at 20°C was added *p*-anisaldehyde (0.223 g, 1.64 mmol). Compound **92** was isolated in 78% yield by crystallization from pentane at -30°C followed by filtration. ^1H NMR (CDCl_3 , 20°C): δ 0.31 (SiMe_3 , 9 H), 0.40 (SiMe_3 , 9 H), 0.64 (*Me*), 1.98 (*Me*), 2.26 (d of d, 13 Hz, 5 Hz, metallacycle C(*H*)), 2.87 ("t", 11 Hz, metallacycle C(*H*)), 3.77 (*OMe*), 5.05 (d of d, 11 Hz, 6 Hz, metallacycle C(*H*)), 6.78 (d, 9 Hz, aromatic proton, 2 H), 7.0-7.4 (aromatic protons, 11 H). $^{13}\text{C}\{^1\text{H}\}$ NMR (CDCl_3 , 20°C): δ 0.8, 3.0, 28.0, 38.4, 55.4, 63.1, 77.7, 83.3, 113.5, 121.0, 122.5, 122.7, 125.0, 125.6, 126.5, 126.7, 128.7, 137.8, 140.5, 143.4, 156.5, 158.2. HRMS calcd for $[\text{M} + \text{H}]^+$: 632.2050 *m/e*. Found (LSIMS): 632.2031 *m/e*.

Reactivity of Arene Complexes with Acetone

A representative reaction: To a C_6D_6 solution of appropriate arene complex was added 1.0 equiv of acetone using a μL syringe. The proposed products, **93** and **94**, and supporting spectroscopic data are discussed in the text.

LIST OF REFERENCES

- (1) Collman, J. P.; Hegedus, L. S.; Norton, J. R.; Finke, R. G. *Principles and Applications of Organotransition Metal Chemistry*; University Science Books: Mill Valley, California, 1987.
- (2) Storhoff, B. N.; Lewis, H. C. *Coord. Chem. Rev.* **1977**, *23*, 1.
- (3) Lorente, P.; Carfagna, C.; Etienne, M.; Donnadieu, B. *Organometallics* **1996**, *15*, 1090.
- (4) Durfee, L. D.; Rothwell, I. P. *Chem. Rev.* **1988**, *88*, 1059.
- (5) Scott, M. J.; Lippard, S. J. *Organometallics* **1997**, *16*, 5857.
- (6) Richter-Addo, G. B.; Legzdins, P. *Metal Nitrosyls*; Oxford University Press: New York, New York, 1992.
- (7) Fryzuk, M. D.; Johnson, S. A. *Coord. Chem. Rev.* **2000**, *200-202*, 379.
- (8) Laplaza, C. E.; Cummins, C. C. *Science* **1995**, *268*, 861.
- (9) Trofimenko, S. *Chem. Rev.* **1993**, *93*, 943, and references therein.
- (10) Nugent, W. A.; Haymore, B. L. *Coord. Chem. Rev.* **1980**, *31*, 123.
- (11) Wigley, D. E. *Prog. Inorg. Chem.* **1994**, *42*, 239.
- (12) Nugent, W. A.; Mayer, J. M. *Metal-Ligand Multiple Bonds*; Wiley: New York, New York, 1988.
- (13) Haymore, B. L.; Maatta, E. A.; Wentworth, R. A. D. *J. Am. Chem. Soc.* **1979**, *101*, 2063.
- (14) Parkin, G.; van Asselt, A.; Leahy, D. J.; Whinnery, L.; Hua, N. G.; Quan, R. W.; Henling, L. M.; Schaefer, W. P.; Santarsiero, B. D.; Bercaw, J. E. *Inorg. Chem.* **1992**, *31*, 82.
- (15) Jørgensen, K. A. *Inorg. Chem.* **1993**, *32*, 1521.
- (16) Barrie, P.; Coffey, T. A.; Forster, G. D.; Hogarth, G. *J. Chem. Soc., Dalton. Trans.* **1999**, 4519.

- (17) Lorber, C; Choukroun, R.; Donnadiou, B. *Inorg. Chem.* **2002**, *ASAP Article*.
- (18) Lappert, M. F.; Power, P. P.; Sanger, A. R.; Srivastava, R. C. *Metal and Metalloid Amides: Syntheses, Structures, and Physical and Chemical Properties*; Halsted Press: New York, 1980.
- (19) Chisholm, M. H.; Rothwell, I. P. *Comprehensive Coordination Chemistry*; Pergamon: Oxford, 1987, vol 2, p. 161.
- (20) Kempe, R. *Angew. Chem., Int. Ed. Engl.* **2000**, *39*, 468.
- (21) McKnight, A. L.; Waymouth, R. M. *Chem. Rev.* **1998**, *98*, 2587.
- (22) Gade, L. H. *Chem. Commun.* **2000**, 173.
- (23) Verkade, J. G. *Acc. Chem. Res.* **1993**, *26*, 483.
- (24) Schrock, R. R. *Acc. Chem. Res.* **1997**, *30*, 9.
- (25) Blake, A. J.; McInnes, J. M.; Mountford, P.; Nikonov, G. I.; Swallow, D.; Watkin, D. J. *J. Chem. Soc., Dalton Trans.* **1999**, 379, and references therein.
- (26) Scollard, J. D.; McConville, D. H.; Payne, N. C.; Vittale, J. J. *Macromolecules* **1996**, *29*, 5241.
- (27) Ortiz, C. G.; Abboud, K. A.; Boncella, J. M. *Organometallics* **1999**, *18*, 4253.
- (28) Skinner, M. E. G.; Cowhig, D. A.; Mountford, P. *Chem Commun.* **2000**, 1167.
- (29) (a) Roussel, P.; Tinker, N. D.; Scott, P. *J. Alloys Compd.* **1998**, *271-273*, 150. (b) Roussel, P.; Scott, P. *J. Am. Chem. Soc.* **1998**, *120*, 1070.
- (30) Gade, L. H.; Mountford, P. *Coord. Chem. Rev.* **2001**, *216-217*, 65.
- (31) Trösch, D. J. M.; Collier, P. E.; Bashall, A.; Gade, L. H.; McPartlin, M.; Mountford, P.; Radojevic, S. *Organometallics* **2001**, *20*, 3308.
- (32) Swallow, D.; McInnes, M.; Mountford, P. *J. Chem. Soc., Dalton. Trans.* **1998**, 2253.
- (33) Thorman, J. L.; Guzei, I. A.; Young, V. G.; Woo, L. K. *Inorg. Chem.* **2000**, *39*, 2344.
- (34) Thorman, J. L.; Woo, L. K. *Inorg. Chem.* **2000**, *39*, 1301.
- (35) Zuckerman, R. L.; Krska, S. W.; Bergman, R. G. *J. Am. Chem. Soc.* **2000**, *122*, 751.
- (36) Ackermann, L.; Bergman, R. G. *Org. Lett.* **2002**, *4*, 1475.

- (37) Shi, Y.; Ciszewski, J. T.; Odom, A. L. *Organometallics* **2001**, *20*, 3967.
- (38) Ong, T.-G.; Yap, G. P. A.; Richeson, D. S. *Organometallics* **2002**, *21*, 2839.
- (39) Benett, J. L.; Wolczanski, P. T. *J. Am. Chem. Soc.* **1997**, *119*, 10696.
- (40) VanderLende, D. D.; Abboud, K. A.; Boncella, J. M. *Organometallics* **1994**, *13*, 3378.
- (41) Huff, R. L.; Wang, S.-Y.; Abboud, K. A.; Boncella, J. M. *Organometallics* **1997**, *16*, 1779.
- (42) Vaughan, W. M.; Abboud, K. A.; Boncella, J. M. *J. Am. Chem. Soc.* **1995**, *117*, 11015.
- (43) Wang, S.-Y. S.; Abboud, K. A.; Boncella, J. M. *J. Am. Chem. Soc.* **1997**, *119*, 11990.
- (44) Wang, S.-Y. S.; VanderLende, D. D.; Abboud, K. A.; Boncella, J. M. *Organometallics* **1998**, *17*, 2628.
- (45) Wang, S.-Y. S. *Ph.D. Dissertation*; University of Florida, Gainesville, FL: 1999.
- (46) Cameron, T. M.; Ortiz, C. G.; Ghiviriga, I.; Abboud, K. A.; Boncella, J. M. *Organometallics* **2001**, *20*, 2032.
- (47) Ortiz, C. G.; Abboud, K. A.; Cameron, T. M.; Boncella, J. M. *Chem. Commun.* **2001**, 247.
- (48) Mills, R. C.; Abboud, K. A.; Boncella, J. M. *Organometallics* **2000**, *19*, 2953.
- (49) Mills, R. C.; Wang, S.-Y. S.; Abboud, K. A.; Boncella, J. M. *Inorg. Chem.* **2001**, *40*, 5077.
- (50) Mills, R. C.; Abboud, K. A.; Boncella, J. M. *Chem. Commun.* **2001**, 1506.
- (51) Cameron, T. M.; Abboud, K. A.; Boncella, J. M. *Chem. Commun.* **2001**, 1224.
- (52) Galindo, A.; Ienco, A.; Mealli, C. *New J. Chem.* **2000**, *2*, 73.
- (53) Frisch, M. J.; Trucks, G. W.; Schlegel, H. B.; Scuseria, G. E.; Robb, M. A.; Cheeseman, J. R.; Zakrzewski, V. G.; Montgomery, J. A.; Stratmann, R. E.; Burant, J. C.; Dapprich, S.; Millam, J. M.; Daniels, A. D.; Kudin, K. N.; Strain, M. C.; Farkas, O.; Tomasi, J.; Barone, V.; Cossi, M.; Cammi, R.; Mennucci, B.; Pomelli, C.; Adamo, C.; Clifford, S.; Ochterski, J.; Petersson, G. A.; Ayala, P. Y.; Cui, Q.; Morokuma, K.; Salvador, P.; Dannenberg, J. J.; Malick, D. K.; Rabuck, A. D.; Raghavachari, K.; Foresman, J. B.; Cioslowski, J.; Ortiz, V. J.; Baboul, A. G.; Stefanov, B. B.; Liu, G.; Liashenko, A.; Piskorz, P.; Komaromi, I.; Gomperts, R.; Martin, R. L.; Fox, D. J.; Keith, T.; Al-Laham, M. A.; Peng, C. Y.;

- Nanayakkara, A.; Challacombe, M.; Gill, P. M. W.; Johnson, B.; Chen, W.; Wong, M. W.; Andres, J. L.; Gonzalez, C.; Head-Gordon, M.; Replogle, E. S.; Pople, J. A. Gaussian, Inc., Pittsburgh PA, 2001.
- (54) Laaksonen, L. *J. Mol. Graphics* **1992**, *10*, 33.
- (55) Bergman, D. L.; Laaksonen, L.; Laaksonen, A. *J. Mol. Graphics & Modelling* **1997**, *15*, 301.
- (56) Adams, R. D.; Collins, D. M.; Cotton, F. A. *Inorg. Chem.* **1974**, *13*, 1086.
- (57) Klingler, R. J.; Butler, W.; Curtis, M. D. *J. Am. Chem. Soc.* **1975**, *97*, 3535.
- (58) CX (X = N, O) multiple bond cleavage reactions are more common. See: (a) Hall, K. A.; Mayer, J. M. *J. Am. Chem. Soc.* **1992**, *114*, 10402. (b) Su, F.-M.; Bryan, J. C.; Jang, S.; Mayer, J. M. *Polyhedron* **1989**, *8*, 1261. (c) Miller, R. L.; Wolczanski, P. T.; Rheingold, A. L. *J. Am. Chem. Soc.* **1993**, *115*, 10422. (d) Meyer, K. E.; Walsh, P. J.; Bergman, R. G. *J. Am. Chem. Soc.* **1995**, *117*, 974. (e) Schrock, R. R.; Listemann, M. L.; Sturgeoff, L. G. *J. Am. Chem. Soc.* **1982**, *104*, 4291.
- (59) (a) Proulx, G.; Bergman, R. G. *J. Am. Chem. Soc.* **1994**, *116*, 7953. (b) Atagi, L. M.; Over, D. E.; McAlister, D. R.; Mayer, J. M. *J. Am. Chem. Soc.* **1991**, *113*, 870. (c) Cummins, C. C.; Schrock, R. R.; Davis, W. M. *Inorg. Chem.* **1994**, *33*, 1448.
- (60) (a) Cotton, F. A.; Matonic, J. H.; Murillo, C. A.; Wang, X. *Bull. Soc. Chim. Fr.* **1996**, *133*, 711. (b) Cotton, F. A.; Daniels, L. M.; Murillo, C. A.; Wang, X. *Inorg. Chem.* **1997**, *36*, 896. (c) Agadorn, J. R.; Arnold, J. *Organometallics* **1994**, *13*, 4670.
- (61) Bonanno, J. B.; Henry, T. P.; Neithamer, D. R.; Wolczanski, P. T.; Lobkovski, E. B. *J. Am. Chem. Soc.* **1996**, *118*, 5132.
- (62) (a) Kleckley, T. S.; Bennet, J. L.; Wolczanski, P. T.; Lobkovski, E. B. *J. Am. Chem. Soc.* **1997**, *119*, 247. (b) Gray, S. D.; Weller, K. J.; Bruck, M. A.; Briggs, P. M.; Wigley, D. E. *J. Am. Chem. Soc.* **1995**, *117*, 10678.
- (63) (a) Tayebani, M.; Gambarotta, S.; Yap, G. P. A. *Angew. Chem., Int. Ed. Engl.* **1998**, *37*, 3002. (b) Tayebani, M.; Gambarotta, S.; Yap, G. P. A. *Organometallics* **1998**, *17*, 3639. (c) Tayebani, M.; Feghali, K.; Gambarotta, S.; Bensimon, C. *Organometallics* **1997**, *16*, 5084.
- (64) Chisholm, M. H.; Folting, K.; Huffman, J. C.; Leonelli, J.; Marchant, N. S.; Smith, C. A.; Taylor, C. E. *J. Am. Chem. Soc.* **1985**, *107*, 3722.
- (65) Gutowsky, H. S.; Holm, C. H. *J. Chem. Phys.* **1956**, *25*, 1228.

- (66) Ortiz, C. G. *Ph.D. Dissertation*; University of Florida, Gainesville FL: 1999.
- (67) Arduengo, A. J., III; Harlow, R. L.; Kline, M. J. *J. Am. Chem. Soc.* **1991**, *113*, 361.
- (68) Bourissou, D.; Guerret, O.; Gabbai, F. P.; Bertrand, G. *Chem. Rev.* **2000**, *100*, 39.
- (69) Weskamp, T.; Böhm, V. P. W.; Herrmann, W. A. *J. Organomet. Chem.* **2000**, *600*, 12.
- (70) Arduengo, A. J., III. *Acc. Chem. Res.* **1999**, *32*, 913.
- (71) Liu, C.-Y.; Chen, D.-Y.; Lee, G.-H.; Peng, S.-M.; Liu, S.-T. *Organometallics* **1996**, *15*, 1055.
- (72) Fischer, E. O.; Hollfelder, H.; Friedrich, P.; Kreissl, R. K.; Huttner, G. *Chem. Ber.* **1977**, *110*, 2467.
- (73) Tolman, C. A.; *Chem. Rev.* **1977**, *77*, 313.
- (74) Kubas, G. J.; Ryan, R. R.; Swanson, B. I.; Vergamini, P. J.; Wasserman, H. J. *J. Am. Chem. Soc.* **1984**, *106*, 451.
- (75) Kubas, G. J. *Acc. Chem. Res.* **1988**, *21*, 120.
- (76) Crabtree, R. H. *Acc. Chem. Res.* **1990**, *23*, 95.
- (77) Crabtree, R. H. *Angew. Chem., Int. Ed. Engl.* **1993**, *32*, 789.
- (78) Jessop, P. G.; Morris, R. H. *Coord. Chem. Rev.* **1992**, *121*, 155.
- (79) Heinekey, D. M.; Oldham, W. J., Jr. *Chem. Rev.* **1993**, *93*, 913.
- (80) Sabo-Etienne, S.; Chaudret, B. *Coord. Chem. Rev.* **1998**, *178-180*, 381.
- (81) Esteruelas, M. A.; Oro, L. A. *Chem. Rev.* **1998**, *98*, 577.
- (82) Kubas, G. J. *Metal Dihydrogen and σ -Bond Complexes*; Kluwer Academic / Plenum: New York, New York, 2001.
- (83) Maltby, P. A.; Schlaf, M.; Steinbeck, M.; Lough, A. J.; Morris, R. H.; Klooster, W. T.; Koetzle, T. F.; Srivastava, R. C. *J. Am. Chem. Soc.* **1996**, *118*, 5396.
- (84) Luther, T. A.; Heinekey, D. M. *Inorg. Chem.* **1998**, *37*, 127.
- (85) Hamilton, D. G.; Crabtree, R. H. *J. Am. Chem. Soc.* **1988**, *110*, 4126.
- (86) Crabtree, R. H. *Acc. Chem. Res.* **1990**, *23*, 95.

- (87) Bautista, M. T.; Earl, K. A.; Maltby, P. A.; Morris, R. H.; Schweitzer, C. T.; Sella, A. *J. Am. Chem. Soc.* **1988**, *110*, 7031.
- (88) Morris, R. H. *Can. J. Chem.* **1996**, *74*, 1907.
- (89) Desrosiers, P. J.; Cai, L.; Lin, Z.; Richards, R.; Halpern, J. *J. Am. Chem. Soc.* **1991**, *113*, 4173.
- (90) Morris, R. H.; Wittebort, R. *J. Mag. Res. Chem.* **1997**, *35*, 243.
- (91) Cameron, T. M.; Ortiz, C. G.; Ghiviriga, I.; Abboud, K. A.; Boncella, J. M. *J. Am. Chem. Soc.* **2002**, *124*, 922.
- (92) Reid, S. M.; Neuner, B.; Schrock, R. R.; Davis, W. M. *Organometallics* **1998**, *17*, 4077.
- (93) Wang, C.; Friedrich, S.; Younkin, T. R.; Li, R. T.; Grubbs, R. H.; Bansleben, D. A.; Day, M. W. *Organometallics* **1998**, *17*, 3149.
- (94) Boncella, J. M.; Wang, S.-Y. S.; VanderLende, D. D. *J. Organomet. Chem.* **1999**, *591*, 8.
- (95) Crabtree, R. H. *The Organometallic Chemistry of the Transition Metals*; John Wiley & Sons: New York, New York, 2001.
- (96) Fontaine, F.-G.; Zargarian, D. *Organometallics* **2002**, *21*, 401, and references therein.
- (97) Abdur-Rashid, K.; Faatz, M.; Lough, A. J.; Morris, R. H. *J. Am. Chem. Soc.* **2001**, *123*, 7473.
- (98) (a) Datta, S.; Wreford, S. S.; Beatty, R. P.; McNeese, T. J. *J. Am. Chem. Soc.* **1979**, *101*, 1053. (b) Beatty, R. P.; Datta, S.; Wreford, S. S. *Inorg. Chem.* **1979**, *18*, 3139.
- (99) Erker, G.; Wicher, J.; Engel, K.; Rosenfeldt, F.; Dietrich, W.; Kruger, C. *J. Am. Chem. Soc.* **1980**, *102*, 6346.
- (100) (a) Yasuda, H.; Kajihara, Y.; Mashima, K.; Lee, K.; Nakamura, A. *Chem. Lett.* **1981**, 519. (b) Yasuda, H.; Kajihara, Y.; Mashima, K.; Lee, K.; Nakamura, A. *Organometallics* **1982**, *1*, 388.
- (101) A Cambridge Structural Database compilation of Group 3, 4, and 5 η^4 -*s-cis*-transition metal butadiene complexes see: Dahlmann, M.; Erker, G.; Fröhlich, R.; Meyer, O. *Organometallics* **1999**, *18*, 4459, supporting information.
- (102) For a compilation of examples see: (a) Wang, L.-S.; Fettingner, J. C.; Poli, R. J. *J. Am. Chem. Soc.* **1997**, *119*, 4453. (b) Mashima, K.; Fukumoto, H.; Tani, K.;

- Haga, M.; Nakamura, A. *Organometallics* **1998**, *17*, 410, and references therein.
(c) Strauch, H. C.; Erker, G.; Frohlich, R. *Organometallics* **1998**, *17*, 5746.
- (103) Selected examples: see Dahlmann, M.; Erker, G.; Frohlich, R.; Meyer, O. *Organometallics* **1999**, *18*, 4459.
- (104) (a) Hilt, G.; du Mesnil, F.-X. *Tetrahedron Lett.* **2000**, *41*, 6757. (b) Paik, S.-J.; Son, S. U.; Chung, Y. K. *Organic Lett.* **1999**, *13*, 2045. (c) Matsuda, I.; Shibata, M.; Sato, S.; Izumi, Y. *Tetrahedron Lett.* **1987**, 3361. (d) tom Dieck, H.; Diercks, R. *Angew. Chem., Int. Ed. Engl.* **1983**, *22*, 778. (e) Mach, K.; Antropiusová, H.; Petrusová, L.; Turecek, F.; Hanus, V. *J. Organomet. Chem.* **1985**, *289*, 331. (f) Murakami, M.; Ubukata, M.; Itami, K.; Ito, Y. *Angew. Chem., Int. Ed. Engl.* **1998**, *37*, 16. (g) Murakami, M.; Itami, K.; Ito, Y. *J. Am. Chem. Soc.* **1997**, *119*, 7163.
- (105) (a) Wender, P. A.; Jenkins, T. E. *J. Am. Chem. Soc.* **1989**, *111*, 6432. (b) Jolly, R. S.; Luedtke, G.; Sheehan, D.; Livinghouse, T. *J. Am. Chem. Soc.* **1990**, *112*, 4965. (c) Wender, P. A.; Smith, T. E. *J. Org. Chem.* **1996**, *61*, 824. (d) McKinstry, L.; Livinghouse, T. *Tetrahedron* **1994**, *50*, 6145. (e) O'Mahony, D. J. R.; Belanger, D. B.; Livinghouse, T. *Synlett* **1998**, 443. (f) Gilbertson, S. R.; Hoge, G. S. *Tetrahedron Lett.* **1998**, *39*, 2075. (g) Gilbertson, S. R.; Hoge, G. S.; Genov, D. G. *J. Org. Chem.* **1998**, *63*, 10077. (h) Kumar, K.; Jolly, R. S. *Tetrahedron Lett.* **1998**, *39*, 3047. For a review of transition metal-mediated cycloaddition reactions see: Lautens, M.; Klute, W.; Tam, W. *Chem. Rev.* **1996**, *96*, 49.
- (106) Strauch, J. M.; Petersen, J. L. *Organometallics* **2001**, *20*, 2623, and references therein.
- (107) Homoleptic Mo(d⁶) butadiene and derivative complexes (synthesis and structure): (a) Skell, P. S.; Van Dam, E. M.; Silvon, M. P. *J. Am. Chem. Soc.* **1974**, *96*, 626. (b) Skell, P. S.; McGlinchy, M. J. *Angew. Chem., Int. Ed. Engl.* **1975**, *14*, 195. (c) Gausing, W.; Wilke, G. *Angew. Chem., Int. Ed. Engl.* **1981**, *20*, 186. (d) Bogdanovic, B.; Bonnemann, H.; Goddard, R.; Startsev, A.; Wallis, J. M. *J. Organomet. Chem.* **1986**, *299*, 347. (e) Yun, S. S.; Kang, S. K.; Suh, I.-H.; Choi, Y. D.; Chang, I. S. *Organometallics* **1991**, *10*, 2509. Nonhomoleptic systems (synthesis and reactivity) (f) Le Grogne, E.; Poli, R.; Richard, P. *Organometallics* **2000**, *19*, 3842. (g) Poli, R.; Wang, L.-S. *Polyhedron* **1998**, *17*, 3689. (h) Wang, L.-S.; Fetting, J. C.; Poli, R.; Meunier-Prest, R. *Organometallics* **1998**, *17*, 2692. (i) Galindo, A.; Gutierrez, E.; Monge, A.; Paneque, M.; Pastor, A.; Perez, P. J.; Rogers, R. D.; Carmona, E. *J. Chem. Soc., Dalton Trans.* **1995**, *23*, 3801. (j) Kingsbury, K. B.; Carter, J. D.; Mc-Elwee-White, L.; Ostrander, R. L.; Rheingold, A. L. *Organometallics* **1994**, *13*, 1635. (k) Vong, W.-J.; Peng, S.-M.; Lin, S.-H.; Lin, W.-J.; Liu, R.-S. *J. Am. Chem. Soc.* **1991**, *113*, 573. (l) Benyunes, S. A.; Binelli, A.; Green, M.; Grimshire, M. J. *J. Chem. Soc., Dalton Trans.* **1991**, 895. (m) Hunter, A. D.; Legzdins, P.; Einstein, F. W. B.; Willis, A. C.; Bursten, B. E.; Gatter, M. G. *J. Am. Chem. Soc.* **1986**, *108*, 3843. (n) Davidson, J. L.; Davidson, K.; Lindsell, W. E.; Murrall, N. W.; Welch, A. J. *J. Chem. Soc., Dalton Trans.* **1986**, 1677. (o)

- Brookhart, M.; Cox, K.; Cloke, F. G. N.; Green, J. C.; Green, M. L. H.; Hare, M. P.; Bashkin, J.; Derome, A.; Grebenik, P. D. *J. Chem. Soc., Dalton Trans.* **1985**, 423. (p) Hunter, A. D.; Legzdins, P.; Nurse, C. R.; Einstein, F. W. B.; Willis, A. C. *J. Am. Chem. Soc.* **1985**, *107*, 1791.
- (108) Cameron, T. M.; Ghiviriga, I.; Abboud, K. A.; Boncella, J. M. *Organometallics* **2001**, *20*, 4378.
- (109) Newton, M. D.; Schulmann, T. M.; Manus, M. M. *J. Am. Chem. Soc.* **1974**, *96*, 17.
- (110) Yamamoto, H.; Yasuda, H.; Tatsumi, K.; Lee, K.; Nakamura, A.; Chen, J.; Kai, Y.; Kasai, N. *Organometallics* **1989**, *8*, 105.
- (111) Mills, R. C. *Ph.D. Dissertation*; University of Florida, Gainesville, FL: 2001.
- (112) Krüger, C.; Müller, G.; Erker, G.; Dorf, U.; Engel, K. *Organometallics* **1985**, *4*, 215.
- (113) Pastor, A.; Galindo, A.; Gutiérrez-Puebla, E.; Monge, A. *J. Organomet. Chem.* **1998**, *566*, 211.
- (114) Schmidt, T. *Chem. Ber. Recueil* **1997**, *130*, 453, and references therein.
- (115) Schuster, D. M.; White, P. S.; Templeton, J. L. *Organometallics* **2000**, *19*, 1540.
- (116) (a) Templeton, J. L. *Adv. Organomet. Chem.* **1989**, *29*, 1, and references therein. (b) Baker, P. K. *Adv. Organomet. Chem.* **1996**, *40*, 45, and references therein.
- (117) (a) Templeton, J. L.; Ward, B. C. *J. Am. Chem. Soc.* **1980**, *102*, 3288. (b) Templeton, J. L.; Ward, B. C. *J. Am. Chem. Soc.* **1980**, *102*, 1532. (c) Tatsumi, K.; Hoffmann, R.; Templeton, J. L. *Inorg. Chem.* **1982**, *21*, 466.
- (118) Allen, F. H.; Kennard, O.; Watson, D. G.; Brammer, L.; Orpen, G. A.; Taylor, R. *J. Chem. Soc., Perkin Trans.* **1987**, S1-S19.
- (119) Lefebvre, C.; Baumann, W.; Tillack, A.; Kempe, R.; Görls, H.; Rosenthal, U. *Organometallics* **1996**, *15*, 3486.
- (120) (a) Berno, P.; Gamarotta, S. *Organometallics* **1995**, *14*, 2159. (b) Gately, D. A.; Norton, J. R.; Goodson, P. A. *J. Am. Chem. Soc.* **1995**, *117*, 986. (c) Buchwald, S. L.; Watson, B. T.; Wannamaker, M. W.; Dewan, J. C. *J. Am. Chem. Soc.* **1989**, *111*, 4486. (d) Tunge, J. A.; Gately, D. A.; Norton, J. R. *J. Am. Chem. Soc.* **1999**, *121*, 4520.
- (121) A Mo(H) η^2 -imine complex has been reported and presumably arises via C-H activation of an amide ligand. Tsai, Y.; Johnson, M. J.; Mindiola, D. J.;

- Cummins, C. C.; Klooster, W. T.; Koetzle, T. F. *J. Am. Chem. Soc.* **1999**, *121*, 10426.
- (122) (a) Clark, J. R.; Fanwick, P. E.; Rothwell, I. P. *Organometallics* **1996**, *15*, 3232. (b) Durfee, L. D.; Hill, J. E.; Fanwick, P. E.; Rothwell, I. P. *Organometallics* **1990**, *9*, 75. (c) Durfee, L. D.; Fanwick, P. E.; Rothwell, I. P.; Folting, K.; Huffman, J. C. *J. Am. Chem. Soc.* **1987**, *109*, 4720. (d) Chiu, K. W.; Jones, R. A.; Wilkinson, G.; Galas, A. M. R.; Hursthouse, M. B. *J. Chem. Soc., Dalton Trans.* **1981**, 2088; *J. Am. Chem. Soc.* **1980**, *102*, 7978.
- (123) Wolczanski, P. T.; Bercaw, J. E. *J. Am. Chem. Soc.* **1979**, *101*, 6450.
- (124) Alexander, J. B.; Glueck, D. S.; Yap, G. P. A.; Rheingold, A. L. *Organometallics* **1995**, *14*, 3603.
- (125) Makioka, Y.; Taniguchi, Y.; Fujiwara, Y.; Takaki, K.; Hou, Z.; Wakatsuki, Y. *Organometallics* **1996**, *15*, 5476, and references therein.
- (126) Takai, K.; Ishiyama, T.; Yasue, H.; Nobunaka, T.; Itoh, M.; Oshiki, T.; Mashima, K.; Tani, K. *Organometallics* **1998**, *17*, 5128.
- (127) C-N single-bond length 1.45 Å and C-N double-bond length 1.27 Å. Burkr-Laing, M.; Laing, M. *Acta Crystallogr.* **1976**, *32B*, 3216.
- (128) Addison, A. W.; Rao, T. N.; Reedijk, J.; Rijn, J. *J. Chem. Soc., Dalton Trans.* **1984**, 1349.
- (129) Reviews: (a) Buchwald, S. L.; Nielsen, R. B. *Chem. Rev.* **1988**, *88*, 1047. (b) Broene, R. D.; Buchwald, S. L. *Science* **1993**, *261*, 1696. (c) Negishi, E. *Chem. Scr.* **1989**, *29*, 457. (d) Negishi, E.; Takahashi, T. *Acc. Chem. Res.* **1994**, *27*, 124.
- (130) (a) Kablaoui, N. M.; Buchwald, S. L. *J. Am. Chem. Soc.* **1995**, *117*, 6785. (b) Kablaoui, N. M.; Buchwald, S. L. *J. Am. Chem. Soc.* **1996**, *118*, 3182. (c) Crowe, W. E.; Rachita, M. J. *J. Am. Chem. Soc.* **1995**, *117*, 6787.
- (131) (a) Kablaoui, N. M.; Hicks, F. A.; Buchwald, S. L. *J. Am. Chem. Soc.* **1996**, *118*, 5818. (b) Crowe, W. E.; Vu, A. T. *J. Am. Chem. Soc.* **1996**, *118*, 1557.
- (132) (a) Cantrell, G. K.; Geib, S. J.; Meyer, T. Y. *Organometallics* **1999**, *18*, 4250. (b) Cantrell, G. K.; Geib, S. J.; Meyer, T. Y. *Organometallics* **2000**, *19*, 3562. (c) Schrock, R. R.; Luo, S.; Lee, J. C.; Zanetti, N. C.; Davis, W. M. *J. Am. Chem. Soc.* **1996**, *118*, 3883.
- (133) Bodenhausen, G.; Ruben, D. J. *Chem. Phys. Lett.* **1980**, *69*, 185.
- (134) Bax, A.; Summers, M. F. *J. Am. Chem. Soc.* **1986**, *108*, 2093.


- (135) (a) States, D. J.; Haberkorn, R. A.; Ruben, D. J. *J. Magn. Reson.* **1982**, *48*, 286.
(b) Bodenhausen, G.; Kogler, H.; Ernest, R. R. *J. Magn. Reson.* **1984**, *58*, 370. (c)
Wider, G.; Macura, S.; Kumar, A.; Ernst, R. R.; Wuthrich, K. *J. Magn. Reson.*
1984, *56*, 207.
- (136) Eileen Frish, M. J. F. *Gaussian 98 User's Reference*; 2nd Edition ed.; Gaussian, Inc.: Pittsburgh, 1999.

BIOGRAPHICAL SKETCH


Thomas Michel Cameron was born July 29, 1975 in Smiths Falls Ontario, to parents Lucile and Gerald Cameron. His younger sister, Dominique, was born two years later, and the Cameron family of four moved from Perth (Ontario) to Ottawa (Ontario), then Puerto Rico and finally to Montreal. Tom attended high school and college in the Montreal area. He left Montreal to attend school at Mt. Allison University in Sackville, New Brunswick, from which he graduated in 1997.

Tom began his laboratory experience at Mount Allison under the direction of Professor Steven A. Westcott. After graduating, Tom went to Los Alamos National Labs for one year and gained valuable lab experience while working with Dr. R. Tom Baker. Tom left Los Alamos to pursue a graduate degree at the University of Florida under the direction of advisor Professor James M. Boncella. The work in this manuscript is a fairly complete record of what has been accomplished during his 4.5 years at UF. Upon his graduation, Tom will return to Los Alamos where his wife, Melissa, is waiting for him.

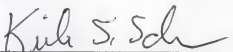
I certify that I have read this study and that in my opinion it conforms to acceptable standards of scholarly presentation and is fully adequate, in scope and quality, as a dissertation for the degree of Doctor of Philosophy.


James M. Boncella, Chair
Professor of Chemistry


I certify that I have read this study and that in my opinion it conforms to acceptable standards of scholarly presentation and is fully adequate, in scope and quality, as a dissertation for the degree of Doctor of Philosophy.


Daniel R. Talham
Professor of Chemistry

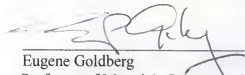
I certify that I have read this study and that in my opinion it conforms to acceptable standards of scholarly presentation and is fully adequate, in scope and quality, as a dissertation for the degree of Doctor of Philosophy.


Kirk S. Schanze
Professor of Chemistry

I certify that I have read this study and that in my opinion it conforms to acceptable standards of scholarly presentation and is fully adequate, in scope and quality, as a dissertation for the degree of Doctor of Philosophy.


Michael J. Scott
Associate Professor of Chemistry

I certify that I have read this study and that in my opinion it conforms to acceptable standards of scholarly presentation and is fully adequate, in scope and quality, as a dissertation for the degree of Doctor of Philosophy.


Eugene Goldberg
Professor of Materials Science and
Engineering

This dissertation was submitted to the Department of Chemistry in the College of Liberal Arts and Sciences and to the Graduate School and was accepted as partial fulfillment of the requirements for the degree of Doctor of Philosophy.

December 2002

Dean, Graduate School

LD
1780
2002

.C182

